



You are cordially invited to attend

MinWien2023

17 to 21 September 2023

A joint meeting of the three Mineralogical Societies



Topics: Mineralogical, Petrological, Geochemical Sciences, deposits & related disciplines (basic, applied & industrial topics)

Programme

Sunday, 17 September 2023

Mineralogy for the public

Young Scientists meet each other

Opening Ceremony

Together Party

Pre-conference

Male K...

16-17 S...

Guides: P. Bačík I. Bros...

Abstracts, O - Z

Thursday,

September 2023

Scientific sessions

Poster presentations

Industrial exhibition

Conference dinner

Wednesday 20 September 2023

Festival Hall, Vienna's City Hall

Half-day tours

18-21 September, 2023

Poster Prizes for young scientists

DMG - General Assembly

Public lecture



Conference Site: Alma Mater Rudolfina - University of Vienna

Geozentrum - UZAI, Josef-Holaubek-Platz 2, 1090 Vienna

Organisation: Institut für Mineralogie und Kristallographie

Further information: <https://minwien2023.univie.ac.at>

e-mail: minwien2023.mineralogie@univie.ac.at

Photo on courtesy of Stephan Wolfsried

DOI: <https://doi.org/10.23689/fidgeo-6024>

Fahlore analyses from a prehistoric work and settlement site in Kundl, Tyrol

L. Oettel¹, P. Tropper¹, L.M. Eß²

¹University of Innsbruck, Institute of Mineralogy and Petrography

²University of Innsbruck, Institute of Archaeology

e-mail: lena.oettel@uibk.ac.at

Between 2018 and 2019, the largest prehistoric area excavation in North Tyrol to date took place in Kundl (district of Kufstein). On an area of about 11,600 m² in the Wimpissinger gravel pit, horizons from the 1st millennium BC were uncovered.

The excavated work area offers a unique large-scale insight into the work stages between mining and metal production. The phases of use of this work area extend from the Early Bronze Age to the late Iron Age.

During the excavations, in addition to hundreds of slag remains from the Early and Late Bronze Age, three storage vessels were excavated, which can also be assigned to the Late Bronze Age (Eß, unpublished). Around one of the storage vessels fahlore ore lumps were draped and examined in the context of an origin determination of the smelted ores.



Figure 1. Storage vessel with fahlore wreath (picture: Talpa GnbR 2019)

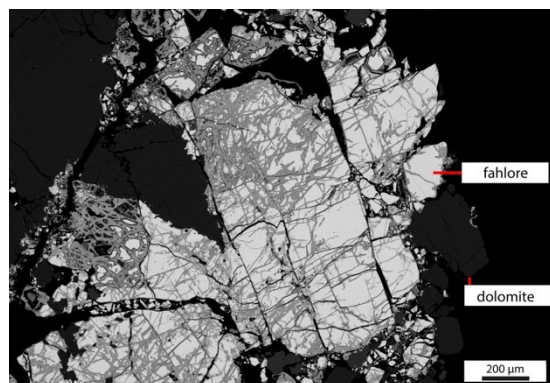


Figure 2. BSE picture of an analysed stone, which was draped around the storage vessel (picture: L. Oettel 2020)

Electron probe microanalysis of these fahlore minerals were undertaken for putting possible provenance constraints on the ores. Since this examination did not yield a satisfying match within the HiMAT mineral chemical database, the source of the smelted fahlores could yet not be determined. For this reason, additional 37 samples of fahlores were taken from a wide variety of localities/tectonic units (e.g. Northern Limestone Alps, Engadin Window) and examined by electron beam microprobe to increase the chemical database considerably.

Micro-CT analyses from a prehistoric work and settlement site in Kundl, Tyrol

L. Oettel¹, P. Tropper¹, G. Degenhart²

¹University of Innsbruck, Institute of Mineralogy and Petrography

²Core facility μ CT at the Medical University Innsbruck

e-mail: lena.oettel@uibk.ac.at

Prehistoric mining and production sites for copper are known from the Eastern Alps, reaching back to the beginning of the Early Iron Age, but the further processing of the copper products (bronze foundries etc.) could so far only be localized indirectly.

A key site for the production step between mining and metal processing, which has hardly been investigated so far, is offered by the Late Bronze and Iron Age workshop area of Kundl in the Tyrolean Lower Inn Valley, which was used over a long period of time, from the late 11th century BC, with an interruption in the 8th/7th century, until the 1st century BC. In Kundl (district of Kufstein), the largest archaeological excavation in North Tyrol to date was carried out in 2018 and 2019, during which nearly 31,000 finds were recovered. The excavation area of around 11,000 m² in the area of the Wimpissinger gravel pit is located directly next to the Iron Age burial ground of the Fritzens-Sanzeno culture discovered in the 1970s.

During the more recent excavations, Late Bronze Age as well as Iron Age use horizons were discovered, which were separated from each other by meter-thick gravel layers, resulting in an excellent preservation of the finds and features (Staudt et al. 2021).



Figure 1. Oven battery with roasting bed (picture: Talpa GnbR, 2019)

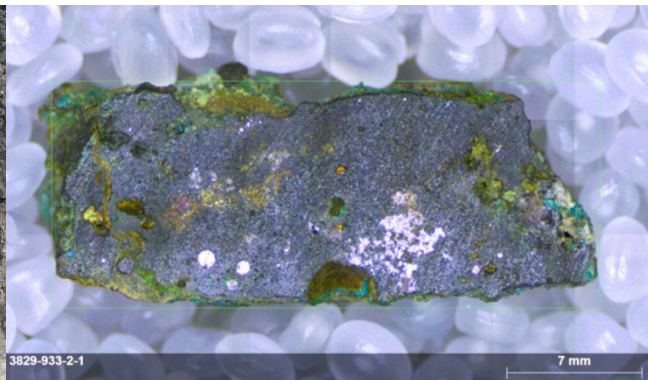


Figure 2. Heterogenous slag from early bronze age horizon (picture: L. Oettel, 2021)

Due to the temporal diversity of the slag finds (Bronze Age to Iron Age), the Kundl site is an ideal pilot project for slag investigations using microcomputed tomography, as this allows to visualize the improvement of the production process of copper to be traced as a function of time. Early as well as Middle and Late Bronze Age slag finds were excavated from various horizons. Furthermore, within the horizons there are samples of all slag categories (heterogeneous slag, plate slag, slag sand and furnace slag), which have preserved the different working steps.

Staudt M, Bader M, Eß LM, Lueger D, Oettel LS, Tropper P, Trebsche P (2021): Eine Werksiedlung aus der Bronze- und Eisenzeit bei Kundl (Nordtirol). - Vorbericht über die Ausgrabungen 2018–2019 in der Schottergrube Wimpissinger. In: *Archaeol Austr* 105, 249-282

Phosphorus in the deep Earth: An experimental investigation of Ca-phosphates at upper- to lower-mantle P-T conditions

T. Pausch¹, B. Joachim-Mrosko¹, A.C. Withers², T. Ludwig³, J. Vazhakuttiyakam¹,
J. Konzett¹

¹*Institute for Mineralogy and Petrography, University of Innsbruck*

²*Bayerisches Geoinstitut, Universität Bayreuth*

³*Institute of Earth Sciences, Heidelberg University*

e-mail: tristan.pausch@uibk.ac.at

During subduction and dehydration of oceanic crust, P can be transported into the mantle wedge by fluids or melts, and either enters silicate phases, in particular garnet and olivine, or, if bulk P concentrations are sufficiently high, forms apatite. This P-enriched peridotite will then be dragged down with the subducted slab into the deep mantle. When apatite reaches its upper pressure stability limit, the anhydrous Ca-phosphate tuite will form. While the role of Ca-phosphates in the global P-cycle is well understood for the crust and shallow upper mantle, this is not the case for the deep silicate Earth near and below 660 km depth.

In this study we investigated the *P-T* stability, phase relations, and compositional evolution of tuite in a peridotitic bulk composition at *P-T* conditions of the upper- to lower-mantle transition. For this purpose, multianvil experiments were performed at 15 to 25 GPa and 1600 to 1800 °C. A synthetic peridotite, based on the composition of a moderately fertile spinel lherzolite, was used as starting material. This peridotite was doped with 3% synthetic β -Ca₃(PO₄)₂, 1% of a trace element mix containing a range of HFSE, LILE and REEs, and approx. 2200 µg/g of Br and Cl each.

The coexisting phases stable within the studied *P-T* range include tuite, majoritic garnet, ringwoodite, forsterite, clinoenstatite, bridgmanite, davemaoite, ferropericlase, and melt. Tuite breaks down between 1700 and 1750 °C at 20 to 25 GPa and between 1750 and 1800 °C at 15 GPa, which yields a negative slope for the tuite-out reaction.

Beyond the *P*-stability of apatite, tuite and/or garnet are the main P carriers in a typical peridotite dependent upon the bulk P content. With increasing depth, the modal amount of Ca-phosphates decreases due to a progressive phosphate-to-silicate P transfer, leading to P contents of up to 4.8 wt% P₂O₅ in majoritic garnet at 1600 °C and 20 GPa. However, as soon as garnet reaches its stability limit, tuite is very likely the most important P-carrying phase at subsolidus conditions while bridgmanite and davemaoite contain small to negligible P (< 60 µg/g and <380 µg/g respectively) even when buffered by tuite.

NanoExtrem-NanoExtrem2: Nano-focus end-station for experiments at ID27 at ESRF

**L. Pennacchioni¹, M. Mezouar², C. L. Sahle², W. Morgenroth¹, S. Jahn³, M. Herrmann³,
M. Schulze³, A. Pakhomova², B. Wehinger², G. Garbarino², S. Bauchau², K. Martel², F. Gerbon²,
D. Andrault⁴, M. Wilke¹**

¹University Potsdam, Potsdam, Germany

²European Synchrotron Facility, ESRF, Grenoble, France

³University of Cologne, Cologne, Germany

⁴Université Clermont Auvergne, Clermont-Ferrand, France

e-mail: lea.pennacchioni@uni-potsdam.de

Research groups from the Universities of Potsdam and Cologne contributed to the construction and improvement of an end station for nano-focused X-ray diffraction (XRD), fluorescence (XRF), and imaging (XRI) at the ID27 high-pressure beamline at the ESRF, Grenoble, in a BMBF project ‘Nanoextrem’. A second BMBF project, ‘Nanoextrem2’, was funded to expand the experimental possibilities with the addition of a high-resolution X-ray emission (XES) spectrometer and pulsed laser heating to the beamline.

An end station for in situ XRD, XRF, XRI and XES at extreme conditions will allow to investigate samples in the field of high-pressure materials and solid state physics in an unprecedented manner.

The end station allows for different focusing schemes by Kirkpatrick-Baez (KB) mirror systems (covering an energy range of 15 to 60 keV) arranged to serve either a nano focus setup, a laser-heating setup, a micro focus arrangement for spatial flexibility and heavy load setups. A Soller slit system was developed and implemented to reduce the Compton scattering of complex sample environments.

Highlights of the setup that have been already characterized : (i) the focusing of the nano-beam (available in the energy range between 15 and 25 keV) to 300×300 nm; (ii) the gain of a factor 70 in flux obtained using a submicron-focused pink beam compared to the monochromatized microbeam (FWHM for pink and monochromatic beam is $0.8 \mu\text{m} \times 0.8 \mu\text{m}$ at $0.3738 \text{ \AA} / 33.17 \text{ keV}$).

As an example, preliminary results on high-pressure XRD experiments on hydrous and anhydrous SiO₂ glasses up to 40 GPa will be presented, as well as performance parameters. In particular, pressure induced structural changes in the SiO₂-H₂O system will be discussed and the first results of a laser-heating experiment up to 4000 K to study the structures of the respective melts will be shown.

Discerning different nucleation mechanisms in synthetic trachybasalts: example from three Titanomagnetite populations in single experiments

S. Peres¹, T.A. Griffiths¹, F. Colle², S. Iannini Lelarge³, M. Masotta^{3,4}, A. Pontesilli⁵, L. Mancini⁶

¹Department of Lithospheric Research, University of Vienna, Josef-Holaubek-Platz 2, 1090 Wien, Austria

²Dipartimento di Scienze Chimiche, della Vita e della Sostenibilità Ambientale, Università di Parma, Campus Universitario, Parco Area delle Scienze 157A, 43124, Parma, Italy

³Dipartimento di Scienze della Terra, University of Pisa, Via Santa Maria 53, 56126 Pisa, Italy

⁴CISUP, Centro per l'Integrazione della Strumentazione Università di Pisa, Lungarno Pacinotti 43, 56125 Pisa, Italy

⁵Istituto Nazionale di Geofisica e Vulcanologia, Via di Vigna Murata 605, 00143 Roma, Italy

⁶ZAG - Slovenian National Building and Civil Engineering Institute,

Dimičeva ulica 12, 1000 Ljubljana, Slovenia

e-mail: stefano.peres@univie.ac.at

Heterogeneous nucleation, i.e. nucleation on a pre-existing surface, is energetically more favourable than homogeneous nucleation because it requires overcoming a lower energetic barrier in order to form a critical nucleus. In most natural and experimental crystallizing magmas, heterogeneous nucleation is suggested to be the main nucleation mechanism, but robust criteria to prove the heterogeneous nucleation origin of a given crystal or phase in natural rocks and ex-situ samples are lacking.

Here we apply multiple analytical methods in order to assess the nucleation mechanism of titanomagnetite (Tmt) crystals that crystallized in the proximity of clinopyroxene (Cpx) crystals in a synthetic trachybasaltic melt (with 2 wt.% added H₂O) in crystallisation experiments carried out in a piston-cylinder apparatus at a constant pressure of 4 kbar. After 30 minutes of superheating at 1300 °C, the samples were cooled at a rate of 80°C / min to the final resting temperatures of 1150 °C and 1100 °C. These temperatures correspond to a respective undercooling (ΔT expressed as $T_{\text{liquidus}} - T_{\text{experiment}}$) of 30° and 80°. The dwell times at these temperatures were 30 minutes and 8 hours, respectively.

3D image processing and 3D image analysis of high-resolution synchrotron X-ray computed microtomography (SR μ CT) data resulted in a precise phase segmentation of Cpx, Tmt, glass and bubbles. Moreover, it was possible to discriminate three main Tmt populations spatially distributed alongside Cpx crystals but morphologically different to each other: a) Tmt grains > 100 μ m in size, skeletal in shape, and mostly isolated in the melt (population 1); b) Tmt grains between up to 100 μ m in size, anhedral to partially skeletal in shape, and always decorating Cpx grains edges and tips (population 2); c) needle-to-flattened Tmt grains almost completely enclosed within Cpx grains (population 3).

The pair correlation function $g(r)$, i.e. a measure of the frequency of an interpoint distance (of r), has been evaluated for the 3D point pattern composed by the centroids of each Tmt population, extracted from several VOIs inside 3D scans of the samples. Tmt grains of population 1 have an unclear 3D point pattern characterized by $g(r)$ near 1, a possible sign of a randomly distributed point pattern. Populations 2 and 3 show clear clustered 3D point patterns, characterized by $g(r) > 1$ and interpoint distances r up to 200 μ m.

Electron backscatter diffraction (EBSD) analysis enables us to clarify the crystallographic orientation relationships (CORs) between Cpx and Tmt crystals which share boundaries. Less than 60 % of the total shared Cpx-Tmt boundary length of population 1 Tmt crystals is characterized by the presence of CORs. Individual crystals of this population show no CORs between the two crystal phases at all, or boundary misorientations dispersed around known specific CORs. In contrast, more than 85% of the total shared Cpx-Tmt boundary length in Tmt populations 2 and 3 follows a COR. Locally, clusters of multiple Tmt decorating single Cpx crystals show more than 95% of the cumulative shared length characterized by the presence of CORs.

Considering the skeletal-to-euhedral shape, the unclear 3D point pattern distribution and the lack of CORs in some Cpx-Tmt pairs classified as Population 1, we suggest that the isolated single grains from this class are most likely formed by homogeneous nucleation. Individual large grains of this same population showing CORs may represent unusually large heterogeneously nucleated Tmt grains, Cpx grains heterogeneously grown on a pre-existing Tmt crystal, or potentially Tmt-Cpx interaction after nucleation apart.

Considering the anhedral or acicular shape, the highly clustered point pattern, and the ubiquitous presence of CORs, we interpret Population 2 and 3 Tmt grains to have formed by heterogeneous nucleation on top of pre-existing Cpx crystals.

In conclusion, multiple Tmt morphologies and distributions coupled with different COR systematics imply different nucleation mechanisms and growth histories for the three populations. Notably, the different Tmt nucleation mechanisms occurred during or right after a single cooling event. Multiple microstructural populations of crystals in natural magmas should be carefully assessed before inferring the existence of complex thermal (or other) histories. A multi-methodological approach which combines 3D SR μ CT data with 2D crystallographic one is indispensable to confidently discern between homogeneous and heterogenous nucleation mechanisms.

Funded by the Austrian Science Fund (FWF): P 33227-N

Mineral reactions in thermally treated calcareous clays for brick production

P.R. Pesek¹, C.L. Lengauer¹, R. Abart², A. Kurka³, G. Früh⁴, W. Gaggl⁴

¹University of Vienna, Department of Mineralogy and Crystallography,
Josef-Holaubek-Platz 2, 1090 Vienna, Austria

²University of Vienna, Department of Lithospheric Research, Josef-Holaubek-Platz 2, 1090 Vienna, Austria

³Wienerberger AG, Wienerbergerplatz 1, 1100 Vienna, Austria

⁴Wienerberger AG, Hauptstraße 4, 2332 Hennersdorf, Austria

e-mail: patrick.pesek@univie.ac.at

The commercial production of bricks usually requires firing temperatures in the range of 800-1000 °C. Some raw materials for brick production may contain up to several wt% carbonates. These carbonates thermally decompose in the range of 600-900 °C and subsequently induce the formation of new mineral phases and microporosity. This allows the production of high thermal insulating clay blocks which contribute for an energy efficient building stock, however, the additional release of CO₂ is an unfavorable side effect regarding the overall carbon footprint. Strongly supporting the European Green Deal, Wienerberger AG is striving to find solutions for a reduction of these raw material related process emissions. Therefore, an approach was targeted to find and evaluate additives, which allow lower firing temperatures in the range of decomposition temperatures of carbonates concurrently keeping the physico-technical parameters of the fired products comparable to available products. In this context, it is particularly important that the pure clay-type raw material and its thermal behavior is foremost characterized so that comparisons with clay-additive mixtures can later be made.

Test specimens were extruded, dried, and fired at 620 °C, 700 °C, 760 °C and 880 °C. The mineral phases, chemical composition and thermal behavior of the green body and the fired sherds were determined using PXRD, XRF and TA, respectively. SEM-EDX and EPMA were used for high-resolution images of microstructures and phase identification as well as for identifying mineral reactions.

The results revealed a multitude of processes occurring during the firing process of the investigated calcareous clay. A selection of relevant mineral reactions is listed below:

(i) Individual clay minerals were dehydroxylated at 620 °C, while the matrix was visibly molten at a firing temperature of 880 °C (Fig. 1A). Within the reduction core, a higher level of melting was present than at the rim, possibly due to FeO that rather acts as a fluxing agent than Fe₂O₃ (Fischer 1987).

(ii) The beginning of decomposition of carbonates was observed at 620 °C. Decomposing carbonates can react with clay minerals, which leads to a densification of sherds at 600 °C (Fischer 1987). Small dolomite grains displayed an advanced level of decomposition at 700 °C with grains exhibiting a dolomite-type core surrounded by MgO and a Ca-rich shell. This degree of decomposition was also visible within larger dolomite grains at 760 °C. Calcite was also partially decomposed and consisted of a calcite-type core surrounded by a Ca-rich shell. At 880 °C almost all of the carbonate grains had vanished. Remaining MgO or pores with or without carbonate residues were surrounded by a rim of Ca-Mg-Al-silicates due to significant diffusion of Ca and Mg into the matrix (Fig. 1B). PXRD exhibited newly formed gehlenite and akermanite at this temperature.

(iii) Pyrite thermally decomposed between 300-600 °C, gaseous SO₂-SO₃ was formed (c.f. Schmidt, 1968) and confirmed by evolved gas analysis. The SO₂-SO₃ gas, however, stayed at most in the sherds and reacted with MgO and CaO of the decomposing carbonates thus forming sulfates (Schmidt 1968). Low concentrations of S were detected in carbonates at 700 °C. The amount of detected S increased with increasing firing temperature. Domains with elevated S contents were formed along the rims of the remaining carbonate grains at 760 °C. At a firing temperature of 880 °C, S could be found in the residues of former carbonates and in the Ca-Mg-Al-silicate reaction rims (Fig. 1B).

(iv) Some Na-rich feldspars exhibited a K-enriched rim at 880 °C (Fig. 1C) due to an exchange of Na⁺ for K⁺ (Riccardi et al. 1999). Collapsed clay minerals (Riccardi et al. 1999) and partially collapsed muscovite (Ionescu & Hoeck 2011) can be considered as sources of K⁺.

(v) Some quartz grains were characterized by a rim enriched in Al, Na, K and Fe at 880 °C (Fig. 1C). The interaction of these foreign elements indicates a softening or partially melting of quartz grains (Ionescu & Hoeck 2011).

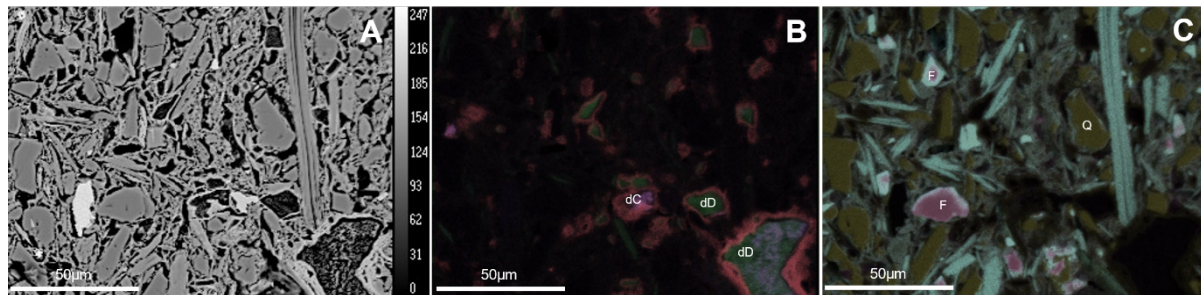


Figure 1. (A) BSE-image of a calcareous clay fired at 880 °C; (B) Stacked element maps of Mg (green), Ca (red) and S (purple); (C) Stacked element maps of Si (yellow), Na (magenta) and K (cyan). Abbreviations: dC decomposed calcite, dD decomposed dolomite, F feldspar, Q quartz.

The outlined observations made are an important basis for firing experiments of clay-additive mixtures. Various mineral reactions were identified, and observations reported in literature were confirmed. The two most significant processes observed in detail are the gradual decomposition of carbonates starting from 620 °C and the melting of the matrix between 760-880 °C. Especially, the role of sulfur during the decomposition of carbonates provides important information for brick producing processes, since the formation of water-soluble sulfates causes severe efflorescence (Schmidt 1961).

Fischer P (1987): Die Bildung des grobkeramischen Scherbens beim Brennen, Teil II. – ZI-Jahrbuch 88, 96

Ionescu C, Hoeck V (2011): Firing-induced transformations in Copper Age ceramics from NE Romania – Eur J Miner 23, 937-958

Riccardi MP, Messiga B, Duminuco P (1999): An approach to the dynamics of clay firing – Appl Clay Sci 15, 393-409

Schmidt E (1961): Ausblühungen. – Die Ziegelindustrie 5, 132

Schmidt E (1968): Die physikalischen und chemischen Veränderungen beim Ziegelbrand – ZI-Jahrbuch 68, 208

Coherent lamellar intergrowth from exsolution of alkali feldspar

E. Petrishcheva, D. Heuser, R. Abart

*Department of Lithospheric Research, University of Vienna
e-mail: elena.petrishcheva@univie.ac.at*

We investigate coherent lamellar intergrowth resulting from exsolution in alkali feldspar. This structure forms when an initially homogeneous alkali feldspar of intermediate composition enters the miscibility gap during cooling below about 550°C and separates into lamellae of more Na-rich and lamellae of more K-rich composition. As the lattice parameters of alkali feldspar are strongly compositional dependent, formation of these lamellae induces strains and stresses within the structure. In coherent intergrowth the elastic and chemical strains interact in such a way that coherent boundaries are maintained between the lamellae.

The presence of elastic deformation affects the system's free energy and consequently influences its equilibrium phase relations such as binodal points and the miscibility gap. In earlier papers, due to the problem of having fewer equations than unknown variables, certain simplifying assumptions were made regarding the strains. In particular, the strains lying in the plane parallel to the lamellar interfaces were assumed to be zero, which we deem unphysical. Instead, we take advantage of the principle that the system tends towards the state with the minimum energy among all possible equilibrium states.

To determine the elastic stresses and strains and their impact on the system's free energy, we calculate and minimize the overall elastic energy of the lamellar structure. The elastic energy acts against the separation of Na-rich and K-rich lamellae, leading to binodal points deviating from the expectations based solely on chemical equilibrium in an unstrained state. By accounting for the elastic energy, we obtain both the corrected binodal points and the miscibility gap as represented by the so-called *coherent solvus*, which now is not unique and depends on the composition of the homogeneous precursor feldspar.

The main mathematical challenge lies in the fact that calculation of the elastic energy requires knowledge of the binodal points, the latter in turn, are determined by the total free energy of the system. To overcome this challenge, we employ a method of successive approximations. Observed lamellar orientations agree well with our calculations. These results represent a significant improvement and generalization of earlier work by Robin (1974).

Micro-CT and micro-XRF investigations of an Early Bronze-Age smelting crucible fragment

M. Piccolruaz¹, P. Tropper¹, G. Degenhart²

¹University of Innsbruck, Institute of Mineralogy and Petrography, 6020 Innsbruck, Austria

²Medical University of Innsbruck, Institute of Radiology, 6020 Innsbruck, Austria
e-mail: peter.tropper@uibk.ac.at

In this investigation, a fragment of an early Bronze Age smelting crucible fragment with an adherent slag crust was examined. Together with ore fragments, raw copper and copper objects this fragment documents the evidence of small-scale smelting activity at the early Bronze Age site Buchberg near Wiesing in the Inn valley.

The sample was analyzed by electron microprobe analysis as well as micro-XRF. Mineralogically and chemically three different areas can be distinguished. The first area (Bereich A) away from the slag crust is unmelted and consists mainly of clay minerals and different temper components (orthogneiss, quartz, plagioclase, K-feldspar, muscovite). The second area (Bereich B) closer to the slag crust shows melting and thus consists mainly of a glass matrix with occasional inclusions of covellite (CuS). The third area (Bereich C) represents the slag crust and contains clinopyroxenes in a glass matrix, and also small amounts of acanthite (Ag₂S). Furthermore, abundant Cu-Sb-Fe-Zn-O phases (possibly the alteration phase theisite, Cu₅Zn₅(AsO₄,SbO₄)₂(OH)₁₄) and chalcocite (Cu₂S) occur. The glass in area C contains high concentrations of phosphorus, arsenic and antimony and the SiO₂ content decreases strongly in the glass from area B to area C.

The crucible fragment was scanned using a micro-CT, which resulted in a three-dimensional image illustrating the distribution of high-density phases in the crucible fragment and the slag crust. Quantitative evaluation of the CT results of the slag crust yielded in very little pore space of 3 vol.%, whereas the amount of the high-density phases (Cu-Sb-Fe-Zn-O phases) is 43 vol.% and thus is clearly concentrated in the slag crust.

Finally, the results show that the ores used for copper smelting in the Early Bronze Age were As-rich tetradrites deriving most likely either from the Devonian Schwaz Dolomite or the carbonates of the Schwaz Triassic (the occurrence of acanthite points towards it). The high phosphorous contents in the slag can either be interpreted as resulting from firing plant materials (wood) or the possible addition of bone apatite to the smelting process.

STOE Diffractometers empowering Mineralogical Crystallography

T. Pippinger¹

*¹STOE & Cie GmbH, Darmstadt, Germany
e-mail: pippinger@stoe.com*

STOE, established in 1887, manufacturing equipment for the optical examination of crystals, has been at the forefront of powder and single crystal X-ray diffraction since the 1960s. STOE invented and patented the transmission geometry technique for Powder XRD and additionally, they developed the first pixel detector XRD system with an open Eulerian cradle for single crystals.

Headquartered in Darmstadt, Germany, STOE maintains complete in-house capabilities for research and development, software programming, electrical and mechanical engineering, and production. This integrated approach enables STOE to offer both standard and customized solutions to its customers. Whenever it comes to quality, STOE accepts no compromises.

STOE's latest instruments facilitate precise profile and Rietveld analyses, as well as ultrafast single crystal diffraction experiments on even the tiniest crystals. Furthermore, high-temperature and high-pressure accessories are available, which can be seamlessly integrated in the hardware and software, allowing for the convenient simulation of non - ambient inner earth conditions.

These solutions tailored to Mineralogical Crystallography and more will be discussed in the presentation.

Clays from the Westerwald area as a source for high reactive main cement constituent

C. J. Piribauer¹, R. Diedel¹, H. Knapp¹, W. Heuser¹, M. Schellhorn¹

¹Stephan Schmidt Group,
e-mail: christoph.piribauer@stephan-schmidt.group

The cement and concrete industry are currently in a state of transition due to high CO₂ emissions. According to a study of the vdz (Deutscher Verband der Zementindustrie), there are three main levers to lower the emissions: alternative fuels, CCS / CCU and clinker reduced cements. As most of the emissions are so called process emissions and the potential for CCS / CCU is limited in a close range to the cement producers, there is a strong focus on the development and usage of clinker reduced cements. Calcined clays play an important role here as a substitute for the cement clinker made from limestone. To meet the decarbonisation targets of the German cement industry, 6.8 to 7.5 million tonnes/a of clay will be needed by 2030 (Basten, 2022). In order to cover this very high demands for clays, waste clays from treatment processes, such as filter cakes and clays from sludge ponds, are considered in addition to conventionally mined clays. As these secondary raw materials occur only in relatively small quantities with strongly varying compositions, they are likely to play only a minor role in the future due to the strong influence of the mineralogical-chemical composition on the calcination conditions and therefore on the resulting reactivities and technological properties.



Figure 1. Mine Wimpsfeld 3, white kaolinitic-illitic clays with an overburden of bentonites and basalt. – Picture: Stephan Schmidt Group

Stephan Schmidt KG operates 20 open-cast clay mining operations in Germany, 16 in the Westerwald area. From these deposits, more than 100 clays were selected for a screening process not only focussing on their basic suitability for calcination, but also with regards to a long-time availability for a constant material supply of a calciner. In a first screening step, the carbonate content (< 5 mass-%), the sulphide concentration (< 1.5 mass-%) and the clay mineral/quartz ratio (> 50 %) were assessed. Clays that met these requirements were calcined at 750 °C and subjected to a test for pozzolanic properties. The Surana method (Surana and Joshi, 1990) was chosen to determine the pozzolanicity. By chemically treating the calcinates after Surana, the available reactive Si and Al ions could be determined via ICP-OES. At a concentration $>80,000$ ppm (Al+Si), suitability as a clinker substitute is ensured, comparable to the performance of blast furnace slag and fly ash (Schulze and Rickert, 2019). Next to this information, also the influence of the calcined clays on the early strength can be estimated, as a higher Al content leads to the formation of CA phases. The final step in the evaluation of calcined clays involves the testing of CEM I cements (activity index/EN 450-1; water demand/EN 196-3; compressive strength/EN 196-1), in which 25 % of the cement clinker phase is replaced by calcined clays.

Based on this knowledge, 2 main supply areas have been identified. While the raw material mixture from Arbon/Wimpfeld 3 (Fig. 1) has a high smectite content, the Sedan mixture is kaolinitic-illitic dominated. Each site allows the delivery of 250,000 t clay/a, which corresponds to the production of 200,000 t/a of calcinate.

Basten M (2022): Die Nachfrage nach Primär- und Sekundärrohstoffen der Steine-und-Erden-Industrie bis 2040 in Deutschland. - Bundesverband Baustoffe Steine und Erden e.V. Berlin

Surana M, Joshi S (1990): Estimating reactivity of pozzolanic materials by a spectrophotometric method. - Advances in Cement Research 3, 81-83

Schulze S, Rickert J (2019): Suitability of natural calcined clays as supplementary cementitious material. - Cement and Concrete Composites 1, 92-97

An uncommon terrestrial rock that was believed to be a meteorite

L. Pittarello^{1,2}, S. Chernonozhkin³, H. Downes⁴, O. Marchhart², S. Merchel², A. Wieser²,
F. Vanhacke⁵, J. Villeneuve⁶, S. Goderis⁷

¹Naturhistorisches Museum, Vienna, Austria

²University of Vienna, Austria

³Montanuniversität Leoben, Austria

⁴Birkbeck University of London, United Kingdom

⁵Ghent University, Belgium

⁶CRPG, Université de Lorraine, Vandœuvre les Nancy, France

⁷AMGC, Vrije Universiteit Brussel, Belgium

e-mail: lidia.pittarello@nhm.at

Ureilites are achondrite meteorites, which can be associated to mantle restites, but containing up to 8 wt% carbon and which have experienced melting, smelting, and shock (e.g., Goodrich 1992; Goodrich et al. 2007). In the framework of a research project on isotopic zoning across olivine grains from selected ureilites (Chernonozhkin et al. *subm.*), a chip from Dyalpur was loaned from the Natural History Museum London (sample BM.51185). Petrographic and geochemical analysis of this sample revealed some features, which are not consistent with the previous characterization of Dyalpur and ureilites in general. However, as clasts with peculiar characteristics are not uncommon among ureilites (e.g., clast ALM-A with a trachyandesitic composition; Bischoff et al. 2014), we decided for further investigations. Oxygen isotopic ratios are close to the terrestrial fraction line, but this can also indicate mixing of different components by impact on the parent body (e.g., for angrites, Rider-Stokes et al. 2023). However, cosmogenic radionuclide measurements by accelerator mass spectrometry (Lachner et al. 2021) finally confirm a terrestrial origin of the sample. The (yet preliminary) upper limit of $^{26}\text{Al}/^{27}\text{Al}$ 4.4×10^{-12} corresponding to 0.3 dpm/kg (^{26}Al) measured is >60 times lower than the one of true Dyalpur sample, and also far lower than literature values for ureilites including Dyalpur (e.g., Aylmer et al. 1990).

The typically terrestrial features, including the occurrence of pargasite-hornblende amphibole and hazlewoodite (a Ni-sulfide), both never described before in ureilites, are associated with other features, which are quite uncommon for terrestrial rocks, such as the presence of carbon-rich veins inducing chemical reduction along their margin, and a Fo₉₁ groundmass, embedding sub-rounded amphibole clasts. Geothermobarometric estimates (e.g., Hammarstrom & Zen 1986; Ridolfi & Renzulli 2012; etc.) on amphibole resulted in pressure estimate of 6-7 kbar and temperature estimate of 790-840 °C.

Terrestrial rocks presenting similar features are rare, mostly consisting of metasomatized peridotite-xenoliths in basalts recording breakdown of amphibole due to heating and decompression during transport (e.g., Ban et al. 2005; Kaeser et al. 2007). Further studies are planned to identify the nature of the sample and to reconstruct the case leading to its classification as Dyalpur ureilite in the collection of the NHM London.

- Aylmer D, Vogt D, Herzog GF, Klein J, Fink D, Middleton R. (1990): Low ^{10}Be and ^{26}Al contents of ureilites: Production at meteoroid surfaces. - *Cosmochim Acta* 54, 1775-1784
- Ban M, Witt-Eickschen G, Klein M, Seck HA. (2005): The origin of glasses in hydrous mantle xenoliths from the West Eifel, Germany: incongruent break down of amphibole. - *Contrib Mineral Petrol* 148, 511-523
- Bischoff A, Horstmann M, Alix Barrat J-A, Chaussidon M, Pack A, Herwartz D, Ward D, Vollmer C, Decker S (2014): Trachyandesitic volcanism in the early Solar System. - *P Natl Acad Sci USA* 111, 12689 -12692
- Chernozhukhin SM et al. (subm.): Early differentiation and core formation on the ureilite parent body recorded in the stable isotopic signatures of Fe, Zn and Mg.
- Goodrich CA (1992): Ureilites. A critical review. - *Meteoritics* 27, 327-352
- Goodrich CA, Orman vanJA, Wilson L (2007): Fractional melting and smelting on the ureilite parent body. - *Geochim Cosmochim Acta* 71, 2876
- Hammarstrom JM, Zen E (1986): Aluminum in hornblende: An empirical igneous geobarometer. - *Amer Mineral* 71, 2876-2895
- Kaaser B, Kalt A, Pettke T (2007): Crystallization and breakdown of metasomatic phases in graphite-bearing peridotite xenoliths from Marsabit (Kenya). - *J Petrol* 48, 1725-1760
- Lachner J, Martschini M, Kalb A, Kern M, Marchhart O, Plasser F, Priller A, Steier P, Wieser A, Golser R (2021): Highly sensitive ^{26}Al measurements by Ion-Laser-InterAction Mass Spectrometry. - *Int J Mass Spectrom* 465, 116576
- Rider-Stokes BG, Greenwood RC, Anand M, White LF, Franchi IA, Debaille V, Goderis S, Pittarello L, Yamaguchi A, Mikouchi Z, Claeys P (2023): Impact mixing among rocky planetesimals in the early Solar System from angrite oxygen isotopes. - *Nat Astron* (2023). <https://doi.org/10.1038/s41550-023-01968-0>
- Ridolfi F, Ranzulli A (2012): Calcic amphiboles in calc-alkaline and alkaline magmas: thermobarometric and chemometric empirical equations valid up to 1,130°C and 2.2 GPa. - *Contrib Mineral Petrol* 163, 877-895

U-Pb garnet, zircon, and rutile petrochronology of eclogite xenoliths from the Navajo Volcanic Field (USA)

J.E. Pohlner¹, R. Albert¹, S. Aulbach¹, S. Hao¹, A. Gerdes¹, J.B. Walters¹, D.J. Schulze², H. Helmstaedt³

¹*Institut für Geowissenschaften and Frankfurt Isotope and Element Research Center (FIERCE),
Goethe-Universität Frankfurt*

²*Department of Earth Sciences and Department of Chemical and Physical Sciences, University of Toronto,
Mississauga, Canada*

³*Department of Geological Sciences and Geological Engineering, Queen's University, Kingston, Canada
e-mail: pohlner@em.uni-frankfurt.de*

Complementary insights from multiple mineral geochronometers are often indispensable to disentangle the complex multi-stage history of subduction-related rocks. Previous geochronological work on eclogite xenoliths of the Navajo Volcanic Field (NVF) sparked controversies about their origin, especially whether they are derived from oceanic crust of the Farallon plate, or from older continental lithosphere, based on occasional Proterozoic zircon U-Pb ages. We present new LA-ICP-MS U-Pb data from garnet, zircon, and rutile alongside geochemical and geothermobarometric data to test models for the origin and evolution of the NVF xenoliths.

The NVF comprises intrusions of serpentinized ultramafic microbreccia (SUM) which intruded the Colorado Plateau at ~30 Ma. Eclogite xenoliths from this SUM are mineralogically unusual, strongly resembling orogenic rather than typically biminerally kimberlite-borne equivalents. Besides ubiquitous rutile, many contain zoisite pseudomorphs after lawsonite (with rare lawsonite relics), matrix monazite, and/or abundant pyrite along with rare coesite. Previous studies obtained peak P-T conditions around 4 GPa and 600°C. Chemically, some of the eclogites resemble mid-ocean ridge basalts, whereas most experienced varying degrees of multi-stage metasomatism. Zoned omphacite with Na-rich rims accompanied by an increase of whole-rock Na₂O contents (up to 11 wt%) and omphacite modes (sometimes >90%) reflects interaction with a siliceous fluid. Mg-rich garnet rims with mantle-like δ¹⁸O are interpreted to reflect a massive hydration event just prior to entrainment in the SUM. The latter is also thought to have caused the crystallization of monazite with published ~30 Ma ages.

The various xenoliths yield variable garnet U-Pb dates, indicating garnet growth at different stages, but exclusively from the Cretaceous to shortly before SUM formation. The non-uniform garnet data may suggest that the NVF eclogite xenolith suite was assembled from rocks that entered the eclogite facies diachronously over tens of Myr. Metamorphic zircon ages cover a range similar to the garnet ages. Various stages of potential interaction with internally-derived (from lawsonite dehydration) and externally-derived (metasomatic) fluids may have induced (re)crystallization and/or partial re-setting of geochronometer minerals over a considerable time span.

There is currently no evidence for pre-Mesozoic metamorphism in the eclogites. By contrast, the hypothesis of a Proterozoic protolith origin is still under consideration, and can only be tested by dating rare igneous zircon cores. A zircon and rutile U-Pb dating campaign planned for the near future will reveal how the resultant ages relate to those obtained from garnet.

Blue- and green-spotted "K2 gneiss" from the Goldberggruppe, Austria

J. Portenkirchner¹, E. Libowitzky²

¹*Department of Lithospheric Research, University of Vienna*

²*Department of Mineralogy and Crystallography, University of Vienna*

e-mail: eugen.libowitzky@univie.ac.at

"K2 gneiss" or "K2 granite" is a grey to white (meta)granite with cm-sized round blue (and sometimes green) spots stained by fine-grained azurite (and sometimes malachite). Due to its attractive appearance it has been carved to various stone artefacts and traded world-wide. Although this rock-type has been known exclusively from the slopes of the K2 in the Himalaya Mountains (hence the name), a second occurrence has been found in the Goldberggruppe in Austria some two years ago.

This special gneiss (Fig. 1) from the N wall of Hoher Sonnblick, Rauris Valley, Salzburg, has never been described in previous literature, although the mapping of the area has been done in great detail (Exner 1962, 1964). Extended field trips during the past years were not successful to confirm "K2 gneiss" in the neighboring areas SW - NW of Hoher Sonnblick peak. Only a special rock with similar appearance has been known from the "Weiße Wand" at Stanziwurten, Möll Valley, Carinthia, some 6 km SSW of Hoher Sonnblick. However, this rock shows a matrix of barite, calcite and quartz with blue and green spots of azurite and malachite.

Besides of normal petrographic investigations with the polarizing microscope (i.e. quartz, feldspar, muscovite, calcite), the blue and green spots were probed with micro-Raman spectroscopy. By comparison with reference spectra from the RRUFF data base (Downs 2006) azurite (Fig. 2) and malachite were unambiguously identified in all samples.

While the barite rocks from "Weiße Wand" contain also tiny chalcopyrite and tennantite grains as obvious primary source of copper, "K2 gneiss" from Hoher Sonnblick lacks any primary copper sulfides; only tiny striated cubes of pyrite have been observed (note the relics of tiny brown spots of limonite in the center of Fig.1).

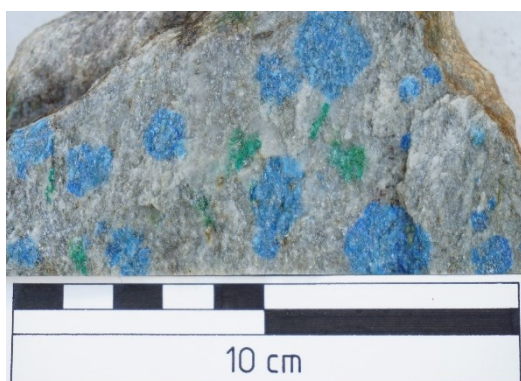


Figure 1. "K2 gneiss" from the Goldberggruppe with spots of azurite (blue) and malachite (green)

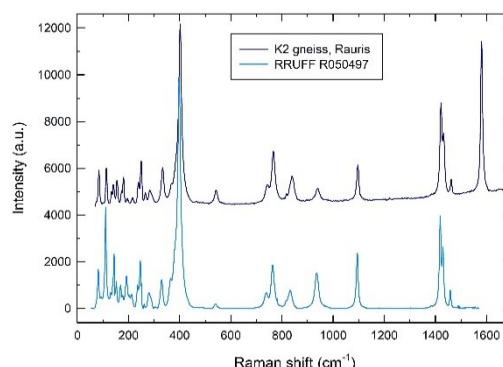


Figure 2. Micro-Raman spectra of azurite from "K2 gneiss" compared to an azurite reference from the RRUFF data base (Downs 2006).

Downs RT (2006): The RRUFF Project: an integrated study of the chemistry, crystallography, Raman and infrared spectroscopy of minerals. – Progr Abstr 19th General Meeting IMA, Kobe, Japan, O03-13

EXNER C (1962): Geologische Karte der Sonnblickgruppe, 1:50000. – Verlag der Geologischen Bundesanstalt, Wien

EXNER C (1964): Erläuterungen zur Geologischen Karte der Sonnblickgruppe, 1:50000. – Verlag der Geologischen Bundesanstalt, Wien

Electron Diffraction – Structure Elucidation of Nano-Crystalline Materials

A. Portieri¹, P. Simoncic¹

¹*Eldico Scientific, Badenerstraße 790, 8048 Zurich-Altstetten, Switzerland
e-mail: simoncic@eldico.ch*

Electron diffraction (known also as ED, 3D ED or microED) performing nano-crystallography on crystals smaller than 1 μm is increasingly gaining momentum in science and industry. Complementary to neutron-, powder-, and single-crystal X-ray diffraction, the disruptive technology of electron diffraction opens up fascinating new perspectives for a wide variety of compounds in the fields of chemical, pharmaceutical, and advanced materials research. The recent introduction of dedicated instrumentation to perform ED experiments is a key aspect of the continued growth and success of this technology. ELDICO Scientific presents the electron diffractometer ED-1, a smart combination of a 5-axis nanometer-precise goniometer, a large sample chamber, radically simplified electron optics, and an ultra-high-speed hybrid-pixel Dectris Quadro® camera for diffraction data acquisition. Several examples of data collected on ELDICO ED-1 are showcased to demonstrate the potential and advantages of a dedicated electron diffractometer, covering selected applications and challenges of electron diffraction: 1) polymorphism, 2) crystal mapping and extrapolation to powder XRD, and 3) structure elucidation of energy storage materials as well as zeolites and minerals.

Thracian marbles from Archaic to Roman Times – Imports or local production?

W. Prochaska, S. Ladstätter, V. Anevlavi

*Austrian Archaeological Institute, Austrian Academy of Sciences, Franz Klein-Gasse 1, 1190 Vienna, Austria
e-mail walter.prochaska@oeaw.ac.at*

Marble use and trade in the region of Thracia took place extensively already before it became Roman province in 46 AD. Within this territory some of the most prominent and renowned marble sources of antiquity are located (e.g., Prokonnesos or Thasos). The coastal regions at the Aegean, Marmara, and Black Sea, as well as the islands, were shaped by Greek culture and these marbles were widely exported throughout the empire. Accordingly, the marble trade in these coastal or island regions was always connected to the international commerce. Recent extensive studies in the course of the project “Fingerprinting White Marbles - Quarries and Cities of Roman Thrace, 1st-3rd century AD” (Austrian Science Fund) revealed that these marbles also were extensively used not only in the coastal areas but also in the larger inland cities of Thrace. In contrast to these renowned international marbles, the numerous marble deposits in the interior, in particular in today's Bulgaria, have received far less attention, however, as will be shown in this paper, they were of considerable economic importance.

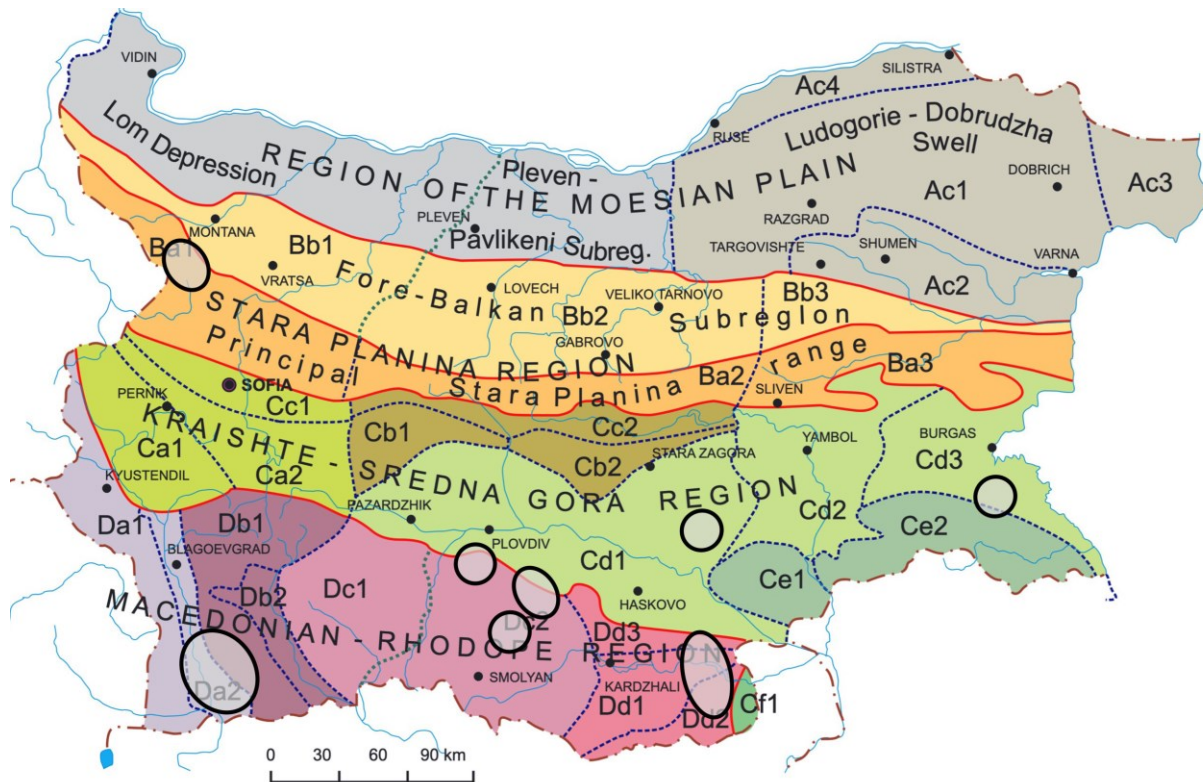


Figure 1. Geologic/geomorphological zonation of Bulgaria (Zagorchev 2009) with the marble producing areas.

The integration of the territory into the Roman Empire was followed by urbanisation and the extension of the infrastructure. Evidence of Roman marble production in the inland territory of Thrace is known in different areas: The most important geologic unit for economic marble production are the Rhodope Mountains with high-grade marble deposits. In the eastern parts of the Sredna Gora region further marble deposits occur with different metamorphic grades. Furthermore, in greenschist facies series of the NW Balkan Mountains near the town of Berkovitsa fine-grained marbles occur. Initial analyses indicate that these marbles were not only employed in the province itself, but were also exported. On the other hand, architecture and sculpture in the province of Thrace reveal striking connections to Asia Minor. By means of a sampling of the Thracian quarries on one hand and of Roman artefacts throughout the province on the other hand, the question regarding marble trade as well as the cultural and technological transfer will be discussed in the presentation. One example of far distant trade of the marble of that region is the “boarhunt” found during excavations in 2010 in Felix Romuliana in today’s Serbia sculptured from Berkovitsa marble.



Figure. 2: The sculpture “boarhunt” made of marble from Berkovitsa SW of the town of Montana in today’s Bulgaria. The sculpture or its marble was transported along a distance of more than 100 km in beeline.

More than 1400 samples from ancient quarries in Thrace and samples from artefacts in the museums all over the region were analysed in order to assign the marble of a given artefact to a corresponding quarry or quarry area. To achieve reliable results a multi method approach was applied using stable isotope analysis (O- and C-isotopes), trace element analysis by ICP-MS and petrographic investigations. Naturally, this large number of variables analysed has to be evaluated by statistical means. We used the programme packages STATISTICA and SPSS. On this basis the different marbles of Thracia can be told apart, and a very precise correlation of the artefacts to the corresponding sources can be achieved.

Zagorchev I (2009): Geomorphological zonation of Bulgaria. Principles and state of the art. - Proceedings of the Bulgarian Academy of Sciences 628(8), 981-992.

Prochaska W Zivic M (2018): The marbles of the sculptures of Felix Romuliana in Serbia. in Proceedings of the XI ASMOSIA Conference (Split May 2015) pp 301-311

Modern non-ambient X-ray diffraction for the investigation of minerals, metals and industrial materials of any type

B. Puhr¹, A.O.F. Jones¹, B. Schrode¹, M. Kremer¹, P. Vir¹, A. Paiva¹

¹Anton Paar GmbH, Graz, Austria
e-mail: barbara.puhr@anton-paar.com

Modern powder X-ray diffraction (XRD) systems must nowadays be able to meet the challenges faced by multi-user and multi-application facilities. Instruments must be capable not only of routine XRD measurements, but also have to offer advanced capabilities such as measurements under non-ambient conditions (varying temperature, pressure, gas atmosphere, humidity, ...) which can drastically change material properties.

The recently launched XRDynamic 500 automated multipurpose powder X-ray diffractometer from Anton Paar (Fig. 1) has set new standards in terms of data quality, automation and efficiency for laboratory powder diffractometers. The core of XRDynamic 500 is the TruBeam™ concept that comprises a large goniometer radius and evacuated optics units, automatic change of the beam geometry and all optics components, and automated instrument and sample alignment routines. All of these features combine to deliver outstanding data quality that can be measured with high efficiency in a straight-forward manner. The high level of automation means that you can perform measurements on one or many samples with different geometries and instrument configurations in one batch with no user intervention needed.

XRDynamic 500 can also be equipped with different non-ambient attachments to perform measurements under non-ambient conditions. These attachments are perfectly integrated into the hard- and software (plug-and play mode, integrated control unit, built-in connections) and guarantee best-in-class convenience for your non-ambient XRD studies.

To highlight the potential of XRDynamic 500, we will present key instrument features and benefits in addition to recent application data on non-ambient diffraction. Examples include in-situ structural changes of bentonite samples and materials used for technical applications (Fig. 2), how salt mineral compositions change under the influence of gas and humidity, and the study of the tempering temperature on the properties of steel.



Figure 1. The XRDynamic 500 automated multipurpose powder X-ray diffractometer from Anton Paar.

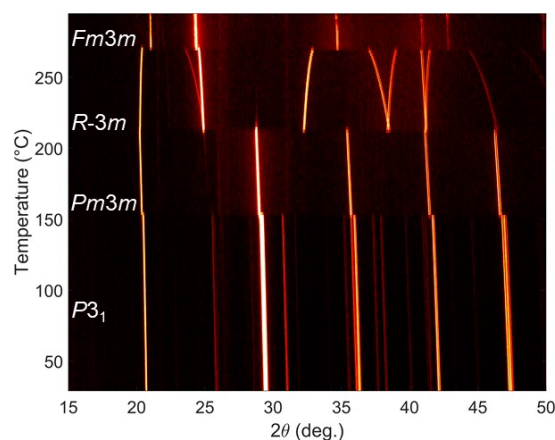


Figure 2. Temperature-induced phase transitions of RbNO₃ (Weidenthaler & Ternieden, 2022).

Machine learning-assisted pyrite indicator mineral approach in mineral exploration

S. Raič¹, F. Molnár², N. Cook³, P. Nikkola⁴, K. Szentpéteri⁴, H. O'Brien⁴,
A. Taivalkoski⁵, J.-P. Ranta⁵

¹*Institute of Applied Geosciences, University of Technology, Graz, Austria*

²*Department of Mineralogy, Institute of Geography and Earth Sciences, Eötvös Loránd University, Budapest, Hungary*

³*Sustainable Minerals Institute, University of Queensland, Indooroopilly, Queensland, Australia*

⁴*Geological Survey of Finland, Espoo, Finland*

⁵*Oulu Mining School, University of Oulu, Oulu, Finland*

e-mail: sara.raic@tugraz.at

Discovering new ore deposits that supply and satisfy the growing industrial demand for green transition metals is becoming more important than ever for transitioning into a non-fossil fuel future. This task however, appears to be unprecedented, when considering the required amount of technology metals. It becomes therefore highly relevant to develop and implement innovative and sustainable, but time- and cost-efficient exploration methods for deeply buried, undiscovered mineral deposits. A way to tackle this challenge is by using known European mineral deposits as testing grounds for new exploration technologies. For this purpose, the domestic mineral resources in northern Finland provide an ideal ecosystem and diversity of profitable green transition metals such as nickel, copper, cobalt and gold. The glaciated terranes in which these mineral systems occur, however, require special exploration methods such as the indicator mineral approach. Indicator minerals (e.g. sulfides, oxides and native gold) are recovered from glacial sedimentary samples and their individual grains are used for trace element analysis by LA-ICP-MS, which ideally could provide key information on the character of their source bedrocks, type of mineralization, as well as the glacial transport direction.

In this study we have tested the indicator mineral approach in the Rompas-Rajapalot Au-Co project areas in the Paleoproterozoic Peräpohja belt in northern Finland, by analyzing and comparing the trace element geochemistry of pyrite grains from bedrock and till samples. A machine learning-based approach was implemented using unsupervised self-organizing maps (SOM) and k-means clustering for mineralization-related pattern recognition. The obtained results show that pyrite grains recovered from till can be discriminated and clustered based on their compositions, and further correlated with pyrite from two hydrothermal deposit types within the study area: (i) the Au-Co mineral system at Rajapalot, and (ii) the vein-style Au system at Rompas. Mapping of recognized patterns, in accordance with ice flow directions, assists in (i) the localization of potential target-areas, (ii) and improves our understanding of similar mineral systems.

Tungsten mineralization in East Tyrol – repeated recycling of W in the crust?

J. G. Raith¹, F. Altenberger¹, F. Hutter², J. Weilbold³, C. Auer³

¹Montanuniversität Leoben, Leoben

²GeoSphere Austria, Vienna

³geo.zt gmbh, Hall in Tirol

e-mail: johann.raith@unileoben.ac.at

Geochemical tungsten anomalies and occurrences were discovered in the Lienz area in the 1980-ies during regional W prospecting campaigns (e.g., Neinavaie & Ronge 1985) and are summarized as "Polymetallic skarn district Drauzug-Gurktal nappe system Lienz-Hochstein" in the IRIS data base. Low- to medium grade metamorphic Austroalpine units were intruded by a pluton west of Lienz in the Oligocene (Edenwald intrusion, ≈30 Ma). A km-sized contact metamorphic aureole with metapelitic hornfels developed around the composite intrusion especially at its western to southern contacts (Linner et al. 2013).

Three types of scheelite mineralization are distinguished in the region: (1) Strata-bound scheelite in low-grade metamorphic metabasites in the Early Palaeozoic Thurntal Quartzphyllite (disseminations, stringers, deformed quartz veinlets; e.g., Tafinalpe). The association of W-As (arsenopyrite) is specific for this type (Portugaller 2010); (2) Sulfide-scheelite skarn mineralization (disseminations, veins; e.g., Edenwald). Massive sulfides (pyrrhotite, chalcopyrite etc.) are associated with thin intercalations of marble and calc-silicate rocks (Ca amphiboles, calcian plagioclase, grossular, diopside-hedenbergite, vesuvianite, wollastonite) (Hutter 2022). This type is interpreted as a reduced magmatogenic skarn, a mineralization style very rare in the Eastern Alps. (3) Scheelite in quartz veins and clefts within the intrusive rocks. This pure scheelite mineralization is controlled by brittle division surfaces in the intrusive rocks.

The Oligocene plutonic rocks span a wide petrographic composition from metaluminous (gabbro)diorite, tonalite, to more evolved peraluminous granodiorite/granite. They are magnesian showing calc-alkaline magma characteristics. The high W bulk values (up to hundreds of ppm W) to are due to post-magmatic (type 3) hydrothermal processes.

LA-ICP-MS trace element analyses of scheelite allow to discriminate these different mineralization styles. We present combined micro-textural features (obtained from CL imaging) and trace element data of scheelite in their geological/petrographic context, we discuss the possible applications for exploration and propose that tungsten has undergone several stages of crustal recycling.

Hutter F (2022): Wolframvererzungen und Intrusionsgesteine am Lienzer Schlossberg, Osttirol. - Masterarbeit, Montanuniversität Leoben

Linner M, Reitner JM, Pavlik W (2013) Geologische Karte 179, Lienz 1:50.000.- Geologischen Bundesanstalt, Wien

Neinavaie MH, Ronge W (1985): Wolframprospektion 1984 in Teilen Osttirols, Kärntens, Niederösterreichs und der Steiermark sowie petrographische Untersuchungen an neu aufgefundenen Wolframvererzungen im Arbeitsgebiet. - Unveröffentlichter Ber VOEST-ALPINE, Eisenerz

Portugaller T (2010): Scheelitvererzungen im Thurntaler Quarzphyllitkomplex, Osttirol: Petrographische und chemische Untersuchungen an Nebengesteinen und Bachsedimenten. - Masterarbeit, Montanuniversität Leoben

Expanding the magmatic and metamorphic geochronological record of the Isua supracrustal belt

A. Ramírez-Salazar^{1,2}, D. Sorger³, T. Müller³, S. Piazzolo¹

¹ School of Earth and Environment, University of Leeds, Leeds

² Instituto de Geología, Universidad Nacional Autónoma de México, Ciudad Universitaria 04510, Mexico City, Mexico

³ Geoscience Centre, University of Göttingen, Goldschmidtstraße 1, Göttingen, Germany
e-mail: r.s.anthonyy@gmail.com

The emplacement history of the protoliths of the Isua supracrustal belt (ISB), southwestern Greenland, goes back to the Eoarchean and is often interpreted to preserve one of the oldest metamorphic records on Earth. Thus, in many studies the metamorphic characteristics of this belt are used to advance our understanding of Archean tectonics. However, the age of its main tectonometamorphic event(s) remains debated with main arguments derived from cross-cutting relationships while direct dating of metamorphic minerals is sparse. Recent microstructural and quantitative P-T analyses (Ramírez-Salazar et al., 2021; Zuo et al., 2021) showed that the ISB experienced a syn-tectonic amphibolite facies event at 550–600 °C and 0.5–0.7 GPa (M₁), followed by a relatively static (lower) amphibolite facies episode at <540 °C and <0.5 GPa (M₂), both later overprinted by greenschist facies fluid-related metamorphism (M₃). In order to constrain the timing of different tectonometamorphic, as well as magmatic, events of the ISB, we combine microstructural and P-T analyses with several geochronometers (Sm-Nd and Lu-Hf in garnet, and U-Pb in rutile and titanite). Our results expand the history of the ISB and reveal new events occurring in its associated rock formation.

Local metamorphism at 650–675 °C and 0.4–0.6 GPa associated with the emplacement of a tonalite-trondhjemite-granodiorite (TTG) body occurring at ≈3,660 Ma is recorded in hornblendite enclaves adjacent to the ISB. Additional information on the magmatic history is provided by an intrusive, garnet-bearing granitoid showing potentially igneous garnet crystallization at ≈3,550 Ma. Sm-Nd and Lu-Hf dates derived from metamorphic garnets within ISB supracrustal rocks show no evidence of a regional, major tectonometamorphic event (M₁) prior to ≈3,400 Ma. Instead, the analysis of syn-tectonic garnets suggests that M₁ most likely occurred at ≈2700 Ma. Moreover, new U-Pb data of post-tectonic titanite suggest that static post-tectonic metamorphism (M₂) occurred during the Neoproterozoic (≈2,700–2,600 Ma), whereas late retrogression event(s) are most likely Paleoproterozoic (<2,200 Ma) in age.

Our findings highlight that the observed main regional ISB metamorphism and concomitant deformation did not occur in the Eoarchean. While results of this study cannot fully discriminate between different geodynamic interpretations, our results suggest that the main tectonometamorphic event forming the current structures of the ISB are not related to pre 3,400 Ma Early Earth, but rather to late Archean geodynamics.

Ramírez-Salazar A, Müller T, Piazzolo S, Webb AAG, Hauzenberger C, Zuo J, Haproff P, Harvey J, Wong TK, Charlton C (2021): Tectonics of the Isua Supracrustal Belt 1: P-T-X-d constraints of a poly-metamorphic terrane. - *Tectonics* 40, doi:10.1029/2020TC006516

Zuo J, Webb AAG, Piazzolo S, Wang Q, Müller T, Ramírez-Salazar A, Haproff PJ (2021): Tectonics of the Isua Supracrustal Belt 2: Microstructures reveal distributed strain in the absence of major fault structures: *Tectonics* 40, doi:10.1029/2020TC006514

Pressure prediction in a poly-metamorphic terrain based on μ -EDXRF. An example from the Archean Vumba Schist Belt, Botswana

D. Rammlmair¹

¹Leibniz University Hannover, Germany
e-mail: d.rammlmair@mineralogie.uni-hannover.de

The Archean Vumba Schist Belt in the NE of Botswana comprises komatiitic successions, bimodal volcanics, sediments, Archean soils, banded iron formation, rodingites, and is intruded by several generations of granitoids, late pyroxenite and dolerite dykes. The belt experienced three metamorphic events, where due to strong uplift and tilting a shift of metamorphic centers from high grade in the NW to medium grade in the center and low grade in the SE can be observed. Shear zone and quartz vein hosted gold deposits are related to the late low grade metamorphic impact.

Several hundred rock slices were mapped by the μ EDXRF M4 Tornado, Bruker nano. The measurement was performed in 20 μ m steps, 2msec acquisition time using a Rh-tube at 50kV and 600 μ A, a poly-capillary beam guide, no filters, two silicon drift detectors arranged in 180°, 90° to the tube with 51° take off or incidence angle, respectively.

The mapping provided bulk area chemical information and phase distribution for the very same area. Phase distribution was obtained by supervised endmember-based classification using the spectral angle mapper (SAM) algorithm of the hyperspectral software ENVI for 165 spectral regions of interest. The minimum per channel per pixel was obtained for both detectors to widely omit diffraction signals of individual grains. Both, area chemistry and modality were used to select samples of similar chemistry along strike from NW to SE to compare the metamorphic impact. A series of mafic rocks was selected and investigated in detail putting focus on the amphibole chemistry by masking all other phases and applying a second SAM classification based on amphibole solid solution endmembers only. The amphibole endmembers were derived from EPMA analyses and amphibole classification by Li et al. (2022) following the classification scheme of Hawthorne et al. (2012). This second classification is the key to differentiate the impact of individual metamorphic events within individual mafic rock slices by visualizing amphiboles classified according to chemistry representative for different PT environments. The pressure estimation provided by Li et al. (2022), referring to the method of Hollister et al. (1987), was used for pressure prediction of amphiboles in individual samples across the belt. The dominant pressure is around 8.9 kb, but relics indicate values of >10 kb, and retrograde alteration shows values of > 4 kb.

Automated mineralogy applied to μ EDXRF, provided a detailed endmember data base exists, is a fast and easy to apply method, despite obscuring effects such as grain boundaries, grain size, shape as well as orientation-based diffraction. Information on rock and mineral chemistry, modality, and mineral sub-classes can be obtained for large sample numbers for preselection of most adequate samples for polished thin sections and EPMA investigations.

Li X, Zhang C, Behrens H, Holtz F (2020): Calculating amphibole formula from electron microprobe analysis data using a machine learning method based on principal components regression. - *Lithos* 362-363, 105469, 10.1016/j.lithos.2020.105469.

Hawthorne FC, Oberti R, Harlow GE, Maresch WV, Martin RF, Schumacher JC, Welch MD (2012): Nomenclature of the amphibole supergroup. - *Amer Mineral* 97, 2031–2048

Hollister LS, Grissom GC, Peters EK, Stowell HH, Sisson VB (1987): Confirmation of the empirical correlation of Al in hornblende with pressure of solidification of calc-alkaline plutons. - *Amer Mineral* 72, 231–239

Diabases are petrologists best friends: quantitative P - T constraints on the Eoalpine metamorphic gradient in the Ötztal Complex using diabase dikes

G. Raso¹, P. Tropper¹, D. Rammlmair²

¹University of Innsbruck, Institute of Mineralogy and Petrography, A-6020 Innsbruck, Austria

²Institute of Mineralogy, Leibniz University, Hannover, Germany

e-mail: peter.tropper@uibk.ac.at

The Ötztal Complex (ÖC) is a large crystalline complex in the western part of the Austroalpine units. The ÖC consists of quartzofelspathic and metapelitic metasediments with various intercalations of orthogneisses, amphibolites and rare metacarbonates. The oldest metamorphic event is Ordovician in age (460 – 490 Ma), leading to the formation of orthogneisses and scattered occurrences of migmatites. The Variscan metamorphic overprint ranges from 390 – 295 Ma and the first stage of the Variscan event was a high-pressure metamorphism around 373 – 359 Ma, leading to the formation of eclogites in the central part of the ÖC. The conditions of the eclogite-facies metamorphism were estimated to be 650 – 750 °C and 20 – 28 kbar. The dominant Variscan amphibolite-facies metamorphism occurred around 330 – 350 Ma with estimated P - T conditions of 570 – 640 °C and 5.8 – 7.5 kbar for the northwestern part of the ÖC. Subsequently after Variscan amphibolite-facies metamorphism diabase dikes intruded into the polymetamorphic basement. The youngest metamorphic event in this Austroalpine basement occurred during the Cretaceous Eo-Alpine orogeny (100 – 73 Ma). The intensity of the Eo-Alpine overprint varies within the ÖC and increases from NW (lower greenschist-facies) to SE (epidote-amphibolite facies) and reaches 550 - 600°C and ≥ 11 kbar in the Schneeberg Complex. Unfortunately, so far, no quantitative data concerning the P - T conditions of the Eoalpine metamorphic overprint in the NW of the ÖC exist. This is where the post-Variscan diabase dikes come in.

The importance of these diabase dikes lies in the fact that field- and textural investigations revealed a post-Variscan emplacement since these dikes only show Eoalpine metamorphism and deformation. The mineral assemblage of these dikes is amphibole + plagioclase + epidote + biotite + muscovite + titanite + quartz +/- garnet. Changes in plagioclase and amphibole chemistry are concordant with a prograde metamorphic evolution. Plagioclase changes from almost pure albite ($X_{An} < 0.1$) to intermediate plagioclase with $X_{An} = 0.3-0.4$. Amphiboles show a strong increase in Al^6 and Al^4 as well as Na^B and Na^A from NW to SE. This is qualitatively indicative of increasing P - T conditions. The P - T calculations were done using the programs Thermocalc v.3.21 and v.3.33 and mode-2 calculations (only using linearly independent reactions and statistical evaluation). The increase in T is from 400°C in the NW to almost 600 °C in the SE at the Timmelsjoch. Similarly P increases from 6-7 kbar in the NW to almost 12 kbar in the SE using Thermocalc v.3.33. Calculations using Thermocalc v.3.21 yielded slightly different P - T conditions from 300 °C and 3 kbar in the NW to 600 °C and 9 kbar in the SW. These differences are due to the use of different activity models for amphibole solid solutions, which has a profound impact on the calculations. Nonetheless these data represent the first quantitative P - T estimates for the Eoalpine metamorphic gradient north above the chloritoid isograd.

Recycling of Mineral Waste Materials by Geopolymerization – First Results

**B. Ratz¹, T. Sattler¹, F. Steindl², S. Raič², I. Zögl², S. Radinger², O. Rudić³,
F. Mittermayr³, C. Grengg²**

*¹Montanuniversitaet Leoben, Chair of Waste Processing Technology and Waste Management,
Franz-Josef-Straße 18, 8700 Leoben, Austria*

²Institute of Applied Geosciences, Graz University of Technology, Rechbauerstraße 12, 8010 Graz, Austria

*³Institute of Technology and Testing of Construction Materials, Graz University of Technology,
Inffeldgasse 24, 8010 Graz, Austria
e-mail: bettina.ratz@unileoben.ac.at*

The building and construction industry is responsible for 40 % of the anthropogenic CO₂ emissions and consumes enormous amounts of resources. In recent decades, there has been a significant increase in the production of waste, of which mineral waste is the largest stream in Austria, accounting for 76 % of the total waste. It is currently mostly disposed in landfills. To counteract the negative environmental impact of building and construction and to reduce the amount of landfilled waste, a Christian Doppler Laboratory for waste-based geopolymer construction materials in the CO₂-neutral circular economy (GECCO₂) was launched at Graz University of Technology. The goal is to produce environmentally friendly, highly resilient and Portland-cement-free geopolymer construction materials, also known as alkali-activated materials, from currently unexploited mineral waste materials. These geopolymers are then to be used in, for example, the environment of biochemically aggressive waste systems, such as sewer manholes, tanks and basins, or biowaste treatment facilities. Tasks of the Chair of Waste Processing Technology and Waste Management at the Montanuniversitaet Leoben, include the identification and selection of relevant mineral waste streams and the mineralogical, chemical and environmental characterization of selected waste materials, and elaboration of potential pretreatment strategies. With the obtained results, a material portfolio of suitable Austrian waste materials and industrial by-products will be created. First results will be presented regarding the mineralogical and chemical characterization of the selected waste materials.

Preliminary EBSD analysis and interpretation of Spinel-Olivine-Plagioclase pseudomorphs in skarnoid xenoliths from Southern Slovakia

L. Reato¹, M. Huraiová¹, T. Griffiths², G. Habler², R. Abart², V. Hurai³, P. Konečný⁴

¹Comenius University, Faculty of Natural Sciences, Department of Mineralogy, Petrology and Economic Geology, Ilkovičova 6, 842 15 Bratislava, Slovakia

²University of Vienna, Department of Lithospheric Research, Josef-Holaubek-Platz 2, 1090, Vienna

³Slovak Academy of Sciences, Institute of Earth Sciences, Dúbravská Cesta 9, 840 05 Bratislava, Slovakia

⁴State Geological Institute of Dionýz Štúr, Department of Special Laboratories, Mlynská Dolina 1, 817 04 Bratislava, Slovakia

e-mail: reato1@uniba.sk

Calc-silicate skarnoid xenoliths, with dimensions of up to 20 cm in diameter, were collected from Pleistocene alkali basalts of Southern Slovakia. Their general mineralogy and petrology have been described in Reato et al. (2022). They are composed of layers of relict augitic diopside, skeletal olivine and interstitial ternary feldspar (An₅₇₋₈₆), alternating with layers of anorthite (An₉₅₋₁₀₀) ± high Al, Fe³⁺ clinopyroxenes [Ca(Al,Fe³⁺)AlSiO₆] ± melilite inclusions. Such a mineral assemblage is indicative of thermal metamorphism in a high *f*O₂ environment and can be found in skarn or paralava (Foit et al. 1987; Pascal et al., 2005). Occasional pockets and veins of calcite ± aragonite can be present in both layers. Most of the xenoliths contain pseudomorphs comprising olivine (Ol), spinel (Spl), and ternary feldspar with an integrated average composition resembling tschermakitic amphibole. The pseudomorphs are characterised by very fine grained (1-100 μm²) skeletal to dendritic olivine and spinel, surrounded by interstitial ternary feldspar. The interstitial ternary feldspar within the pseudomorphs (An₅₃₋₉₆) has compositions similar to the one in the diopside + olivine layer (An₅₇₋₈₆). A sharp chemical boundary between the pseudomorphs and the anorthite layer is present. The olivine within the pseudomorphs is richer in Mg and has a more restricted composition (Fo₈₅₋₈₈) compared to olivine outside the pseudomorphs (Fo₆₆₋₈₈), which is characterised by much bigger (>100 μm) crystals, growing perpendicular to the elongation direction of the pseudomorphs.

The sample's lineation and foliation were determined by X-ray micro-computed tomography using an industrial v|tome|x L 240 tomograph from the Institute of Earth Sciences - SAS in Banská Bystrica, and thin sections were cut parallel to the lineation and perpendicular to the foliation. Locations with interesting micro-structural features were selected through transmitted light microscopy. The mineralogy of the selected areas was quantified through EMPA at the State Geological Survey of Slovakia in Bratislava, using a CAMECA SX-100 electron microprobe. EBSD analysis, together with EDS maps, were produced at the Laboratory for Field-Emission Scanning Electron Microscopy and Focused Ion Beam Applications at the University of Vienna, using the FEI Quanta™ 3D FEG instrument. After this, data were re-indexed and processed using EDAX OIM Analysis™ at the University of Vienna, and the Matlab™ toolbox MTEX (Bachmann et al. 2010).

A region containing a pseudomorph at the contact between the anorthite layer and the diopside + olivine layer was selected to determine the microstructural characteristics of the three different domains and their interactions. Both anorthite and ternary feldspar outside the pseudomorph keep the same crystal orientation inside the pseudomorph, despite their change in composition. The grain boundary misorientation angle distribution between olivine and spinel inside the pseudomorph shows a peak at 56°. When only the Spl-Ol boundary segments in the range 55°-57° misorientation angle are considered, a very strong misorientation axis

peak, suggestive of a near-specific crystallographic orientation relationship (COR), was observed. This was confirmed by plotting Spl directions with respect to Ol for the selected boundaries, revealing alignment of one of the $\{111\}$ Spl planes with the (100)Ol plane and one of the $\{110\}$ Spl planes with (001)Ol, with minor dispersion (generally $<5^\circ$) around the perfect relationship.

The observed COR between spinel and olivine implies an interaction between the two lattices, most likely during simultaneous growth. Similar plane relationships have been found in experimental petrology studies and were related to the exsolution of spinel from olivine occurring in the mantle transition zone (Hamaya & Akimoto 1982; Green, 1984). However, the xenoliths' protolith was formed and transformed within the crust (Reato et al. 2022), implying a different simultaneous growth process is responsible for the COR in this case. Concerning the behaviour of plagioclase within the pseudomorph, we can conclude that it has likely grown after olivine and spinel, using the plagioclase crystals from outside the pseudomorphs as a template for its growth within them, analogous to the formation of myrmekites (Phillips and Evans, 1980; Yuguchi & Nishiyama 2008). This feature is typical of rapid cooling systems, which is in accordance with the geological context and history of the xenoliths, which are thought to have undergone high-T thermal metamorphism before being collected by the host alkali basalt (Reato et al. 2022).

- Bachmann F, Hielscher R, Schaeben H (2010): Texture Analysis with MTEX – Free and Open-Source Software Toolbox. *Sol. St. Phen* 160, 63–68
- Foit FF, Hooper RL, Rosenberg PE (1987): An unusual pyroxene, melilite, and iron oxide mineral assemblage in a coal-fire buchite from Buffalo, Wyoming. - *Amer Mineral* 72, 137-147
- Hamaya N, Akimoto SI (1982): On the mechanism of the olivine-spinel phase transformation. - *Phys Earth Plan In* 29, 6-11
- Green HW (1984): How and why does olivine transform to spinel? - *Geophys Res Lett* 11, 817-820
- Phillips ER (1980): On polygenetic myrmekite. - *Geol Mag* 117, 29-36
- Pascal M, Katona I, Fonteilles M, Verkaeren J (2005): Relics of high-temperature clinopyroxene on the join Di–CaTs with up to 72 mol.% Ca(Al,Fe³⁺)AlSiO₆ in the skarns of Ciclova and Magureaua Vatei, Carpathians, Romania. - *Can Mineral* 43, 857–881
- Reato L, Huraiová M, Konečný P, Marko F, Hurai V (2022): Formation of esseneite and kushiroite in tschermakite-bearing calc-silicate xenoliths ejected in alkali basalt. - *Minerals* 12, 156
- Yuguchi T, Nishiyama T (2008): The mechanism of myrmekite formation deduced from steady-diffusion modeling based on petrography: Case study of the Okueyama granitic body, Kyushu, Japan. - *Lithos* 106, 237-260

Metamorphism induced strength inversion at high-pressure conditions

A. Rogowitz^{1,2}, S. Schorn¹, B. Huet³, L. Menegon⁴, B. Grasemann^{B.2}

¹*Institute of Earth Sciences, University of Graz, Austria*

²*Department of Geology, University of Vienna, Austria*

³*GeoSphere Austria, Vienna, Austria*

⁴*Njord Centre, University of Oslo, Norway*

e-mail: anna.rogowitz@uni-graz.at

We present structural, microstructural and petrographical data from an eclogite-facies shear zone of the Hohl locality (Koralpe, Eastern Alps, Austria). The shear zone spans over about 6 meter in thickness and shows a pronounced foliation (average: 047/63) characterized by alternating layers of proto- to ultramylonitic eclogite with different mineralogical content. Two stretching lineations have been identified: (1) a penetrative NW-SE striking mineral lineation (average: 122/27) defined by the shape and orientation of prismatic minerals and (2) a N-S striking stretching lineation (average: 354/20) which occurrence is limited to ultramylonitic layers. The latter appears to cross-cut the NW-SE striking lineation and is therefore considered as younger. The shear zone bears rocks with two distinct eclogite facies mineral assemblages of which one is dominated by clinozoisite, amphibole and garnet. This lithology occurs as foliated sigmoidal lenses hosted by typical eclogite containing omphacite, garnet, clinozoisite, amphibole, quartz, kyanite and rutile.

Both lithologies derived from NMORB gabbro which intruded during Permian rifting. Whole rock geochemical data shows that the lenses are enriched in Al and depleted in Mg and Fe when compared to the eclogite matrix. Protolith assemblage calculations suggest that lenses have originally been plagioclase-rich cumulates within a clinopyroxene-plagioclase gabbro matrix. Considering experimentally derived flow-laws on clinopyroxene-plagioclase aggregates (Dimanov & Dresen, 2005) indicates that lenses were less competent than the gabbro. However, the sigmoidal shape of lenses surrounded by ultramylonitic eclogite suggests that the lenses were stronger during shear zone development.

Microstructural investigations reveal an ultramylonitic fabric dominated by fine-grained (~50 µm) euhedral clinopyroxene within the host eclogite. Triple- and quadro-junctions, open grain boundaries and a lack of intracrystalline strain suggest that eclogite dominantly deformed by fluid supported grain boundary sliding. On the other hand, the microstructure of lenses is dominated by coarse-grained elongated clinozoisite (~300 µm) and amphibole aggregates (~2 mm). Amphibole aggregates are sigmoidal and characterized by a coarse-grained highly strained clast and strain free slightly elongated crystals in strain shadows. These observations indicate that lenses deformed by combined dislocation and dissolution-reprecipitation creep.

Our data shows how mineral replacement resulted in a strength inversion whereas the lenses, initially weaker than their host, are stronger than the surrounding eclogite after metamorphism at eclogite-facies conditions (720 ± 20 °C, 21 ± 3 kbar). The switch in strength caused stress concentration at the lithological contacts and subsequent strain localization in the weaker eclogitic mineral assemblage. Activation of fluid assisted grain boundary sliding in eclogite ultramylonites is assumed to have further weakened the eclogite, causing drastic strain partitioning. Later N-S-directed deformation subsequently solely localized within the weaker ultramylonitic eclogite.

Structural peculiarities in $(1-x)\text{Na}_{0.5}\text{Ba}_{0.5}\text{TiO}_3-x\text{BaTiO}_3$ at the morphotropic phase boundary studied by high-pressure XRD and Raman spectroscopy

C. Rösche¹, T. Boffa-Ballaran², T. Malcherek¹, C. Paulmann¹,
R. J. Angel³, B. Mihailova¹

¹FB Erdsystemwissenschaften, Universität Hamburg, Germany

²Bayerisches Geoinstitut, Universität Bayreuth, Germany

³Istituto di Geoscienze e Georisorse, CNR, Padova, Italy

e-mail: constanze.roesche@uni-hamburg.de

Perovskite-type (ABO_3) ferroelectric solid solutions are widely used functional materials, whose properties are utilized, for example, in sensors and actuators. The currently market-leading ferroelectric ceramics $\text{Pb}_{1-x}\text{Zr}_x\text{TiO}_3$ contain lead, which is undesirable from an environmental point of view. The solid solution $\text{Na}_{0.5}\text{Bi}_{0.5}\text{TiO}_3-x\text{BaTiO}_3$ (NBT- x BT) is one of the promising lead-free alternatives, however, its properties still need to be accurately constrained. Compositional variations may change the symmetry of the ferroelectric phase and shape the nanoscale structure, allowing to tune the properties by chemical substitutions. At the morphotropic phase boundary (MPB) with $x = 0.05 - 0.06$ for NBT- x BT the dielectric permittivity, piezoelectric coefficient, and electromechanical coupling factor are enhanced (Ge et al. 2011) due to an increased structural flexibility (de la Flor et al. 2019), making such compositions a good starting point for improvement by additional chemical doping. For an effective modification of the material, better understanding of the relation between the chemical composition and the nanoscale structural features in NBT- x BT is needed.

In this study, we have analyzed the response of the structure of NBT-0.048BT to external hydrostatic stress by performing high-pressure single-crystal X-ray diffraction (XRD) and Raman spectroscopic experiments up to 9 GPa, using the diamond-anvil-cell technique. It is known that in the case of Pb-based relaxor ferroelectrics pressure suppresses the polar order, while it enhances the antiferrodistortive order. Thus, the complementary high-pressure analyses of Bragg scattering, informative of long-range order, X-ray diffuse scattering (XDS), indicative of intermediate-range order and Raman scattering, sensitive to the intermediate-/short-range order can help to reveal subtle structural features, which are hard to detect at ambient pressure (Mihailova et al. 2011). The combination of different experimental methods allows us to obtain a comprehensive picture of the pressure-induced structural transformations ranging from the local to the long-range scale. At ambient and low pressure the deviations from the average pseudo-cubic perovskite structure produce strong diffuse scattering, which evolves into sharp Bragg peaks with increasing pressure [see Fig. 1 (a) and (c)]. The appearance of additional Bragg peaks indicates a phase transition between 4.4 and 5.5 GPa. The Raman data [Fig. 1 (b) and (d)] resolve the multistep local scale structural changes that lead to the change in symmetry. First a reduction of the Ba-induced local BO_6 anisotropy is taking place at 0.5 - 0.9 GPa, followed by decoupling of adjacent A- and B-site dipoles near 1.2 GPa. This allows for development of antipolar order of A-cation off-center displacements starting above 1.9 GPa, similar as it has been observed by Kreisel et al. (2003) in pure NBT at lower pressures. Furthermore, there is a strong amplification and increase in correlation length of octahedral tilts above 2.7 GPa and a change in the tilt pattern at 4 - 4.5 GPa.

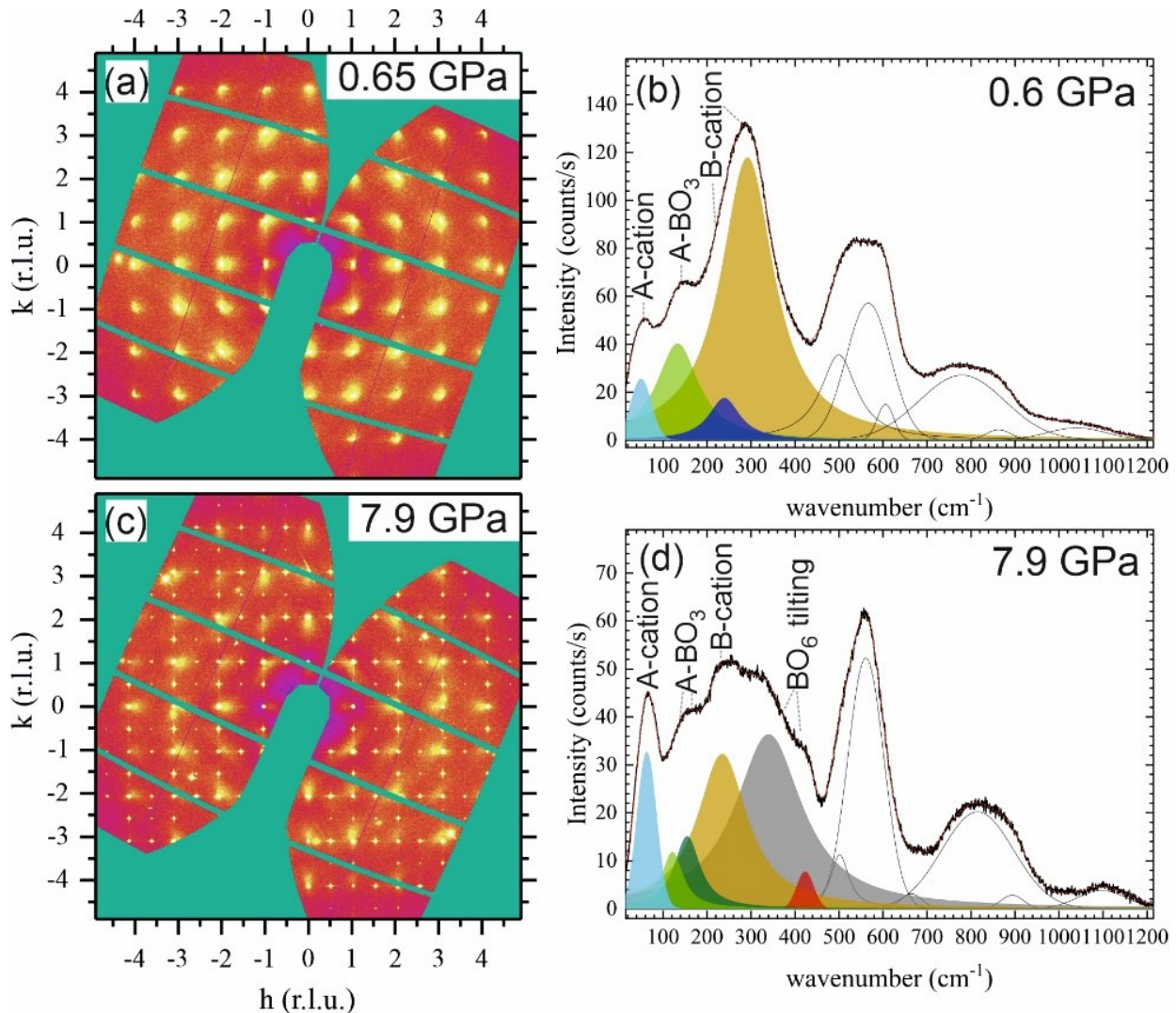


Figure 1. X-ray diffraction pattern in $hk0$ plane (a) and (c) and Raman scattering (b) and (d) of NBT-0.048BT at ~ 0.6 GPa and 7.9 GPa. The colored peaks in (b) and (d) are associated with A-cation off-centering vibrations (light blue), A- BO_3 translations (light and dark green), B-cation off centering vibrations (dark blue and orange) and BO_6 tilting vibrations (grey and red).

Ge W, Cao H, DeVreugd C, Li J, Viehland D, Zhang Q, Luo H (2011): Influence of BaTiO_3 content on the structure and properties of $\text{Na}_{0.5}\text{Bi}_{0.5}\text{TiO}_3$ crystals. - J Amer Ceram Soc 94, 3084-3087

De La Flor G, Gorfman S, Mihailova B (2019): Local-scale structural response of $(1-x)\text{Na}_{0.5}\text{Bi}_{0.5}\text{TiO}_3-x\text{BaTiO}_3$ to external electric fields. - Appl Phys Lett 114, 42901

Mihailova B, Angel RJ, Maier BJ, Welsch AM, Zhao J, Gospodinov M, Bismayer U (2011): The structural state of lead-based relaxor ferroelectrics under pressure. - IEEE Trans Ultrason Ferroelectr Freq Control 58, 1905-1913

Kreisel J, Bouvier P, Dkhil B, Thomas PA, Glazer AM, Welberry TR, Chaabane B, Mezouar M (2003): High-pressure x-ray scattering of oxides with a nanoscale local structure: Application to $\text{Na}_{1/2}\text{Bi}_{1/2}\text{TiO}_3$. - Phys Rev B68, 14113

**Turning toolboxes into an ecosystem:
How to make research software interoperable?
Moderator**

Thomas Rose^{1,2}

¹*Goethe-Universität Frankfurt, Institut für Geowissenschaften, Frankfurt, Germany*

²*Forschungsbereich Archäometallurgie, Leibniz-Forschungsmuseum für Georessourcen /
Deutsches Bergbau-Museum Bochum, Bochum, Germany
e-mail: thomas.rose@em.uni.frankfurt.de*

I am an archaeologist and geochemist by training, currently working in the German National Research Infrastructure consortium for the Earth System Sciences (*NFDI4Earth*). The aim of the consortium is to provide a central access point for all resources related to research data management and data science in the Earth System Sciences. In addition, I am a core team member of *GlobaLID*, the Global Lead Isotope Database. *GlobaLID* aims to become an infrastructure for the publication, curation and access of lead isotope data in archaeology. Moreover, *GlobaLID* further aims to bring the lead isotope community closer together, to create collaboration opportunities for researchers from less wealthy countries, and to provide training materials for the lead isotope method. In addition, I am author of the R package *ChronochRt*.

At the heart of all these endeavours lies my strong believe, that high-quality research can only be maintained in the future when its transparency is increased and hurdles (e.g. financial, infrastructural) are lowered. Besides making research data FAIR – findable, accessible, interoperable, reusable –, research software is a key component to turn this vision into reality. However, it won't be enough to have lots of tools at hand, as efficient and user friendly they may be. A crucial aspect is to design them, and the structure of the data processed by them, in a way that allows seamless passing of data between different software and, ideally, enable different software to directly communicate with each other. Consequently, not only the data but also the software must become interoperable.

Currently, there seems to be little coordination between the different groups working on research software in mineralogy, geochemistry, and neighbouring fields. However, aligning our efforts towards a common vision would be beneficial for all people involved in the development of such software and the community in general.

Hydrothermal pyritization of nano-magnetite and the record of biominerals in ancient sulfide systems

E.A. Runge^{1,2}, T.H. Chiu³, M. Mansor³, A. Kappler^{3,4}, J.-P. Duda^{1,2}

¹*Geobiology, Geoscience Center, University of Goettingen, Germany,*

²*Sedimentology & Organic Geochemistry, University of Tuebingen, Germany*

³*Geomicrobiology, University of Tuebingen, Germany*

⁴*Cluster of Excellence EXC 2124, Controlling Microbes to Fight Infection, University of Tuebingen, Germany*
e-mail: eric.runge@uni-tuebingen.de

The microbial formation of magnetite nanoparticles in hydrothermal environments can be driven by enzymatically controlled reactions or occur as a by-product of microbial Fe cycling. The resulting biogenic magnetite has characteristic traits that distinguish it from its abiotic counterpart, which makes it a potential biosignature. Furthermore, the precipitates may preserve chemical and isotopic information that provide valuable insights into conditions during their formation; hence, they might be used as environmental proxies. However, sulfidic diagenesis driven by hydrothermal fluids and microbial S cycling may cause the rapid transformation of microbial magnetite to Fe sulfide minerals, potentially altering or erasing biosignatures and proxies encoded in the primary precipitates. Thus, understanding the mechanisms, and characterizing the products of such sulfidation reactions is crucial for reading the record of biominerals in ancient hydrothermal sulfide deposits. Here, we present sulfidation experiments with synthetic and biogenic magnetite at physical and chemical conditions relevant to microbial niches in hydrothermal environments (<121 °C, excess S/Fe). By integrating multiple analytical techniques (e.g., scanning electron microscopy, sequential Fe extraction, Raman spectroscopy), we demonstrate a potential taphonomic bias against biogenic magnetite in hydrothermal environments and a strong influence of diagenetic fluid-mineral interactions on magnetite preservation. We further suggest that a portion of Fe sulfide minerals in hydrothermal deposits may be secondary products of magnetite sulfidation, highlighting the importance of understanding their diagenetic history for (bio)geochemical analyses. Our approach will aid the identification of biominerals and their transformation products in ancient rocks and pave the way for a more robust reconstruction of microbial evolution and environmental change through geological time.

Highly siderophile element and Re-Os isotope compositions of the 3.5 Ga Tomka Iron Formation, Daitari Greenstone Belt, India

A. Salzmann¹, T. Schulz¹, S. Viehmann², J. Jodder³, A. Hofmann⁴, C. Koeberl¹

¹*Department für Lithosphärenforschung, Universität Wien, Österreich*

²*Institut für Mineralogie, Leibniz Universität Hannover, Deutschland*

³*Evolutionary Studies Institute, University of the Witwatersrand, South Africa*

⁴*Department of Geology, University of Johannesburg, South Africa*

e-mail: a01610854@unet.univie.ac.at

Banded iron formations (BIFs) are Precambrian sedimentary rocks that are the product of chemical precipitation from seawater diagenetic, and metamorphic processes. Their abundance reach a maximum at around 2.4 Ga and appear to correlate with the Paleoproterozoic rise of atmospheric oxygen (Great Oxidation Event) with the subsequent change from anoxic to oxic conditions in the shallow parts of the ancient oceans. BIFs may thus represent robust archives, traced by rare earth elements and Yttrium (REY) and the Sm-Nd isotope system (Viehmann et al. 2015b) for the physico-chemical evolution of early Earth's atmosphere and oceans.

Following earlier studies that applied the redox-sensitive highly siderophile element (HSE) abundances and the Re-Os isotopes system to the Neoproterozoic Temagami BIF (Schulz et al. 2021) and the Neoproterozoic Urucum BIF (Prost 2023), we investigate the application of these geochemical tools to a BIF of the Paleoproterozoic Daitari Greenstone Belt, Singhbhum Craton, India. This multiproxy approach has the potential to record the influence of different source contributions to the BIF forming seawater column (i.e., continental vs. hydrothermal vs. possibly meteoritic). Analyses were conducted using the laboratory and thermal ionization mass spectrometry facilities at the GeoIsotope Core Facility of the Department of Lithospheric Research at the University of Vienna and (for isotope dilution concentration measurements of selected HSEs) in cooperation with the mass spectrometry facilities at the Freie Universität Berlin.

The Tomka, as well as any other, BIF can only serve as a geochemical seawater archive if devoid of detrital contamination and pristine (i.e., devoid of diagenetic, metamorphic, and hydrothermal overprints). The Tomka BIF is a promising candidate to preserve primary seawater signatures, because it was only subjected to greenschist-facies metamorphism, whereas other old iron formations (e.g., Isua BIF) almost exclusively underwent higher grade metamorphism (Nutman et al. 2017; Jodder et al. 2023).

A comparison between literature data for immobile elements such as Zr, and fluid mobile elements, such as Sr (Bau & Möller, 1993; Kamber et al. 2004; Viehmann et al. 2015a, 2016), in combination with the $^{187}\text{Os}/^{188}\text{Os}$ ratios reported in this study for the Daitari BIF layers (chert-, magnetite- and mineralogically mixed layers) might indicate only minor syn- and postdepositional disturbances. Accordingly, most of the analyzed samples have a weak linear correlation in the $^{187}\text{Os}/^{188}\text{Os}$ vs. $^{187}\text{Re}/^{188}\text{Os}$ diagram and scatter around a ~ 3.5 Ga reference isochron. The $^{187}\text{Os}/^{188}\text{Os}$ ratios range from mantle-like values of ~ 0.14 to more radiogenic values up to ~ 0.41 (which is still significantly less radiogenic than the present-day upper continental crust with a value of ~ 1.4 ; Peucker-Ehrenbrink & Jahn 2001). Iridium

contents of the analyzed samples are exclusively crust-like at ~0.03 ppb, thus excluding any extraterrestrial component, while Os concentrations (mostly ranging between 0.1 and 0.3 ppb) can be as high as 1 ppb. More data, including Pt, Ru and Pd concentrations, will be presented at the conference.

- Bau M, Möller P (1993): Rare earth element systematics of the chemically precipitated component in early precambrian iron formations and the evolution of the terrestrial atmosphere-hydrosphere-lithosphere system. - *Geochim Cosmochim Acta* 57, 2239–2249, doi:10.1016/0016-7037(93)90566-F
- Jodder J, Hofmann A, Xie H, Elburg MA, Wilson A (2023): Geochronology of the Daitari Greenstone Belt, Singhbhum Craton, India. - *Precamb Res* 388, 106997, doi:10.1016/j.precamres.2023.106997
- Kamber BS, Bolhar R, Webb GE (2004): Geochemistry of late Archaean stromatolites from Zimbabwe: evidence for microbial life in restricted epicontinental seas. - *Precamb Res* 132, 379–399, doi:10.1016/j.precamres.2004.03.006
- Nutman AP, Bennett VC, Friend CRL (2017): Seeing through the magnetite: Reassessing Eoarchean atmosphere composition from Isua (Greenland) ≥ 3.7 Ga banded iron formations. - *Geosci Front* 8, 1233–1240, doi:10.1016/j.gsf.2017.02.008
- Peucker-Ehrenbrink B, Jahn B (2001): Rhenium-osmium isotope systematics and platinum group element concentrations: Loess and the upper continental crust. - *Geochem Geophys, Geosystems* 2, paper no. 2001GC0001172, 22pp, doi:10.1029/2001GC000172
- Prost T (2023): Direct radiometric dating of a Neoproterozoic iron formation – Rhenium-Os and highly siderophile element systematics of the Urucum Iron Formation, Brazil. - Master's thesis, Univ Vienna, 113 pp
- Schulz T, Viehmann S, Hezel DC, Koeberl C, Bau M (2021): Highly siderophile elements and coupled Fe-Os isotope signatures in the Temagami Iron Formation, Canada: Possible signatures of Neoproterozoic seawater chemistry and Earth's oxygenation history. - *Astrobiology* 21, 924–939, doi:10.1089/ast.2020.2311
- Viehmann S, Bau M, Böhn B, Dantas EL, Andrade FRD, Walde DHG (2016): Geochemical characterisation of Neoproterozoic marine habitats: Evidence from trace elements and Nd isotopes in the Urucum iron and manganese formations, Brazil. - *Precamb Res* 282, 74–96, doi:10.1016/j.precamres.2016.07.006
- Viehmann S, Bau M, Hoffmann JE, Münker C (2015a): Geochemistry of the Krivoy Rog Banded Iron Formation, Ukraine, and the impact of peak episodes of increased global magmatic activity on the trace element composition of Precambrian seawater. - *Precamb Res* 270, 165–180, doi:10.1016/j.precamres.2015.09.015
- Viehmann S, Bau M, Smith AJB, Beukes NJ, Dantas EL, Böhn B (2015b): The reliability of ~2.9 Ga old Witwatersrand banded iron formations (South Africa) as archives for Mesoarchean seawater: Evidence from REE and Nd isotope systematics: *J African Earth Sci* 111, 322–334, doi:10.1016/j.jafrearsci.2015.08.013.

Hydrogen induced changes in the mineralogical phase composition of downhole cements: fundamentals research within the context of Underground Hydrogen Storage

T. Sammer¹, K. Ravi², J. G. Raith¹

¹Chair of Resource Mineralogy, Montanuniversität Leoben

²Chair of Drilling and Completion Engineering, Montanuniversität Leoben

e-mail: thomas.sammer@unileoben.ac.at

Hydrogen is nowadays commonly considered a promising way of storing energy from renewable energy sources, hence increasing the efficiency of renewable energy sources. However, to store large volumes of hydrogen on a seasonal (e.g., winter – summer) time scale fast storage volumes are needed (Reitenbach et. al. 2015). Underground hydrogen storage (UHS, e.g., the idea of using natural geological reservoirs like depleted gas fields) promises exactly that. To make UHS a feasible process, fundamentals research investigating not just the integrity of reservoir and cap rocks, but also the interaction of hydrogen with downhole materials (e.g., cement) used in boreholes is essential. Boreholes provide access to geological reservoirs but are also the bottleneck of any production or storage operation. In general, boreholes are lined with downhole materials, consisting of a steel casing surrounded by cement. The cement acts as a bonding between the steel casing and the wallrock, providing mechanical stability and tightness for the hole. However, the effect that hydrogen might have on the mineralogical phase composition and subsequently on physical and mechanical parameters of downhole cement is still very scarcely known (Reitenbach et. al. 2015). This project, which is part of a PhD programme on H₂ production and storage at Montanuniversität Leoben, Austria aims to contribute to a better understanding of this issue.

The mineralogical phase composition of a cement class G, a standard type portland cement used in the petroleum industry, before and after hydrogen treatment was investigated and the influence was evaluated that potential reactions might have on the physical and mechanical properties.

The mineralogical methods applied were: XRD, FE-SEM, EPMA. Physical parameters such as porosity, pore size distribution and permeability were measured using Hg-porosimetry, N₂ sorption and nitrogen permeation, respectively. The mechanical properties were characterized by determining compressive and tensile strength. Additionally Young's modulus was determined from the stress-strain curves obtained during compressive strength testing.

Additionally, thermodynamic modelling using Gibbs Energy Minimization Software (GEMS) was carried out. The modelling indicates that certain redox-sensitive phases within hardened cement pastes are susceptible to hydrogen alteration caused by the strong reducing character of hydrogen. Especially ferric iron and sulphate bearing phases like brownmillerite, monosulfoaluminate (AFm) and ettringite (AFt) are altered, resulting in the formation of native iron, magnetite, and iron sulphides.

Partial melting of hornblende–epidote eclogite at the pressure maximum (eclogite type-locality, Eastern Alps, Austria)

S. Schorn¹, A. Rogowitz^{1,2}, C. Hauzenberger¹

¹*Institute of Earth Sciences, NAWI Graz Geocenter, University of Graz, Universitätsplatz 2, 8010 Graz, Austria*

²*Department of Geology, University of Vienna, Josef Holaubek-Platz 2, 1090 Vienna, Austria*

e-mail: simon.schorn@uni-graz.at

Pristine hornblende–epidote eclogite from within the eclogite type-locality (Hohl, Koralpe) of the Eastern Alps in Austria preserves cm-thick, concordant leucocratic segregations of coarse-grained euhedral hornblende–epidote–quartz and fine-grained disseminated garnet–omphacite–rutile. Petrographic- and mineral chemical data and phase diagram modelling are interpreted in terms of limited melting at or close to the well-established pressure maximum (21 ± 3 kbar and 680–740 °C) followed by melt crystallization near these conditions. Plagioclase \pm amphibole/ clinopyroxene films formed at sub-eclogite facies conditions from final melt vestiges. Natural variability in rock composition and bulk oxidation state leads to variable mineral modes and calculated high-pressure solidus temperatures for compositional endmembers sampled at Hohl. Oxidized conditions ($X_{\text{Fe}^{3+}} \sim 0.5$) favour hydrous but refractory amphibole–epidote-rich assemblages with a fluid-present solidus temperature of ~ 740 °C at 20 kbar, whereas more reduced rocks ($X_{\text{Fe}^{3+}} \sim 0.2$) are fertile ‘true’ eclogites (>70 vol. % garnet + omphacite) that commence melting at ~ 720 °C. The interlayering of such eclogites constitutes a fluid source–sink couple at appropriate (pressure–)temperature conditions, favouring fluid transfer from neighbouring dehydrating layers to melt-bearing ones down gradients in chemical potential of H_2O ($\mu_{\text{H}_2\text{O}}$). Moderate degrees of fluid-fluxed melting (<10 %) would not alter the peak assemblage provided the resulting melts are removed from the source rock. We suggest that eclogites with a comparable composition and metamorphic history are however unlikely to produce voluminous melts, thus not significantly contributing to adakite magmatism and crustal differentiation in collisional settings.

Thermoelastic properties and phase transition of natural pollucite

J. Schreuer¹, M. Münchhalfen¹, E. Hartman¹

¹*Ruhr-Universität Bochum, Institut für Geologie, Mineralogie und Geophysik,
Universitätsstraße 150, Bochum, 44801, Germany
e-mail: schreuer@rub.de*

Pollucite $(\text{Cs,Na})\text{AlSi}_2\text{O}_6 \cdot y\text{H}_2\text{O}$, a cesium-bearing zeolite belonging to the analcim group characterized by ANA topology of its tetrahedral framework, has long been considered to be a suitable material for use in fixation and deposition of radioactive Cs isotopes in high-level nuclear waste. Particularly favorable properties are the stability and low thermal expansion at high temperatures, the capability to host large amounts of Cs, and the low leaching rate of Cs. However, below about 500 K, the three-dimensional framework gradually changes from an "expanded form" to a "collapsed form" which is accompanied by a significant shrinkage of the unit cell volume without a change of symmetry (e.g., Kobayashi et al. 1997). Phase transformations from the cubic phase to a low-temperature tetragonal phase are also known (e.g., Kobayashi et al. 2006). Both processes can negatively affect the mechanical integrity of pollucite crystals and ceramics. The aim of our work is, therefore, to investigate the thermoelastic behavior of pollucite between 100 K and 673 K using dilatometry and resonant ultrasound spectroscopy.

The elastic properties of our pollucite samples at room temperature are in reasonable agreement with values reported by Sanchez-Valle et al. (2010). The temperature coefficients of the three independent elastic stiffnesses are uncharacteristically positive for stable materials. In the course of the framework "collapse", the longitudinal stiffness c_{11} and the shear resistance c_{44} soften between 673 K and 133 K by nearly 50% and 35%, respectively. At the same time, the deviations from the Cauchy-relations take on negative values, indicating the increasing importance of directional interactions.

Sanchez-Valle C, Chio C-H, Gatta, GD (2010): Single-crystal elastic properties of $(\text{Cs,Na})\text{AlSi}_2\text{O}_6 \cdot \text{H}_2\text{O}$ pollucite: A zeolite with potential use for long-term storage of Cs radioisotopes. - J Appl Phys 108, 093509

Kobayashi H, Yanase I, Mitamura T (1997): A new model for the pollucite thermal expansion mechanism. - J Am Ceram Soc 80, 2161-2164

Kobayashi H, Sumino S, Tamai S, Yanase I (2006): Phase transition and lattice thermal expansion of Cs-deficient pollucite, $\text{Cs}_{1-x}\text{Al}_{1-x}\text{Si}_{2+x}\text{O}_6$ ($x \leq 0.25$). - J Am Ceram Soc 89, 3157-3161

Chemical composition and crystal structure of oxy-dravite from the Beluga occurrence, Nunavut Territory, Canada

L. Skřápková¹, J. Cempírek¹

¹*Departement of Geological Sciences, Faculty of Science, Masaryk University, Kotlářská 2, 602 00 Brno
e-mail: lenka.skrapkova@gmail.com*

A new occurrence of oxy-dravite was found in a composition near its ideal end-member at the Beluga occurrence, Nunavut territory, Canada. Oxy-dravite belongs to the sodic group of the tourmaline supergroup with dominant ^WO, and commonly forms a solid solution with foitite, schorl, and oxy-schorl. Since its original description (Bosi & Skogby 2013) from the quartz-muscovite schist from Osarara (Narok district, Kenya), the mineral has been found at several localities worldwide, typically in metamorphic environments, and typically in solid solution with other species (Čopjaková et al. 2012; Cempírek et al. 2013; Pieczka et al. 2018).

The contribution provides new information about the occurrence, chemical composition, physical and structural properties of the oxy-dravite with a near-endmember composition from the Beluga occurrence. These data improve characterization of physical properties of oxy-dravite, allow examination of oxy-dravite solid solutions with respect to other species, improve the interpretation of Al–Mg disorder among the Y- and Z-sites, and discuss its petrogenetic importance.

The Beluga property is located in the southern part of Baffin Island, Nunavut territory, Canada. The locality is known largely due to the occurrence of sapphire-bearing calc-silicate pods. These pods are hosted in a shelf sequence of clastic rocks and carbonates along with garnet-bearing metasediments of the Lake Harbour Group, Trans-Hudson orogeny (St-Onge et al. 2007).

The tourmaline sample has a relatively homogenous composition, with only minor change from the crystal core to its rims. The X-site is predominantly occupied by Na (up to 0.91 apfu), its Ca content is low (max. 0.12 apfu) and vacancies are minimal. The octahedral Y-site is dominated by Al and Mg (2.77–2.81 apfu), Fe content is low (max. 0.18 apfu); Li content measured using LA-ICP-MS is negligible. The octahedral Z-site is similarly to Y-site also occupied by Al with minor Mg. The T-site is dominated by Si (up to 5.95 apfu), substituted by inconsiderable amount of Al. The V- and W-sites are characterised by high OH (2.92–3.00 apfu) and O contents (0.80–0.95 apfu), with minor F (0.12–0.17 apfu) only.

The crystal structure of the oxy-dravite sample was refined from single-crystal X-ray diffraction data. The refinements were performed using the SHELXTL crystallographic software package (Sheldrick 2008, 2015) of Bruker AXS. Scattering factors for neutral atoms were employed for the cations and ionic factors for O²⁻ were used for oxygen (Hovestreydt 1983). The structure of dravite after Foit and Rosenberg (1979) was introduced as an initial model for refinement that was processed (by refining occupancy of Na at X-site, and Mg Fe vs. Al at the Y and Z sites) to a final R index of ~ 1.45 % for an anisotropic displacement model. The H3-atom site was located in residual electron density maps whereas the H1 site was impossible to locate. The H3-site isotropic displacement parameter was constrained to be equal to 1.2 times of that of the O3-site. The distance of the H3 from the donor oxygen atom was not constrained, and the structure refinement provided O3–H3 = 0.949 Å. The mean bond-lengths of the individual sites are: <X–O> ~ 2.673 Å, <Y–O> ~ 1.999 Å, <Z–O> ~ 1.928 Å, <T–O> ~ 1.621 Å, and <B–O> ~ 1.375 Å.

The Beluga oxy-dravite has trigonal symmetry, space group $R3m$ with $a = 15.9121(2)$ Å, $c = 7.1788(10)$ Å, $V = 1574.12(5)$ Å³ and $Z = 3$. The crystal structure was refined to $R1 = 1.45$ using 1613 unique reflections. The oxy-dravite is optically uniaxial negative, with $\omega = 1.6453(5)$ and $\varepsilon = 1.6074(18)$ and strongly pleochroic – light yellowish-brown colour in the omega direction and colourless in the epsilon direction; its calculated density is 3.069 g.cm⁻³ with a compatibility index 0.016 (superior category).

The Beluga oxy-dravite, ideally $\text{Na}(\text{Al}_2\text{Mg})(\text{Al}_5\text{Mg})(\text{Si}_6\text{O}_{18})(\text{BO}_3)_3(\text{OH})_3(\text{O})$, has similarly to the holotype (Bosi & Skogby 2013) disorder between Y- and Z-site. However, the final form of Mg-disorder between the octahedral sites heads towards $(\text{Mg}_2\text{Al})(\text{Al}_6)$ rather than $(\text{Al}_2\text{Mg})(\text{Al}_5\text{Mg})$. This is the evidence that the oxy-dravite structure has more stable configurations and it is not necessary to divide Mg in ratio of 1:1 between the octahedral sites.

In comparison with other Mg-dominant end-members (oxy-dravite, dravite, fluor-dravite, uvite a Mg-foitite a Mg-lucchesiite), the Beluga oxy-dravite has lower density and comparable to lower values of refractive indexes ω and ε . Similarly, the Beluga oxy-dravite has lower unit cell volume and calculated density, the only exception is magnesiofoitite with the lowest values.

The main petrogenetic environments of oxy-dravites are aluminous metapelites and metapsammities, low-Ca ultramafics and (Cr,V)-rich metasediments (Pieczka et al. 2018). The oxy-dravite holotype was described by Bosi & Skogby (2013) from a quartz-muscovite schist in the Osarara locality. Čopjaková et al. (2012) found oxy-dravite in tourmalinites associated with mica-schist of the Krkonoše-Jizera Crystalline Massif, whereas Pieczka et al. (2018) reported a further occurrence of oxy-dravite from a quartz vein cutting granitic gneisses of the Kowary Unit. Oxy-dravite was also described by Ertl et al. (2003) from a primitive pegmatite vein cutting a gneiss of the Gföhl Unit. Oxy-dravite was also formed in amphibolite (Şek et al. 2022) or in the metaevaporite layers within dolomitic marbles (Krmíček et al. 2021). The Beluga oxy-dravite occurs in calc-silicate pods in association with dolomitic marbles (Belley et al. 2017); the necessary conditions for its crystallization (besides high B₂O₃ content) are increased content of Al and Na, and low content of F in the Mg-rich system.

- Belley PM, Dzikowski TJ, Fagan A, Cempírek J, Groat LA, Mortensen JK, Fayek M, Giuliani G, Fallick AE, Gertzbein P (2017): Origin of scapolite-hosted sapphire (corundum) near Kimmirut, Baffin Island, Nunavut, Canada. - *Can Mineral* 55, 669
- Bosi F, Skogby H (2013): Oxy-dravite, $\text{Na}(\text{Al}_2\text{Mg})(\text{Al}_5\text{Mg})(\text{Si}_6\text{O}_{18})(\text{BO}_3)_3(\text{OH})_3\text{O}$, a new mineral species of the tourmaline supergroup. - *Am Min* 98, 1442-1448
- Cempírek J, Houzar S, Novák M, Groat LA, Selway JB, Šrein V (2013): Crystal structure and compositional evolution of vanadium-rich oxy dravite from graphite quartzite at Bitovánky, Czech Republic. - *J Geosci* 58, 149-162
- Čopjaková R, Škoda R, Vašinová-Galiová M (2012): „Oxy-dravit“ z turmalinitů krkonošsko-jizerského krystalinika. - *Bulletin Min-Pet Odd NM Praha* 20, 37
- Ertl A, Hughes JM, Brandstätter F, Dyar MD, Prasad PSR (2003): Disordered Mg-bearing olenite from a granitic pegmatite at Goslarn, Austria: A chemical, structural, and infrared spectroscopic study. - *Can Mineral* 41, 1363-1370
- Foit FF, Rosenberg PE (1979): The structure of vanadium-bearing tourmaline and its implications regarding tourmaline solid solutions. - *Am Min* 64, 788-798
- Hovestreydt E (1983). On the atomic scattering factor for O²⁻. - *Acta Crystallogr* A39, 268-269
- Krmíček L, Novák M, Trumbull RB, Cempírek J, Houzar S (2021): Boron isotopic variations in tourmaline from metacarbonates and associated calc-silicate rocks from the Bohemian Massif: Constraints on boron recycling in the Variscan orogen. - *Geosci Front* 12, 219-230
- Pieczka A, Ertl A, Sek MP, Twardak D, Zelek S, Szeleg E, Giester G (2018): Oxy-dravite from Wolowa Góra Mountain, Karkonosze massif, SW Poland: Crystallochemical and structural studies. - *Mineral Mag* 82, 913-928

- Sęk MP, Włodek A, Stachowitz M, Woźniak K, Pieczka A (2022): Magnesio-lucchesiite from the Kowary vicinity, Karkonosze Mountains, SW Poland: the third occurrence worldwide. - *Mineral Mag* 87, 60-68
- Sheldrick GM (2008): A short history of SHELX. - *Acta Crystallogr A* 64, 112-122
- Sheldrick GM (2015): Crystal structure refinement with SHELXL. - *Acta Crystallogr C* 71, 3-8
- St-Onge MR, Wodicka N, Ijewliw O (2007): Polymetamorphic evolution of the Trans-Hudson Orogen, Baffin Island, Canada: Integration of petrological, structural, and geochronological data. - *J Petrol* 48, 271-302

Monazite fission-track dating of a heavy mineral sand, NE Sri Lanka

E. Skrzypek¹, S. Jones², B. Kohn², L. Chung², A. Gleadow²

¹*Institute of Earth Sciences, University of Graz*

²*School of Geography, Earth and Atmospheric Sciences, The University of Melbourne
e-mail: etienne.skrzypek@uni-graz.at*

Monazite fission-track (MFT) analysis appears to have potential for ultra-low temperature thermochronology. Recent experiments suggest that the nominal MFT closure temperature is ~25-45 °C (Jones et al., 2021). However, monazite commonly shows a wide range of compositions, so that it is crucial to assess the influence of compositional variations on fission-track systematics. For that, a MFT study of monazite grains from a heavy mineral beach sand (Polmuddai, NE Sri Lanka) was undertaken.

Electron microprobe analyses of 84 grains show significant variations in SiO₂ (0.12 - 2.63 wt.%), CaO (0.13 - 2.03 wt.%), ThO₂ (1.30 - 13.38 wt.%), UO₂ (0.07 - 1.28 wt.%) or Ce₂O₃ (23.94 - 34.31.03 wt.%). The analyses show that actinides were incorporated in monazite through the cheralite and/or huttonite substitutions. Eighty grains statistically define a main age population with a weighted mean Th-U-total Pb age of 502 ± 5 Ma (MSWD=1.3), while four other grains show older dates (ca. 1600 - 1900 Ma).

Spontaneous fission tracks were revealed by etching polished monazite mounts in a H₂O:HCl (1:1 by volume) solution at 90 °C. Due to the variability of monazite compositions, step-etching at five-minute intervals was performed to avoid under-/over-etching and limit surface damage. The majority of grains were well-etched after 10 - 15 minutes, whereas a few required up to 60 minutes. Fission tracks were manually counted using both reflected- and transmitted-light images.

The different monazite grains or domains yield individual MFT dates ranging from 3.90 to 0.25 Ma. It is recommended to use electron microprobe analyses to approximate the density of monazite domains, as it can noticeably influence the MFT age calculation. Only Si appears to show a fair correlation with MFT date, suggesting that higher Si content (SiO₂ = 1.5-2.0 wt.%) slows down FT annealing. This finding is supported by a tendency for Si-richer monazite grains to show longer confined track lengths (> 9 µm) than Si-poor ones (< 9 µm). A remaining question for further investigation is whether FT formation and annealing could also have an impact on U-Th dating of monazite, especially on radiogenic Pb loss.

Jones S, Gleadow A, Kohn B (2021): Thermal annealing of implanted ²⁵²Cf fission tracks in monazite: Geochronology 3, 89–102

Formation of reaction textures in aluminous paragneisses during near-isothermal exhumation

D. Sorger^{1,2}, C.A. Hauzenberger², F. Finger³, M. Linner⁴, E. Skrzypek², S. Schorn²

¹*Geoscience Center, Georg-August-University Göttingen, Goldschmidtstraße 1, Göttingen 37077, Germany*

²*NAWI Graz Geocenter, University of Graz, Universitätsplatz 2, Graz 8010, Austria*

³*Department of Geography and Geology, University of Salzburg, Hellbrunnerstraße 34, Salzburg 5020, Austria*

⁴*Department of Hard Rock Geology, Geological Survey of Austria, Neulinggasse 38, Vienna, 1030, Austria*
e-mail: dominik.sorger@uni-goettingen.de

Two different types of aluminous paragneiss found in the Loosdorf complex in NE Austria, were studied to investigate the post-peak history of the Gföhl unit in the southern Bohemian Massif. Both paragneiss types contain coarse-grained granulite assemblages and retrograde reaction textures. The peak metamorphic conditions, estimated using phase equilibrium modelling, indicate that the Loosdorf complex experienced metamorphism at 0.9-1.1 GPa and 780-820°C. The dominant mineral assemblage during this peak metamorphism includes garnet-biotite-sillimanite-plagioclase-K-feldspar-quartz-granitic melt \pm kyanite \pm ilmenite \pm rutile.

The first type of paragneiss, called Ysper paragneiss, exhibits cordierite moats around garnet and cordierite-spinel or cordierite-quartz symplectites at former garnet-sillimanite interfaces. These textures suggest a post-peak near-isothermal decompression path reaching around 0.4 GPa. The second type, Pielach paragneiss, shows only intermittent cordierite coronae around garnet porphyroblasts and lacks symplectites. The presence of cordierite suggests near-isothermal decompression to 0.4-0.5 GPa and 750-800 °C. This relatively high-temperature decompression path is attributed to the simultaneous exhumation of a large high-pressure-ultrahigh-temperature (HP-UHT) granulite body.

The timing of regional metamorphism in the granulites and the southern Bohemian Massif is well constrained and peaked around 340 Ma. Monazite from the Loosdorf paragneiss samples yield a slightly younger age of approximately 335 Ma. Although these ages overlap within the error, they are interpreted as reflecting near-isothermal decompression and exhumation, which led to the formation of the observed reaction textures.

Tl-retention by jarosite-group minerals in technosoils from the central part of the Allchar deposit, North Macedonia

**F. Stadler¹, T. Đorđević^{2,1}, A. Vaněk³, M. Mihaljevič⁴, T. Serafimovski⁵, G. Tasev⁵,
I. Boev⁵, B. Boev⁵**

¹*Institut für Mineralogie und Kristallographie, Universität Wien, Josef-Holaubek-Platz 2, 1090 Wien, Austria*

²*University Service Centre for TEM, Technische Universität Wien,*

Wiedner Hauptstraße 8-10, 1040 Vienna, Austria

³*Department of Soil Science and Soil Protection, Faculty of Agrobiological Sciences, Czech University of Life Sciences Prague, Kamýcká 129, 165 00, Prague 6, Czech Republic*

⁴*Institute of Geochemistry, Mineralogy and Mineral Resources, Faculty of Science, Charles University, Albertov 6, 128 43, Prague 2, Czech Republic*

⁵*Faculty of Natural Sciences, University "Goce Delčev"-Štip, Goce Delčev 89, 2000 Štip, North Macedonia
e-mail: stadlerfiona63@gmail.com*

Areas naturally enriched in thallium (Tl) represent a severe threat to surrounding ecosystems as the bioavailability of this highly toxic heavy metal strongly depends on its retention by the weathering-induced formation of secondary Tl-minerals. Estimations on the remediation potential of such areas therefore require a detailed mineralogical characterization of included Tl-bearing secondary minerals. This study focusses on the Allchar Sb-As-Tl-Au deposit in the southern part of North Macedonia, as its mineralogical composition is a rarity in the world. It contains remarkable concentrations of Tl, estimated to be around 1,000 tons of metal. In this study, stockpile material from abandoned, surface-exposed mining wastes and surrounding soils of the Sb-rich central part of the Allchar deposit was examined for the presence of secondary Tl-minerals. A combination of optical microscopy, powder X-ray diffraction (PXRD) and scanning electron microscopy with energy dispersive spectroscopy (SEM-EDS) was performed to determine the speciation of Tl in heavily weathered technosoils. The chemical composition of the soils measured by inductively coupled plasma mass spectrometry (ICP-MS) showed Tl-concentrations in the range of 480 to 4600 ppm. The main constituents of the examined samples could be identified as quartz, gypsum, sheet silicates, iron oxides and iron oxyhydroxides, followed by the presence of heavily weathered pyrite, marcasite and realgar, as well as traces of arsenopyrite and stibnite. Further weathering products comprise arsenates such as scorodite, alumopharmacosiderite, arseniosiderite, Ca-antimonates of the roméite-group, tripuhyite and sulfates of the jarosite group. Minor contents of Ce-monazite, apatite, zirkon, rutile, baryte, sphalerite and native gold could also be encountered. This paragenesis is suggesting acidic weathering conditions with pH-values ranging from 2-3. During weathering, dissolved Tl was mainly incorporated in an incomplete solid-solution between jarosite and dorallcharite with Tl concentrations up to 2.2 at%, which consequently represent the main host minerals of Tl. However, Tl could also be encountered in iron oxyhydroxides (up to 0.5 at%) and sheet silicates (up to 0.2 at%). Based on our results, Tl-jarosites are important secondary host phases for Tl in the central part of Allchar. Yet, the instability of jarosite at near-neutral pH conditions also characterizes it as a possible source of soluble Tl. Consequently, it is essential to further examine the role of jarosite-group minerals in Tl-retention under various environmental conditions.

This work was supported by the Austrian Science Fund (FWF) [grant number P 36828-N to T. Đorđević].

The "Schaudepot" for minerals and rocks of the Krauhuletz-Gesellschaft in Eggenburg, Lower Austria

F. F. Steininger¹, A. Rauscher²

¹Neue Gasse 7, 3730 Eggenburg, Austria

²Hofwiesenstrasse 46, 3511 Furth-Aigen, Austria

e-mail: Fritz.Steininger@senckenberg.de

The Krauhuletz-Gesellschaft in Eggenburg, Lower Austria, operates a local but internationally much noticed museum. The three-story main building in the city centre hosts the permanent exhibition accompanied by special presentations mostly with a regional focus which change regularly. The entire area in the north-western part of Lower Austria is noticeable rich in prehistoric and early history besides folklore. But not only remains from the early settlers can be found here. The region belongs to the Bohemian Massif with its very complex geological setting. The exhibits in the museum belonging to Earth's history range from mineralogy to geology and palaeontology. The collection is that large and the number of display items is still growing. Hence two further buildings were provided by the city of Eggenburg. They serve as depots for the extensive scientific collections:

Depot 1 is a former cinema (named "Lichtspielhaus") hosting the extensive paleontological collections. They focus on the many regional geological units (e.g., from the Carboniferous of Zöbing and the Lower Miocene of Eggenburg). Also prehistoric and early historical objects that cannot be shown in the main building are stored here. Worthy to note is the large library compiling Earth science topics besides descriptions of the flora and fauna of the area. It hosts a large collection of offprints, scientific journals, and geological maps. This depot is named in honour of the long-serving governor of Lower Austria "Dr. Erwin Pröll Study Collection".

Depot 2 is a two-storey building used earlier as the production site by a furniture factory, it is known as the "MöFa". It is, besides other objects, dedicated to Geosciences. It combines an exhibition of minerals, rocks, and some fossils from the area in showcases besides the storage of samples for scientific investigations in the future. As the area is heavily forested, outcrops are short-lived. Minerals and rocks originating from sites that will not be accessible without great effort in future (e.g., road constructions, building pits, progress in quarry mining) are preserved. These samples are maintained in the depot's racks. From these two purposes result the name "Schaudepot" that means "look and store".

On the ground floor of the building there is the new two-track exhibition and storage area for minerals and rocks. It includes five rooms with a total area of 183 m². In the entire collection are only mineral specimens and rock samples from the Austrian part of the Bohemian Massif - Waldviertel, the Dunkelsteiner Wald (located south of the Danube between Melk and Krems), and the Mühlviertel (located to the west and belongs already to Upper Austria). The samples were donated by finds and private donations from collectors of this area. So far, there are in total about 7,700 mineral specimens and about 1,500 rock samples stored. The exhibition area comprise five rooms that are briefly characterized here.

Showroom 1 (23 m², 5 showcases) exhibits minerals and rock from some quarries: Among them is Amstall (about 20 km west of Krems), a graphit deposit well known for reddish corundum or xenotime. It is the type locality for Amstallite (a rare Ca-Al-silicate). The Eibenstein quarry (close to the border to the Slovakia) is located in the "Bunte Serie"

(metamorphic rocks including biotite- and hornblende gneisses, amphibolites, calcsilicate rocks, marbles) and exhibits rarely pegmatite veins. The Loya quarry (a few steps north from the Danube and close to Ybbs-Persenbeug) is well known for wollastonite and thulite (a pink variety of zoisite). Pegmatite veins are located in the entire Waldviertel including the Southern Dunkelsteiner Wald and in the Western Mühlviertel. Famous mineral samples found in these pegmatites are smoky quartz (var. morion from Brunn near Fratres), opal (from Waldkirchen), or quartz (cutted samples from Langau).

Also some fossils from the Eggenburg area (Loibersdorf, Eggenburgian, Lower Miocene) are shown here; remarkable is a giant “Herzmuschel“ (Larvicardium kübecki).

Showroom 2 (10 m²) is dedicated to the large variety of rocks occurring in the Waldviertel. The rocks are stored on shelves and might be touched. Slices of Chalcedony and Garnet Pyroxenites are illuminated from the reverse; also these samples are from the Waldviertel.

The **Collection & showroom 3** (Fig. 1) is the largest room and captures nearly half of the entire area (80 m², 16 cabinets). To enable an easy access, samples are stored according to location in an alphabetical order (from Aggsbach-village to Zissersdorf). In one cabinet samples from the southern Lower Austria and the Mühlviertel are stored. Others contain a systematic collection of silicates from the Waldviertel, private collections were handed over in a grateful manner. In some show cases minerals of the Waldviertel are arranged according to their tectonic units. Series of quartz crystals (from Äpfelgschwendt, Loiwein, and Felling), pegmatite minerals (from Wanzenau, Horn, and the Königsalm), opals (from Waldkirchen) are on display.

Despite the large exhibition area, also the window niches are used to store large samples and a hardness scale according to Mohs and Rosiwal. Also a rock cleft is rebuilt.



Fig. 1 View to the main storage (room 3).

The relatively small display **Showroom 4** (10 m²) is dedicated exclusively to the Amethysts from the Waldviertel. Most of them are from Maissau, a small village about 10 km south of Eggenburg. A long time ago farmers when tilling the fields and mineral collectors became aware of Amethyst specimens often with an astonishing bright violet colour and sometimes large in size. The outcrop was excavated by the Krahuletz-Society in 1986 and 1988. The amethyst bearing quartz vein was rich in wonderful samples up to a size of some 0.2 m. Crystals (partly multiple zoned and exhibiting distinct varieties) are shown besides cut slices and polished specimens. Furthermore, finds from other localities in the Waldviertel are on display, among them are samples from Eggenburg, Grafenberg, Maigen, or Kautzen. Spectacular are amethyst sections in transmitted light. Two tubular showcases exhibit polished amethysts from Maissau and Eggenburg, respectively.



Fig. 2: The storage of minerals and rocks (room 5)

The collection **showroom 5** (**Fig. 2**) (60 m²) hosts mineral and rock samples from the Waldviertel that came from former scientific investigations or result from new finds during constructions of roads or other buildings. They are exclusively reserved for scientific investigations in future. The samples stored here reflect the variety of minerals and rocks that can be found in the entire area. The rocksamples range from plutonites to sediments and metamorphites. Cuttings and mineral samples are stored in a systematic order in pull-out cabinets and drawer units. Furthermore, a working area for microscopic investigations, a stone cutting device and a storage of reference literature can be found here.

Opening hours: every 1st Saturday a month (10 am to 4 pm). Information: www.krahuletzmuseum.at. Contact: A. Rauscher (+43 66473571480). Steininger (Fritz.Steininger@senckenberg)

Rauscher A, Steininger F (2023): Kurzführer durch das Schaudapot für Mineralien und Gesteine der Krahuletz-Gesellschaft – 3730 Eggenburg, Museumsgasse 6. – Pub. Krahuletz-Ges. 2023/1: 29 S., 26 Abb., Raumplan, Verkehrsspinne.- Eggenburg (Krahuletz-Gesellschaft)

Inorganic crystal structure database

A. Steudel¹, S. Rühl¹, S. Rehme¹

¹FIZ Karlsruhe – Leibniz-Institute for Information Infrastructure,
Hermann-von-Helmholtz-Platz 1, 76344 Eggenstein-Leopoldshafen, Germany
e-mail: annett.steudel@fiz-karlsruhe.de

ICSD (Inorganic Crystal Structure Database) is the world's largest database for fully determined inorganic crystal structures. It is made available to the scientific community and industry by FIZ Karlsruhe. ICSD contains the crystallographic data of published crystalline inorganic structures, including atom coordinates, dating back to 1913. Organometallic and theoretical structures have been added within the past years. The ICSD data are of excellent quality. Only data that have passed thorough quality checks are included.

The ICSD database now contains more than 280,000 crystal structures. Around 12,000 new structures are added every year. Through our continuous quality assurance, existing content is modified, supplemented or duplicates removed. As a result, and by filling gaps from previous years, even the older content is not static.

Highlights of ICSD:

- All important crystal structure data are available, including unit cell, space group, complete atomic parameters, site occupation factors, Wyckoff sequence, molecular formula and weight, ANX formula, mineral group, etc.
- 80 % of the structures are allocated to about 10,000 structure types. This allows for searches for substance classes.
- Continuous selection and evaluation of theoretical structures. They can serve as a basis for developing new materials through data mining processes.
- Keywords to describe physical and chemical properties are provided.
- Abstracts for a quick grasp of the article content are available.
- Simulation of Powder Diffraction Data

Last year the revision of the mineral names took place, which included a standardization of the mineral names. The standardization of the mineral names was done following the International Mineralogical Association (IMA) and this enabled us to link mineral entries to the two mineral databases "webmineral.com" and "mindat.org", so that further information about the minerals can be retrieved.

For a large part of the minerals, we have also included the hierarchical classification. This makes it easier to find minerals in the same hierarchical level (or below) and thus can also be used in teaching for improved understanding.

Since the last update of ICSD, topological information is included in the database for about half of the inorganic structures in ICSD. As a first step, this information can be used to search for the coordination of a central atom. This coordination can then also be represented visually. The topological data provide much more information which will be made available in future updates.

Crystal chemistry and structural transformations in Fe²⁺-bearing talc studied by Raman spectroscopy

L. Stoeck¹, S. Aspiotis^{1,2}, B. Mihailova¹

¹Department of Earth Sciences, University of Hamburg, Grindelallee 48, Hamburg, 20146, Germany

²Centre for the Study of Manuscript Cultures (CSMC), Cluster of Excellence 'Understanding Written Artefacts', University of Hamburg, Warburgstrasse 28, Hamburg, 20354, Germany
e-mail: lennard.stoeck@studium.uni-hamburg.de

High temperature behaviour of Fe²⁺-bearing hydrous silicates have recently gained much attention, because they are important reservoirs of water and can contribute into volatile cycling as well as into redox processes in the vicinity of subduction zones (Spandler et al. 2007; Bernardini et al. 2023), especially after the discovery of thermally induced reversible Fe²⁺ ↔ Fe³⁺ oxidation in Fe²⁺-bearing double-chain silicates, resulting in the activation of delocalized e⁻ and H⁺ with anisotropic mobility (Mihailova et al. 2021; Rösche et al. 2022). Therefore, Fe-bearing hydrous silicates with a strong anisotropic structure, such as amphiboles, can be an important factor to explain the occurrence of anisotropic conductivity anomalies in the lithosphere.

Talc (Mg₃Si₄O₁₀(OH)₂) is another rock-forming mineral with a highly anisotropic structure and significant implications in several fields, including petrology, geophysics and environmental science (Spandler et al. 2007). Besides talc is among the most important industrial minerals, because of its properties, such as chemical inertness, affinity for organic chemicals and hydrophobicity. These characteristics allow its use in several applications including paper coating, paint, cosmetics and polymer industries, for which the knowledge of the stability field of talc is critical (Ulian et al. 2014). So far temperature-induced changes in the structure and properties of talc have mostly been analyzed via X-ray diffraction, Fourier-transform infrared spectroscopy and thermogravimetry-differential scanning calorimetry (Liu et al. 2014).

In this contribution, we present (i) a new approach to quantify minor amounts of elements such as Fe and Mn in the octahedral sheets of talc using Raman spectroscopy (ii) results analyzing the temperature-induced changes in talc to gain further insight into the oxidation processes at high temperatures and structural transformations on an atomic level scale.

We analyzed a Fe²⁺-bearing sample from Zillertal in Austria, whose exact chemical formula (Mg_{2.93}Fe²⁺_{0.08}Ni_{0.01}Si_{4.04}OH_{1.81}O_{0.19}) was determined by electron microprobe analysis (Aspiotis et al., 2023). Spectra have been collected in two different sample orientations within the temperature range 150K-1400K in ranges from 15-1215cm⁻¹ and 3370-3770cm⁻¹.

We show that the Mg²⁺ (and Fe²⁺+ Mn²⁺) contents can be quantified by fractional intensities of the OH-stretching peaks assigned to various *M1M2M2* local configurations as well as by the wavenumber of the MO₆-vibrational mode near 360 cm⁻¹ (Aspiotis et al., 2023). Heating/cooling experiments demonstrate that the Raman peak at 3660cm⁻¹ associated with the OH-Fe²⁺MgMg stretching mode vanishes at 1250K but recovers when cooling down to room temperature. This clearly indicates the occurrence of reversible oxidation mechanisms at least at 1250K, and the existence of delocalized charge carriers (e⁻ and H⁺). Upon further heating up to 1400K talc undergoes a structural breakdown, decomposing into clinoenstatite

(Wesołowski, 1984). Therefore, we prove the existence of the “oxo-state” for talc between 1250K and 1400K, where Fe^{2+} is oxidized into Fe^{3+} , without a structural breakdown.

The trends for Fe^{2+} -bearing talc will be compared to pure-Mg talc, which is currently being analyzed by in situ-temperature Raman spectroscopy.

Acknowledgements: The research for this study was funded by the Deutsche Forschungsgemeinschaft (DFG, German Research Foundation) under Germany’s Excellence Strategy – EXC 2176 ‘Understanding Written Artefacts: Material, Interaction and Transmission in Manuscript Cultures’, project no. 390893796. The research was conducted within the scope of the Centre for the Study of Manuscript Cultures (CSMC) at Universität Hamburg. We thank Stefanie Heidrich and Peter Stutz, Universität Hamburg, to help with WD-EMPA measurements and sample preparation. We are very grateful to the Mineralogical Museum, Hamburg for kindly providing the talc crystals.

- Aspiotis S et al. (2023) Raman spectroscopy for crystallochemical analysis of Mg-rich layered silicates: serpentine and talc. - to be submitted to J Raman Spectr
- Bernardini S, Della Ventura G, Schlüter J, Mihailova B (2023): Thermally-activated electron hopping in Fe-rich amphiboles: Implications for the high-conductivity anomalies in subduction zones. - *Geochem* 83, 125942
- Liu X, Liu X, Hu Y (2014): Investigation of the thermal decomposition of talc. - *Clays Clay Miner* 62, 137-144
- Mihailova B, Della Ventura G, Waesermann N, Xu W, Schlüter J, Galdenzi F, Marcelli A, Redhammer GJ, Boiocchi M, Oberti R (2021): Atomistic insight into lithospheric conductivity revealed by phonon–electron excitations in hydrous iron-bearing silicates. - *Commun Mater* 2, 57
- Rösche C, Waesermann N, Petrova M, Malcherek T, Schlüter J, Mihailov B (2022): Oxidation processes and thermal stability of actinolite. - *Phys Chem Miner* 49, 47.
- Spandler C, Hermann J, Faure K, Mavrogenes JA, Arculus RL (2008): The importance of talc and chlorite “hybrid” rocks for volatile recycling through subduction zones; evidence from the high-pressure subduction mélange of New Caledonia. - *Contr Mineral Petrol* 155, 181-198
- Ulian G, Tosoni S, Valdrè CG (2014): The compressional behaviour and the mechanical properties of talc $[\text{Mg}_3\text{Si}_4\text{O}_{10}(\text{OH})_2]$: a density functional theory investigation. - *Phys Chem Miner* 41, 639-650
- Wesołowski M (1984): Thermal decomposition of talc: a review. - *Thermochim Acta* 78, 395-421

**Micromorphology meets micro-XRF:
A case study from the Iron Age site of Haselbach (Lower Austria)**

F. Stuffer¹, S. Cereda², P. Tropper¹, P. Trebsche²

¹University of Innsbruck, Institute of Mineralogy and Petrography, 6020 Innsbruck, Austria

²University of Innsbruck, Institute of Archaeologies, 6020 Innsbruck, Austria

e-mail: peter.tropper@uibk.ac.at

In the context of this investigation a chemical characterization of archaeological sediments from Haselbach (Lower Austria) was carried out on six uncovered thin sections by means of micro-XRF analysis. The elemental mapping was carried out with a Bruker M4 Tornado. The analysed thin sections were collected at the boundary between the loess substrate and the fill (cultural layer) of different structures: five come from pit houses and one from a pit. Samples were first examined with a polarization microscope and, subsequently, “objects” of interest were selected to clarify their chemical composition.

The results of the micro-XRF analysis show the exact spatial distribution of the detected elements in thin section: aluminum (Al_2O_3), silicon (SiO_2), magnesium (MgO), calcium (CaO), iron (FeO), phosphorus (P_2O_5), potassium (K_2O), titanium (TiO_2), sulfur (SO_3), and manganese (MnO). False colour maps were also produced to enhance the relative concentration of the aforementioned elements. Furthermore, the objects found in the thin sections could be quickly identified, by combining their morphological characteristics with their elemental composition. They consist of: bone and pottery fragments, aggregates of trampled debris, charcoal, faecal remains, ashes and different types of pedofeatures.

Thanks to the elemental analysis it was also possible to determine that, in all six thin sections, the in-situ loess is mainly composed of the elements Al, Fe, K, Mn, Si, and Ti, while the fill deposits show increasing contents of the elements Ca, P and S. Both microscopic and chemical results show that organic matter occurs in the cultural layer, indicating the influence of humans and animals in the formation of these deposits. The loessy substrate, on the other hand, has remained largely untouched by human and animal activity. Specific archaeological questions, such as the actual use of the pit houses and the pit, could not be answered on the basis of these results alone. Further analyses (i.e., micromorphological and archaeological) are thus required for a comprehensive understanding of these built features.

In-situ $^{40}\text{Ar}/^{39}\text{Ar}$ dating of phenocrysts in the phonolite from Late Quaternary East Eifel Olbrück volcano

M. Sudo¹, U. Altenberger¹, C. Günter¹

¹University of Potsdam, Institute of Geosciences, Potsdam, Germany
e-mail: msudo@geo.uni-potsdam.de

Since 2002, University of Potsdam has started the $^{40}\text{Ar}/^{39}\text{Ar}$ dating laboratory with a CO_2 continuous laser and a pulsed Nd-YAG UV laser, then the in-situ $^{40}\text{Ar}/^{39}\text{Ar}$ dating has been applied to metamorphic rocks with 400-10 Ma ages. However, it was not well known to what extent in-situ $^{40}\text{Ar}/^{39}\text{Ar}$ dating was available to younger samples. In order to investigate the applicability of $^{40}\text{Ar}/^{39}\text{Ar}$ dating to very young samples, we used phonolite from Olbrück volcano, a late Quaternary monogenetic volcano group in the East Eifel, where Lippolt et al. (1990) had reported the presence of excess ^{40}Ar in nosean or hauyne in the phonolites. Sudo et al. (2014) reported for Ar isotopic ratio measurements on natural samples and also preliminary dating results of the first $^{40}\text{Ar}/^{39}\text{Ar}$ dating including assumptions, because the analyses were done more than one year after the neutron irradiation. Since then, three more neutron irradiations and $^{40}\text{Ar}/^{39}\text{Ar}$ dating have been done so far, then those results of the $^{40}\text{Ar}/^{39}\text{Ar}$ dating have been accumulated and are reported here.

For the samples for Ar isotope analyses, thick rock sections with a thickness of about 0.5 mm and a long diameter of up to 12 mm were prepared, then their surfaces were examined in detail by SEM-EDS. Then they are irradiated with fast neutrons for 4 h at the CLICIT facility of the OSTR nuclear reactor at the University of Oregon, USA. In-situ spot analysis of the sample surfaces was then carried out at the University of Potsdam using a UV pulse laser at a wavelength of 266 nm to determine the Ar isotope ratios. In most cases, one spot did not yield enough gas for targets of sanidine, leucite, nosean or groundmass parts, and in the case of nosean, up to 5-6 spots of 200 microns diameter laser irradiation was conducted for a single measurement.

The results of the dating by weighted averaged when they agree within error, as follows; sanidine: 0.42 ± 0.29 Ma (N = 3, error 1sigma), leucite: 0.08 ± 0.16 Ma (N = 3), groundmass 0.71 ± 0.17 Ma (N = 2). These ages agree with the Ar/Ar age of 0.41 ± 0.01 Ma by Lippolt within 2 sigma error from sanidine and leucite. In contrast, the nosean, in which the excess ^{40}Ar has been reported, yielded two results, done in two separate irradiations, as 3.14 ± 0.45 Ma (N = 8), 31.06 ± 4.1 Ma (N = 5) and one outlier 154.5 ± 11.2 Ma. The nosean ages by Lippolt et al. (1990) were 11.2-12.2 Ma, suggesting that the excess ^{40}Ar in nosean is heterogeneously distributed. Sudo et al. (2014) reported the existence of melt inclusions in the nosean and the concentration of Cl in them. This time the correlation was also observed between the excess ^{40}Ar and Cl-derived ^{38}Ar in nosean.

Lippolt HJ, Troesch M, Hess JC (1990): Excess argon and dating of Quaternary Eifel volcanism, IV. Common argon with high and lower-than atmospheric $^{40}\text{Ar}/^{36}\text{Ar}$ ratios in phonolitic rocks, East Eifel, F.R.G. - Earth Planet Sci Lett 101, 19-33

Sudo M, Altenberger U, Günter C (2014): In-situ Ar isotope, $^{40}\text{Ar}/^{39}\text{Ar}$ analysis and mineral chemistry of nosean in the phonolite from Olbrück volcano, East Eifel volcanic field, Germany: Implication for the source of excess ^{40}Ar . – Geophysical Research Abstracts, EGU General Assembly 2014

Digital Microscopy Solutions: Practical Analysis for different applications

A.R. Szalai¹

¹KEYENCE VHX 7000
e-mail: r.szalai@keyence.eu

Due to the high depth of field and depth composition, the system offers fully sharp images within seconds. With tilting and rotating stage, it is possible to inspect the crystals in all angles, giving the user an all-around view of the sample. The 4K resolution provides high quality for a detailed analysis. Keyence VHX lenses can be used with all lightning options such as brightfield, darkfield, transmitted light, diffuser, polarisation, DIC, mix light, and shadow effect mode for the surface analysis. Intuitive software design and a steering console secure comfortable usability for the operator, which makes an experience to microscope.

Next to 2D and 3D measurement, profile- and area measurement are available for perform analysis. Automatic report functions shorten the process of documentation.

Unravelling the true nature of Martian ‘lh’-kieserite

D. Talla¹, M. Wildner¹

¹*Institut für Mineralogie und Kristallographie, Josef-Holaubek-Platz 2, 1090 Wien, Österreich
e-mail: dominik.talla@univie.ac.at*

The confirmed presence of hydrous sulfates on celestial bodies in our solar system such as Mars or the icy moons of Jupiter and Saturn has been a hotly debated topic for several decades (recently e.g., Clark et al. 2005; Bishop et al. 2009; Noel et al. 2010). Especially Mg-sulfate hydrates, with the ability to change their hydration state based on local humidity and temperature, are regarded as one of the key components governing the water budget at equatorial latitudes on Mars (Milliken et al. 2007).

Furthermore, these and other sulfate compounds are supposed to play an important role on the icy moons of Jupiter and Saturn, where their presence, possibly along with pressure-induced structural changes (e.g., Meusburger et al. 2020), influences thermodynamic equilibria leading to the presence of subsurface oceans, potentially even supporting life (Solomonidou et al. 2009).

Especially kieserite, $\text{MgSO}_4 \cdot \text{H}_2\text{O}$, given its broad field of stability compared to the other hydrates, is also believed to form on the surface of the icy moons via decomposition of higher Mg-sulfate hydrates by cosmic rays and UV radiation, with the stability of the sulfate monohydrate strongly enhanced by the surrounding vacuum (Zolotov & Shock 2001).

A still unsolved enigma is the structural and spectroscopic character of the so-called ‘lh’-kieserite polytype (where ‘lh’ stands for ‘low-humidity’), which, according to dehydration experiments under simulated Martian conditions performed by Wang et al. (2009), is presumed to be the dominant variant of monoclinic kieserite on the surface of Mars. Until now, however, no thorough investigation of this new ‘polytype’ has been conducted.

Comparing the powder patterns of ‘lh’-kieserite as documented by Wang et al. (2009) to other sulfate species, we observed a striking resemblance between this enigmatic compound and the tetragonal Mg-hydroxide sulfate hydrate (‘MHSH’) mineral caminite. To date, the latter was found on Earth in an entirely different environment compared to that on the surface of Mars – namely in black smokers on oceanic rift zones, reflecting its experimentally confirmed reverse solubility (e.g., Hochella et al. 1983). An entire range of such MHSH compounds is anticipated, where the cell metrics are dictated by variable occupancy of the Mg and H sites.

Taking the reverse solubility of the MHSH mineral group into account, we designed a novel autoclave prototype, allowing venting of the aqueous solvent at maximum temperature, preventing re-dissolution of the high-temperature phase assemblage upon cooling. Indeed, we were already able to synthesize several representatives of the said tetragonal compounds as single crystals with the expected variability in the Mg- and H-site occupancy, proving the existence of an (at least partial) MHSH solid solution series, with tetragonal ‘MHS’ (Mg-hydroxide sulfate, $c = 12.885 \text{ \AA}$; Fleet & Knipe 1997) and monoclinic kieserite ($2d_{001} = 13.499 \text{ \AA}$; Bechtold & Wildner 2016) as theoretical endmembers. As the Mg-site occupancy decreases in favour of the H content, the tetragonal c -lattice parameter lengthens, conversely to the a axis.

The comparison of powder patterns of 'lh'-kieserite and MSHH shown in Fig. 1 (using CuK α radiation) is quite conclusive: the prominent reflection doublet at 26.5 and 28° 2 θ , along with the characteristic pair at ~55° 2 θ present in both phases, strongly indicates that both compounds are indeed one and the same substance.

This leaves the question as to why the MSHH group has not been previously considered as 'lh'-kieserite. Firstly, naturally occurring minerals belonging to this series are scarce, with only the aforementioned caminite found in nature to date. Secondly, both IR and Raman spectra of kieserite and MSHH bear striking resemblance (Fig. 2), making a spectroscopic discrimination rather ambiguous, more so taking into account the limited signal-to-noise ratio of remote measurements from orbiter instruments.

Our contribution aims to corroborate the existence and properties of the MSHH mineral group, which seems, in light of the newest findings, to represent an important constituent of sulfate assemblages present on celestial bodies in our solar system.

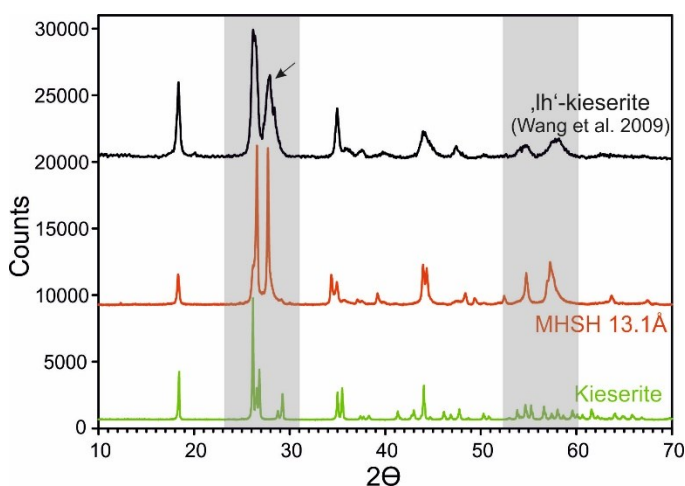


Figure 1. Comparison of the powder pattern of 'lh'-kieserite, MSHH and kieserite. Note the close match between Bragg reflections in 'lh'-kieserite and the MSHH variant with the *c*-cell parameter equal to 13.1 Å (highlighted in grey).

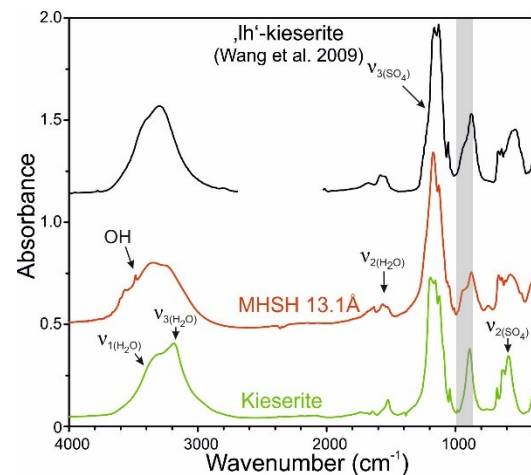


Figure 2. Close resemblance between IR spectra of 'lh'-kieserite, MSHH and kieserite. Apart from a shoulder at ~950 cm⁻¹, diagnostic for MSHH, the spectral envelopes are quite similar.

We gratefully acknowledge financial support of this work by the FWF grant-in-aid P34227-N.

Bechtold A, Wildner M (2016): Crystal chemistry of the kieserite–cobaltkieserite solid solution, Mg_{1-x}Co_x(SO₄)·H₂O: well behaved oddities. - Eur J Miner 28, 43-52

Bishop JL, Parente M, Weitz CM, Noe Dobrea EZ, Roach LH, Murchie LS, McGuire PC, McKeown NK, Rossi CM, Brown AJ, Calvin WM, Milliken R, Mustard JF(2009): Mineralogy of Juventae Chasma: Sulfates in the light-toned mounds, mafic minerals in the bedrock, and hydrated silica and hydroxylated ferric sulfate on the plateau. - J Geophys Res 114, E00D09

Clark BC, Morris RV, McLennan SM, Gellert R, Jolliff B, Knoll AH, Squyres SW, Lowenstein TK, Ming DW, Tosca NJ, Yen A, Christensen PR, Gorevan S, Brückner J, Calvin W, Dreibus G, Farrand W, Klingelhofer G, Waenke H, Zipfel J, Bell III JF, Grotzinger J, McSween, HY, Rieder R (2005): Chemistry and mineralogy of outcrops at Meridiani Planum. - Earth Planet Sci Lett 240, 73-94

Fleet ME, Knipe SW (1997): Structure of magnesium hydroxide sulfate, [2MgSO₄·Mg(OH)₂] and solid solution in magnesium hydroxide sulfate hydrate and caminite. - Acta Cryst B53, 358-363

- Hochella MF, Keefer KD, deJong BHWS (1983): The crystal chemistry of a naturally occurring magnesium hydroxide sulfate hydrate, a precipitate of heated seawater. - *Geochim Cosmochim Acta* 47, 2053-2058
- Meusburger JM, Ende M, Matzinger P, Talla D, Miletich R, Wildner M (2020): Polymorphism of monohydrate sulfate kieserite under pressure and its occurrence on giant icy Jovian satellites. - *Icarus* 336, 113459
- Milliken RE, Mustard JF, Poulet F, Jouglet D, Bibring J-P, Gondet B, Langevin Y (2007): Hydration state of the Martian surface as seen by Mars Express OMEGA: 2. H₂O content of the surface. - *J Geophys Res* 112, E08S07
- Noel A, Bishop JL, Al-Samir M, Gross C, Flahaut J, McGuire PC, Weitz CM, Seelos F, Murchie S (2015): Mineralogy, morphology and stratigraphy of the light-toned interior layered deposits at Juventae Chasma. - *Icarus* 251, 315-331
- Solomonidou A, Coustenis A, Bampasidis G, Kyriakopoulos K, Moussas X, Bratsolis E, Hirtzig M (2011): Water oceans of Europa and other moons: implications for life in other solar systems. - *J Cosmol* 13, 4191-4211
- Wang A, Freeman JJ, Jolliff BL (2009): Phase transition pathways of the hydrates of magnesium sulfate in the temperature range 50°C to 5°C: Implication for sulfates on Mars. - *J Geophys Res* 114, E04010
- Zolotov MY, Shock EL (2001): Composition and stability of salts on the surface of Europa and their oceanic origin. - *J Geophys Res* 106, 32815-32827

An extensible, open, and web-based research environment to understand geochemical data

T. Tamanna¹, D.C. Hezel¹

*Institute of Geosciences, Goethe University, Frankfurt, Altenhöferallee 1, 60438 Frankfurt am Main, Germany
e-mail: tamanna@uni-frankfurt.de*

Introduction: The application of Data Science in Geochemistry and Cosmochemistry is becoming increasingly important and relevant to handle and work with the exponentially growing number of geo- and cosmochemical data over the last few decades. Exploring large databases provides the opportunity to research huge datasets to better understand the Earth's dynamics (Jiao et al. 2018). In the last 20-30 years, geochemical data and standards have been collected in databases such as GeoROC, EarthChem, MetBase, or AusGeochem.

The objective of this project is to create methods to work with databases such as, organising and cleaning of data, visualising data on different kinds of plots, statistical analyses of the geochemical data, detection and checking the influence of outliers, integrate these with existing tools such as pyrolite, IsoplotR, GeoPyTool and implement these tools in a modular, open, and web-based research environment. The overall goal is to combine geochemical data and software, which will enable new routes of research and possibly a new area of original scientific discoveries (Ma 2023).

Methods: The web application was developed using python and deployed through streamlit. The python source codes are publicly available on GitHub.

Results and Discussion: We developed a web page with which geochemical database data can be visualized on a map or various types of plots such as scatter plots (bivariate plots), category plots which show the normalised concentrations with respect to e.g., chondrite, or primitive mantle versus a list of user-defined elements and ternary plots. For this we used GEOROC data as an example. The entire database was initially organized by choosing a subset of required elements needed to complete the various web application components. The nan values were replaced by 0 and the columns with no information were dropped. Boxplots were used to identify the outliers. Those outliers, which might be a result of typing errors, were dropped.

Jiao et al. (2018): Progress and challenges of big data research on petrology and geochemistry. - Solid Earth Sci 3, 105-114

Ma X (2023): Data science for geoscience: Recent progress and future trends from the perspective of a data life cycle. - Geol Soc Amer, Special Paper 558



You are cordially invited to attend

MinWien2023

17 to 21 September 2023

A joint meeting of the three Mineralogical Societies



Topics: Mineralogical, Petrological, Geochemical Sciences, deposits & related disciplines (basic, applied & industrial topics)

Programme

Sunday, 17 September 2023

Mineralogy for the public

Young Scientists meet each other

Opening Ceremony

After Party

Pre-conference

Male K...

16-17 S...

Guides: P. Bačík I. Bros...

Abstracts, A - G

Thursday,

September 2023

Scientific sessions

Poster presentations

Industrial exhibition

Conference dinner

Wednesday 20 September 2023

Festival Hall, Vienna's City Hall

Half-day tours

18-21 September, 2023

Poster Prizes for young scientists

DMG - General Assembly

Public lecture



Conference Site: Alma Mater Rudolphina - University of Vienna

Geozentrum - UZAI, Josef-Holaubek-Platz 2, 1090 Vienna

Organisation: Institut für Mineralogie und Kristallographie

Further information: <https://minwien2023.univie.ac.at>

e-mail: minwien2023.mineralogie@univie.ac.at



You are cordially invited to attend

MinWien2023

17 to 21 September 2023

A joint meeting of the three Mineralogical Societies



Topics: Mineralogical, Petrological, Geochemical Sciences, deposits & related disciplines (basic, applied & industrial topics)

Programme

Sunday, 17 September 2023

Mineralogy for the public

Young Scientists meet each other

Opening Ceremony

After Party

Pre-conference

Male K...

16-17 S...

Guides: P. Bačik I. Bros...

Abstracts, H - N

Thursday,

September 2023

Scientific sessions

Poster presentations

Industrial exhibition

Conference dinner

Wednesday 20 September 2023

Festival Hall, Vienna's City Hall

Half-day tours

18-21 September, 2023

Poster Prizes for young scientists

DMG - General Assembly

Public lecture



Conference Site: Alma Mater Rudolphina - University of Vienna

Geozentrum - UZAI, Josef-Holaubek-Platz 2, 1090 Vienna

Organisation: Institut für Mineralogie und Kristallographie

Further information: <https://minwien2023.univie.ac.at>

e-mail: minwien2023.mineralogie@univie.ac.at



You are cordially invited to attend

MinWien2023

17 to 21 September 2023

A joint meeting of the three Mineralogical Societies



Topics: Mineralogical, Petrological, Geochemical Sciences, deposits & related disciplines (basic, applied & industrial topics)

Programme

Sunday, 17 September 2023

Mineralogy for the public

Young Scientists meet each other

Opening Ceremony

After Party

Pre-conference

Male K...

16-17 S...

Guides: P. Bačík I. Bros...

Abstracts, O - Sch

Thursday,

September 2023

Scientific sessions

Poster presentations

Industrial exhibition

Conference dinner

Wednesday 20 September 2023

Festival Hall, Vienna's City Hall

Half-day tours

18-21 September, 2023

Poster Prizes for young scientists

DMG - General Assembly

Public lecture



Conference Site: Alma Mater Rudolphina - University of Vienna

Geozentrum - UZAI, Josef-Holaubek-Platz 2, 1090 Vienna

Organisation: Institut für Mineralogie und Kristallographie

Further information: <https://minwien2023.univie.ac.at>

e-mail: minwien2023.mineralogie@univie.ac.at



You are cordially invited to attend

MinWien2023

17 to 21 September 2023

A joint meeting of the three Mineralogical Societies



Topics: Mineralogical, Petrological, Geochemical Sciences, deposits & related disciplines (basic, applied & industrial topics)

Programme

Sunday, 17 September 2023

Mineralogy for the public

Young Scientists meet each other

Opening Ceremony

After Party

Pre-conference

Male K...

16-17 S...

Guides: P. Bačík I. Bros...

Abstracts, Sci - Z

Thursday,

September 2023

Scientific sessions

Poster presentations

Industrial exhibition

Conference dinner

Wednesday 20 September 2023

Festival Hall, Vienna's City Hall

Half-day tours

18-21 September, 2023

Poster Prizes for young scientists

DMG - General Assembly

Public lecture



Conference Site: Alma Mater Rudolphina - University of Vienna

Geozentrum - UZAI, Josef-Holaubek-Platz 2, 1090 Vienna

Organisation: Institut für Mineralogie und Kristallographie

Further information: <https://minwien2023.univie.ac.at>

e-mail: minwien2023.mineralogie@univie.ac.at

Defect adamantines: potential materials for photovoltaic applications

Y. Tomm¹, G. Gurieva¹, D. M. Többens¹, S. Schorr^{1,2}

¹Helmholtz-Zentrum Berlin für Materialien und Energie

²Institute of Geological Sciences, Freie Universität Berlin

e-mail: susan.schorr@helmholtz-berlin.de

Compounds of the Adamantine family includes kesterite ($\text{Cu}_2\text{ZnSnS}_4$), currently the most promising material for fully inorganic thin film photovoltaic technology that is free of critical raw-materials and thus provides sustainable solutions.

Ternary adamantines like the chalcopyrites can be transferred by chemical substitution to a quaternary adamantine such as $\text{A}^{\text{I}}_2\text{B}^{\text{II}}\text{C}^{\text{IV}}\text{X}^{\text{VI}}_4$ (e.g., $\text{Cu}_2\text{ZnSnS}_4$) and $\text{A}^{\text{I}}\text{B}^{\text{III}}\text{C}^{\text{IV}}\text{X}^{\text{VI}}_4$ compounds, the latter are called defect adamantines (Pamplin 1981).

Defect adamantines like $\text{Cu}\square\text{GaGeS}_4$ and $\text{Cu}\square\text{GaSnS}_4$ can be seen as a compound within the solid solution between gallite – radvaniceite (Sejkora et al. 2022), $(\text{CuGaS}_2)_{1-x}(\text{GeS}_2)_x$ and gallite – berndtite $(\text{CuGaS}_2)_{1-x}(\text{SnS}_2)_x$, at $x = 0.5$, respectively.

Single crystals of these defect adamantines were grown by chemical vapor transport using iodine as transport agent. Aiming for chemical compositions according to the defect adamantine, chemical analysis of the grown crystals by X-ray fluorescence (XRF) has shown, that crystals in the system $(\text{CuGaS}_2)_{1-x}(\text{GeS}_2)_x$ show $\text{Cu}/(\text{Ga}+\text{Ge})$ ratios between 0.45 and 0.9 as well as $\text{Ge}/(\text{Ga}+\text{Ge})$ ratios between 0.15 and 0.6. Thus the single crystals show a quite strong deviation from the stoichiometric composition ($\text{Cu}/(\text{Ga}+\text{Ge}) = \text{Ge}/(\text{Ga}+\text{Ge}) = 0.5$). We explain this behavior by the flexibility of the crystal structure of the end members and the defect adamantine. Their crystal structures are based on a corner-sharing network of tetrahedra (CuS_4 , GaS_4 , GeS_4 or $\square\text{S}_4$). By multiple energy anomalous synchrotron X-ray diffraction (MEAD) it was shown, that $\text{Cu}\square\text{GaGeS}_4$ crystallizes in the tetragonal chalcopyrite-type structure. It compares to the crystal structure of gallite, but with a higher fraction of vacancies.

The single crystals grown aiming for $\text{Cu}\square\text{GaSnS}_4$ adopt the chalcopyrite-type structure and the $\text{Cu}/(\text{Ga}+\text{Sn})$ values are close to 1. Thus there is only a very limited solubility in the $(\text{CuGaS}_2)_{1-x}(\text{SnS}_2)_x$ system. Berndtite (SnS_2) crystallizes in a trigonal structure type where the Sn^{4+} cations are coordinated by 8 sulfur anions. The very limited solubility between Gallite and Berndtite may be explained by the different coordination of the four-valent cation.

The band gap energy (determined by UV-Vis spectroscopy) of the mixed crystals in the $(\text{CuGaS}_2)_{1-x}(\text{GeS}_2)_x$ system cover a range of 2.1 to 2.4 eV, showing a strong bowing behavior in the dependency on the chemical composition parameter x . The crystals obtained in the system $(\text{CuGaS}_2)_{1-x}(\text{SnS}_2)_x$ have band gap energies within 1.7 and 2.0 eV. Thus, such defect adamantines are interesting materials for photovoltaic applications.

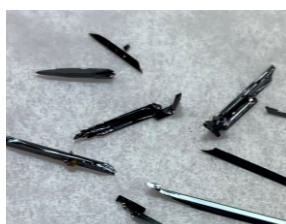


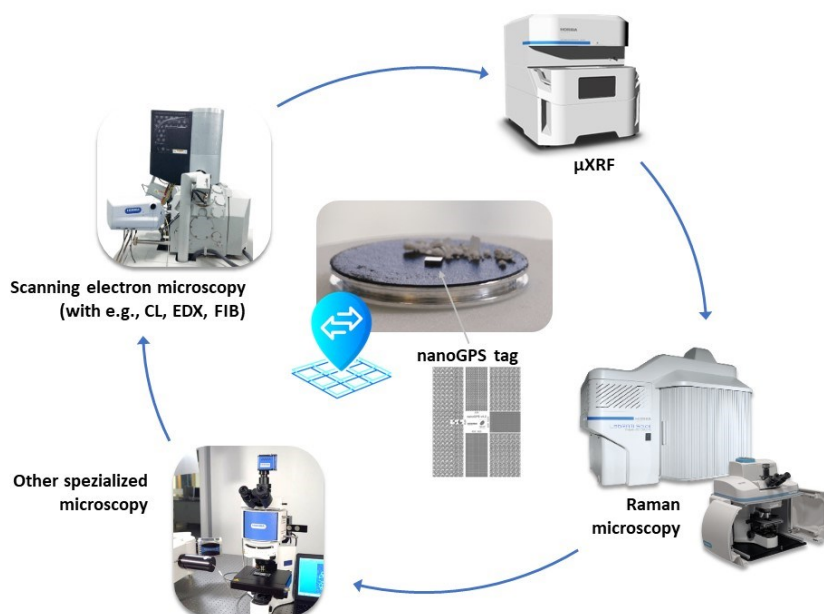
Figure 1. Single crystals of off-stoichiometric $\text{Cu}\square\text{GaGeS}_4$ (left) and $\text{Cu}\square\text{GaSnS}_4$ (right).

nanoGPS navYX™ – HORIBAs collaborative and inter-instrumental solution for correlative microscopy

M. Trapp¹, C. Lenz¹

¹HORIBA Jobin Yvon GmbH, Oberursel, Germany
e-mail: christoph.lenz@horiba.com

A comprehensive characterization of geological or mineralogical samples requires the application of more than one method to combine their complementary strengths. For example, the synergetic combination of μ -XRF (or SEM-EDX) with Raman microscopy provides information on both, the element composition as well as phase and structural properties of a specimen. However, relocation of points of interest (POI) on a μ m-scale is one of the most tedious and time-consuming issue if the specimen is transferred between various instruments, especially if the imaging technique strongly differs (e.g., SEM vs. light microscopic image). Here, we present HORIBAs nanoGPS navYX™ technology that provides a unique solution to this problem and is independent from the respective instrument or manufacturer (Acher et al. 2021). Typical requirements to successfully apply this technique include the option for microscopic sample imaging or visualization (min. 2x to 5x magnification) and software-controlled, motorized sample stage positioning. Nearly all types of microscopy techniques, such as SEM, μ -XRF, AFM, Raman or light microscopy, hence, may be correlated using nanoGPS navYX™. To do so, a small relocation tag with a patented reading pattern is attached to the sample. This tag defines a virtual coordination system that is read by the dedicated navYX™ software and saves all points and measurement sites of interest. On every calibrated instrument, the saved POIs may be easily relocated independently of sample positioning or rotation via direct conversion of the virtual nanoGPS coordinates into the instrument's stage coordinates.



Acher O, Nguyễn T L, Podzorov A, Leroy M., Carles P A, Legendre S (2021): An efficient solution for correlative microscopy and co-localized observations based on multiscale multimodal machine-readable nanoGPS tags. - Meas Sci Technol 32(4) 045402

Visible and invisible complexities in rocks: mineralogical and petrological constraints on the Variscan metamorphic gradient in the Southalpine metamorphic basement (Brixen quartzphyllites)

P. Tropper¹, T. Klotz², A. Wzietek¹, H. Pomella²

¹University of Innsbruck, Institute of Mineralogy and Petrography, 6020 Innsbruck, Austria

²University of Innsbruck, Institute of Geology, 6020 Innsbruck, Austria

e-mail: peter.tropper@uibk.ac.at

The basement of the Southern Alps is represented by the Brixner Quartzphyllite whose Variscan *P-T* conditions correspond to a greenschist-facies metamorphic overprint. This metamorphic basement shows a metamorphic gradient ranging from the lower greenschist-facies in the S to the amphibolite-facies in the N. This metamorphic gradient reached peak metamorphic conditions in the Brixen area and decreases in a southern direction. Due to the emplacement of Permian intrusions into this basement, locally a Permian contact metamorphic overprint can be observed. The aim of this study was to provide mineralogical and mineral-chemical constraints of major mineral phases as well as accessories such as apatite on this gradient and if possible obtain *P-T* conditions along a profile from north to south.

The quartzphyllite samples were collected along a traverse from Reccoaro (TKP054) in the S to Brixen (TKP022) in the N. Petrographic investigations revealed that the metapelites contain quite a complex polyphase mineral assemblage. The mineral assemblage in the S is represented by chlorite + muscovite + albite + quartz. Towards the center of the traverse, biotite occurs in the mineral assemblage, which has subsequently been replaced by chlorite. Samples in the vicinity of the Permian Cima d'Asta intrusion show petrographic evidence for contact metamorphism since K-feldspar, chloritoid and andalusite occur. In the N the mineral assemblage is chlorite + muscovite + plagioclase + quartz + garnet. Therefore, the metapelitic zones of chlorite, biotite and garnet could be observed along the traverse.

Mineral chemical investigations revealed further complexities. The chemical compositions of muscovite, chlorite and plagioclase vary continuously with increasing *P-T* conditions from S to N. Si in muscovite decreases (from 3.3 to 3.1 apfu) with increasing Al⁶ (from 2.4 to 2.7 apfu). Muscovite also shows an increase in the paragonite component from 4% to 13%. Similarly chlorite changes its composition also showing a decrease in Si and an increase in Al⁶. Plagioclase changes from pure albite to anorthite contents of 30%. The data also revealed that the southernmost sample (TKP054) shows evidence for a later *T*-accentuated overprint (Permian?) texturally not visible. Also, the second southern sample (TKP056) from the traverse shows two plagioclase generations, which are also likely due to a later overprint.

The chemical composition of apatite also changes continuously from S to N with slightly increasing F contents. F increases from 3.6 wt.% in the S to 3.8 wt.% in the N. A contemporaneous increase in FeO, Y₂O₃, and Cl has also been observed. Geothermobarometry yielded so far *P-T* conditions of 554 ± 11 °C and 6.49 ± 1.3 kbar in the northernmost sample TKP022. Currently it is planned to apply muscovite-chlorite-quartz geothermobarometry to the rest of the samples of the traverse to obtain more quantitative data on the *P-T* gradient from the southern samples. This study clearly shows that quartzphyllites indeed are able to record complex metamorphic histories hidden in petrographic and mineral chemical data.

Don't drink that stuff: mineralogical constraints on the Ni-anomaly in waters from rock glaciers in the Ötztal Complex

P. Tropper¹, K. Krainer², G. Winkler³, G. Bertolotti², V. Schmit²

¹*University of Innsbruck, Institute of Mineralogy and Petrography, 6020 Innsbruck, Austria*

²*University of Innsbruck, Institute of Geology, 6020 Innsbruck, Austria*

³*University of Graz, Institute of Earth Sciences, 8010 Graz, Austria*

e-mail: peter.tropper@uibk.ac.at

The hydrology of intact rock glaciers is complex and mainly controlled by climatic factors (weather), bedrock composition, size, composition and internal structure. Rock glaciers may serve as aquifers, storing and releasing water over different timescales and thus are of increasing interest as reservoirs for drinking water supply. However, still little is known on the quality (chemistry) of water released from permafrost springs.

Increasing concentrations of ions and heavy metals were detected in two high Alpine lakes, which are impacted by meltwater from rock glaciers. During the last years, abnormally high Ni concentrations (and high concentrations of other elements such as Cu, Co Zn) high above the upper limit for drinking water were recorded from a number of springs released from intact rock glaciers and permafrost-related springs in the Ötztal Alps. High concentrations of Ni, Co, Zn, Mn, Fe and Al were recently recorded from permafrost ice of a core drilled on rock glacier Lazaun. It has previously been shown that creeks and high alpine lakes derived from intact rock glaciers and characterized by low water temperatures, high EC, high sulfate, Mg and Ca, and partly high metal concentrations display a significantly lower biodiversity compared to high alpine creeks and lakes that are not influenced by water derived from permafrost.

In this contribution, we concentrate on nickel because: (1) Ni in drinking water is a toxic heavy metal; (2) Ni occurs in concentrations high above the upper limit for drinking water that is at 0.02 mg/L according to the Drinking Water Regulation (Trinkwasserverordnung – TWV 2023) of the Austrian Government; and (3) Ni-minerals are so far unknown from the rocks of the Ötztal Complex.

In the course of this study, thin sections of paragneiss and amphibolite rock samples from the rock glaciers Krummgampen, Wannekar and Lazaun were prepared and the minerals were analyzed using the electron probe microanalysis, with respect to their Ni contents. Petrographic investigations show that the mineral assemblage (silicates and sulfides) is heavily altered. Sulfides for instance are almost completely replaced by goethite and silicates such as garnet, biotite and staurolite show replacement by chlorite. The results show that the sulfides, namely pyrrhotite contain Ni contents of up to 1.2 wt.% NiO, chalcopyrite on the other hand contains much lower Ni contents of up to 0.2 wt.% NiO. Silicate minerals contain Ni concentrations below 0.1 wt.% NiO. With respect to additional heavy elements (Mn, Zn) present in the waters, garnet contains up to 10 wt.% MnO and staurolite contains up to 1.7 wt.% ZnO. These data show that in the absence of evidence for other heavy element sources, the altered mineral assemblage in the rocks from the rock glaciers are the most obvious source of these elements.

Non-ideal, but how non-ideal? Low-temperature calorimetry of the Al-F-titanite – titanite solid solution

P. Tropper¹, E. Dachs², U. Troitzsch³

¹University of Innsbruck, Institute of Mineralogy and Petrography, 6020 Innsbruck, Austria

²University of Salzburg, Chemie und Physik der Materialien, 5020 Salzburg, Austria

³Research School of Physics, Australian National University, Canberra, Australia

e-mail: peter.tropper@uibk.ac.at

Al-rich titanite [Ca(Ti,Al)(O,F,OH)SiO₄] has been the focus of many previous mineralogical studies, because Al is one of the most common and abundant substituents for Ti in natural titanite. Moreover, the substitution appeared to be pressure and temperature dependent and thus could be of interest for geothermobarometry. The two coupled substitution reactions that account for the formation of Al-bearing titanite are: $\text{Ti}^{4+} + \text{O}^{2-} = \text{Al}^{3+} + \text{F}^-$ and $\text{Ti}^{4+} + \text{O}^{2-} = \text{Al}^{3+} + \text{OH}^-$. Hence Al-rich titanite is made up of the three end-members CaTiOSiO₄ [titanite], CaAlFSiO₄, and CaAlOHSiO₄ (vuagnatite).

Tropper et al. (2018) measured the heat capacity (C_P) data of Al-F-bearing titanite that yielded the standard entropy S°_{298} of F-Al-titanite CaAlFSiO₄ (FAT). C_P of synthetic FAT was measured with relaxation calorimetry and differential scanning calorimetry between 5 and 764 K. The results yielded $S^\circ_{298.15}$ to be 115.4 ± 2.0 J/(mol·K) and subsequently the standard Gibbs free energy of formation from the elements, $\Delta_f G^\circ$, of CaAlSiO₄F to be between -2583 ± 3.0 and -2588 ± 3.0 kJ/mol, and the standard enthalpy of formation from the elements, $\Delta_f H^\circ$, to lie between -2728 ± 3.0 and -2733 ± 3.0 kJ/mol, depending on the thermodynamic data retrieval approach.

This study focusses on the determination of the entropy of mixing along the F-Al-titanite – titanite join. The following compositions (X_{Ti}) were measured: 0.18, 0.33, 0.63, 0.77, 0.82, 0.91. The corresponding values of $S^\circ_{298.15}$ are: 120.2, 127.27, 126.66, 128.43, 127.55, and 130.84 J/(mol·K) \pm 1.6-1.8 J/(mol·K) (2σ). Calculation of the excess entropy S^{ex} yielded a positive deviation from ideality. Due to the scatter of the data and the relatively large errors in S^{ex} , it is possible to use a symmetrical as well as an asymmetrical fit through the data. For simplicity, a regular model was fit through the data in accordance with the regular activity model proposed by Tropper et al. (2002). The corresponding values of the entropic Margules parameter W_S is 28 ± 16 J/(mol·K). In conjunction with data on W_V and estimates on W_H , this value will be another step closer to the comprehensive formulation of a non-ideal activity model for the system Al-F titanite – titanite.

Tropper P, Troitzsch U, Dachs E Benisek A (2018): Heat capacity measurements of CaAlSiO₄F from 5 to 850 K and its standard entropy. - Amer Miner 103, 1165-1168

Geochemical insights into one of the earliest marine habitats on Earth – the reliability of 3.5-billion-year-old jaspillites from the Dresser Fm., Australia

S. Viehmann¹, D. Krämer², C. Koeberl³, S.V. Hohl⁴, M.J. van Kranendonk⁵

¹University of Hannover, Institute of Mineralogy, Hannover, Germany

²Federal Institute of Geosciences and Natural Resources (BGR), Hannover, Germany

³University of Vienna, Department of Lithospheric Research, Vienna, Austria

⁴State Key Laboratory of Marine Geology, Tongji University, Shanghai, P.R. China

⁵University of New South Wales Sydney, Australian Centre for Astrobiology, Sydney, Australia
e-mail: s.viehmann@mineralogie.uni-hannover.de

The ca. 3.5 billion-year-old Dresser Formation in the Pilbara Craton, Western Australia, is famous for its traces of early life in the form of microfossil assemblages and stromatolites. These unique rock types provide fascinating windows into habitats of microbial life and the state of the ambient atmosphere-hydrosphere system. Among several pioneering studies targeting interdisciplinary fields of geo(micro)biology and geochemistry, trace elements in combination with Fe isotopes of jaspillites from different units within the Dresser Formation have recently been reported to reconstruct ancient paleo-environments (Johnson et al. 2022). This geochemical study targeted jaspillites, i.e., chemical sediments that are proposed to directly reflect ancient fluid chemistry from which the jaspillites formed, from four consecutive horizons of the Dresser Formation. They propose severe and fluctuating paleo-environmental changes during the deposition of these units in combination with changing nutrient availability and limitation during land-sea transitions based on Rare Earth's and yttrium (REY) and Fe isotope systematics. While this study provides a crucial milestone in understanding the earliest microbial habitats on Earth, the source of elements providing nutrients among other elements in the ancient Dresser aqueous environments remains still incompletely understood.

To determine the sources affecting water chemistry in the Dresser Formation, we obtained trace element and radiogenic Nd isotope compositions of high pressure-high temperature digestions of jaspillitic cherts directly overlying the famous “candelabra”-stromatolites from a terrestrial hot spring deposit (Djokic et al. 2017). The trace element data corroborate the endmembers (Johnson et al. 2022): endmember I shows seawater-like shale-normalized (subscript SN) REY_{SN} patterns with positive La_{SN}, Gd_{SN} anomalies, heavy REY_{SN} over light REY_{SN} enrichment, and super-chondritic Y/Ho ratios. In contrast, the endmember II is characterized by the lack of typical seawater-like anomalies, sub-chondritic Y/Ho ratios, and light REY_{SN} over heavy REY_{SN}. Positive Eu_{SN} anomalies representing REY contributions from high-temperature, hydrothermal fluids in the ancient Dresser depositional environment are present in both endmembers. Radiogenic Nd isotope compositions, commonly used to determine the local sources of REY in modern and ancient seawater due to the short residence time of Nd, show a significant impact of post-depositional alteration and a reset of the Sm-Nd isotope system in the Dresser Formation jaspillites. A best-fit isochron calculation yields a Sm-Nd age of 2260 Ga ± 180 Ma that overlaps with thermo-tectonic events in Pilbara Craton between 2430 to 2400 Ma and 2215 to 2145 Ma (Rasmussen et al. 2005), respectively, suggesting that Nd isotope of the Dresser Formation jaspillites are unreliable geochemical proxies to reconstruct sources in Dresser fluids 3.5 Ga ago. We – however- strongly emphasize that overall REY distributions and Fe isotope compositions must not necessarily be affected by these events, although the Nd isotope compositions in the Dresser jaspillites show significant disturbances.

- Djokic T, Van Kranendonk MJ, Campbell KA, Walter MR, Ward CR (2017): Earliest signs of life on land preserved in ca. 3.5 Ga hot spring deposits. - *Nat Comm* 8, 15263
- Johnson CM, Zheng X-Y, Djokic T, Van Kranendonk MJ, Czaja AD, Roden EE, Beard BL (2022): Early Archean biogeochemical iron cycling and nutrient availability: New insights from a 3.5 Ga land-sea transition. - *Earth Sci Rev* 103992
- Rasmussen B, Fletcher IR, Sheppard S (2005): Isotopic dating of the migration of a low-grade metamorphic front during orogenesis. - *Geology*, 33, 773-776

Analysis of Vickers indentation tests by means of Atomic Force Microscopy (AFM)

P. Vivanco-Chávez¹, M. Klichowicz², H. Lieberwirth², F. Mertens¹, O. Popov², G. Heide³

¹Institute for Physical Chemistry, Technische Universität Bergakademie Freiberg

²Institute for Mineral Processing Machines and Recycling Systems Technology, Technische Universität Bergakademie Freiberg

³Institute for Minealogy, Technische Universität Bergakademie Freiberg
e-mail: Patricia-Ilein.Vivanco-Chavez@chemie.tu-freiberg.de

The study of the mechanical properties of materials such as fracture toughness (K_{IC}) and Vickers hardness (VH), at micro/nanometric scales is scarce and at the same time a challenge to determine them. Therefore, this research shows a new methodology of analysis and insight in detail regarding the elastic/plastic behaviour of investigated materials with Vickers indenters. In this research five samples were analysed: a fused silica as reference material, a synthetic quartz crystal (SQ \square and SQ \times) and finally quartz grains from granite and granodiorite. A possible tool for the verification of the recorded indentation depths is Atomic Force Microscopy (AFM). Using an AFM allows to measure with great accuracy such as the length of the cracks (l), the depth of residual indentation (h_f) and the indentation marks (d), allowing to determine K_{IC} and HV with greater accuracy, i.e. at the nanoscale.

Keywords: Microhardness; Vickers Indentation; Quartz; Atomic Force Microscopy, Radial Cracks; Cone Crack; Palmqvist Cracks

Background: The importance of realistic modelling of the mechanic behaviour of mineral materials has increased due to its demand and contributions to mineral processing optimization and mining. These models rely on the accurate characterisation of mechanical properties, e.g. fracture toughness (K_{IC}) which characterises the resistance to unstable crack propagation under the crack opening. Since the theory and application of this parameter are described in standard textbooks like Anderson (2017) and Gross & Seelig (2018), the focus is set on the properties which are relevant for minerals, as well as the characterisation of different types of crack morphology that was first observed and analysed by Cook & Pharr (1990).









In contrast to macroscopic measurement approaches, the microscopic fracture toughness is calculated from the size of the cracks, which can be observed as a result of indentation hardness testing with a Vickers pyramid (for details see Roebuck et al. 2008 and ISO 28079:2009). To date, this method has been applied to hard metals (Palmqvist, 1957), technical non-metallic materials like glasses and ceramics (Cook & Pharr, 1990; Moradkhani et al. 2013), and rocks and minerals (Swain & Lawn, 1976; Whitney et al. 2007; Han et al. 2020).

However, this approach presents some challenges as the measurement quality of this parameter is affected by the difficulty of implementing this method on natural minerals, i.e. not all minerals show regular cracks after indentation (Whitney et al. 2007), the type of crack can often only be assumed based on literature references since different crack systems (Glandus et al. 1991), and the crack length measurements via microscope have low accuracy. Therefore, in this study, AFM is used to analyze with high precision the indentation marks and cracks caused by micro indentation tests with a Vickers indenter, thus, increasing the accuracy of mechanical property (K_{IC}) calculation.

Methods: The investigation of microhardness and fracture toughness of mineral phases was carried out using a Shimadzu HMV-G21DT Micro Vickers Hardness Tester, in which each sample underwent 30 indentation tests with a maximum load of $F = 980.7 \text{ mN}$ and a 15-second holding time. Subsequently, the indentation marks were analyzed with Park NX10 AFM to scan the sample surfaces, where the indentation diagonals (d_i) and crack length (l) are determined, and the final depth of the residual hardness impression (h_f) measured on scales ranging from micrometres to a few nanometers.

Results: The following is a synthesis of the crack morphologies found in this study (Table 1) and a summary comparison of the fracture toughness (K_{IC}) of this study with other authors (Figure 1).

Table 1. Summary classification of the different morphologies in the indented samples (30 indentations for each sample).

Sample	Cracks Morphology							
								
	No cracks	PRC	SRC	PRC + SRC	PCC	PCC + SRC	PRC + SCC	PRC + SRC + SCC
FS	5 (16.6%)	-	2 (6.6%)	-	3 (10%)	4 (13.3%)	10 (33.3%)	6 (20%)
SQ _{//}	-	25 (83.3%)	-	5 (16.6%)	-	-	-	-
SQ _⊥	-	5 (16.6%)	-	25 (83.3%)	-	-	-	-
Q-Gr	-	10 (33.3%)	-	20 (66.6%)	-	-	-	-
Q-Bg	-	3 (10%)	7 (23.3%)	20 (66.6%)	-	-	-	-

PRC = Primary Radial Cracks; SRC = Secondary Radial Cracks; PCC = Primary Cone Cracks; SCC = Secondary Cone Cracks

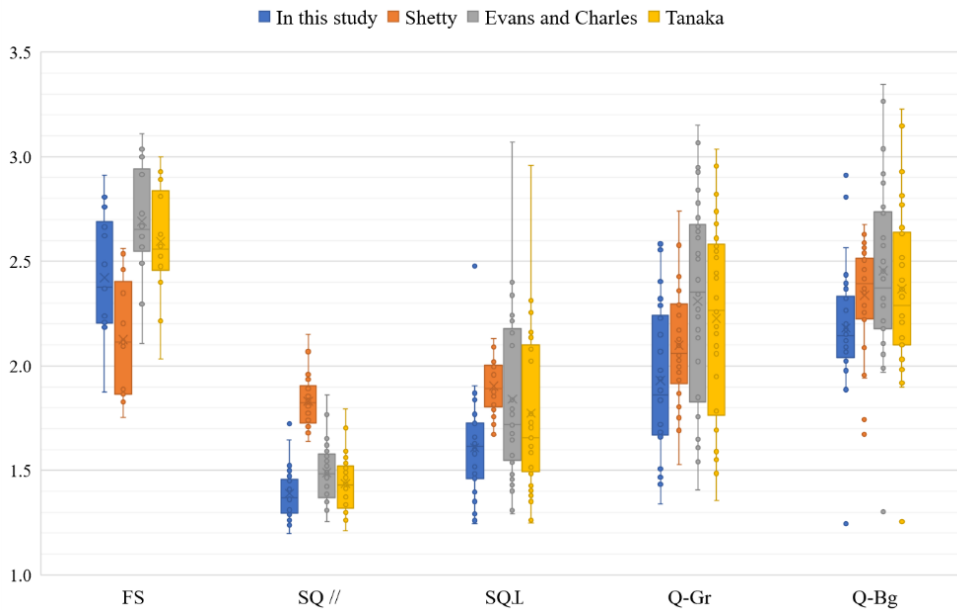


Figure 1. Comparison boxplot between the different K_{IC} values of the authors Deschamps et al. (2013), Tanaka (1987), Evans & Charles (1976) and this present study.

Conclusions:

- In this study, the characterization of the types of crack morphologies are both quantitatively and qualitatively determined (Table 1) and are consistent with models based on the literature review.
- Reconstruction of an indentation profile of the tested material based on the parameters of h_f and h_{max} is established, which is important to explain the elastic/plastic behaviour of the indented minerals.
- The fracture toughness (K_{IC}) values from this study agrees with the models of other authors (Figure 1), and this parameter is inversely proportional to the Vickers hardness (VH).

- Anderson TL (2017): Fracture mechanics: Fundamentals and applications. - Fourth ed, CRC Press Taylor & Francis Group: Boca Raton, Fla., London, New York, ISBN 9781498728133
- Roebuck B, Bennett E, Lay L, Morrell R (2008): Measurement good practice guide No. 9. - Palmqvist Toughness for Hard and Brittle Materials; Teddington, Middlesex, UK, TW11 0LW, ISBN 1368-6550
- Cook RF, Pharr GM (1990): Direct observation and analysis of indentation cracking in glasses and ceramics. - J Amer Ceram Soc 73, 787–817, doi:10.1111/j.1151-2916.1990.tb05119.x
- Evans AG, Charles EA (1976): Fracture toughness determinations by indentation. - J Amer Ceram Soc 59, 371–372, doi:10.1111/j.1151-2916.1976.tb10991.x
- Glandus JC, Rouxel T, Tai Q (1991). Study of the Y-TZP toughness by an indentation method. - Ceram Internat 17, 129–135, doi:10.1016/0272-8842(91)90041-W
- Gross D, Seelig T (2018): Fracture mechanics: With an introduction to micromechanics. - 3rd ed., Springer Internat Publ, Cham, ISBN 9783319710907.
- Han Q, Qu Z, Wang P, Bi G, Qu G (2020): Applications of micro-indentation technology to estimate fracture toughness of shale. - Materials (Basel) 13, doi:10.3390/ma13184208.
- International Organization for Standardization. ISO 28079 (2009): Hardmetals - Palmqvist toughness test (28079)
- Moradkhani A, Baharvandi H, Tajdari M, Latifi H, Martikainen J (2013): Determination of fracture toughness using the area of micro-crack tracks left in brittle materials by Vickers indentation test. - J Adv Ceram 2, 87–102, doi:10.1007/s40145-013-0047-z
- Palmqvist S (1957): Method att Bestamma Segheten hos Spread Material, Sarskit Hardmettaler. - Jernkontorets Annaler 141, 300–307
- Shetty DK, Wright IG, Mincer PN, Clauer AH(1985): Indentation fracture of WC-Co Cermets. - J Mater Sci 20, 1873–1882, doi: 10.1007/BF00555296
- Swain MV, Lawn BR (1976): Indentation fracture in brittle rocks and glasses. - Int J Rock Mech Mining Sci Geomech Abstr 13, 311–319, doi:10.1016/0148-9062(76)91830-1
- Tanaka K (1987): Elastic/plastic indentation hardness and indentation fracture toughness: the inclusion core model. - J Mater Sci 22, 1501–1508. doi: 10.1007/BF01233154
- Whitney DL, Broz M, Cook RF (2007): Hardness, toughness, and modulus of some common metamorphic minerals. - Amer Mineral 92, 281–288, doi:10.2138/am.2007.2212

Tracking transformation processes in the Mg phosphate mineral system – A mineralogical study for environmental applications

R. Volkmann^{1,2}, R. Blukis³, C. Schmidt¹, L. G. Benning^{1,2}

¹German Research Centre for Geosciences Potsdam

²Freie Universität Berlin

³Leibniz-Institut für Kristallzüchtung Berlin

e-mail: rebeccav@gfz-potsdam.de

Phosphorous is an essential component of all living beings and is an important component in fertilizers. It is a scarce element on Earth and mining of phosphorous deposits is environmentally harmful (Manning, 2008). Therefore, recent research is focusing on P-recovery from anthropogenic sources, e.g., from wastewaters. The mineral struvite ($\text{MgNH}_4\text{PO}_4 \cdot 6\text{H}_2\text{O}$) is recovered from wastewater and reutilized as a slow-release nitrogen and phosphorus fertilizer (Le Corre et al. 2009). However, struvite is unstable under atmospheric conditions, leading to its decomposition and transformation into other phosphate phases (Tansel et al. 2018). This subaerial transformation has not yet been characterized and kinetic parameters for the transformation reactions are unknown.

In this study, the decomposition and transformation of struvite was investigated by altering synthetic μm - and mm -sized crystals at different temperatures (22–60 °C) in open and closed systems for up to 10 months. Phase transformations were monitored by optical microscopy and Raman spectroscopy and transformation kinetic parameters were quantified by powder X-ray diffraction (XRD) and Rietveld analysis.

Struvite transformed to different products following different mechanisms. In open systems, and at 22 °C, struvite transformed to newberyite ($\text{Mg}(\text{PO}_3\text{OH}) \cdot 3\text{H}_2\text{O}$) by losing its ammonia and three of its water molecules. However, struvite remained fairly stable and at 22 °C this transformation proceeded only by 15 % even after 10 months. In contrary, at 37 and 60 °C, struvite transformed faster and primarily to another phase - dittmarite ($\text{MgNH}_4\text{PO}_4 \cdot \text{H}_2\text{O}$) which retained its ammonia but lost five out of six water molecules; newberyite occurred only as a minor product (< 5 wt.-%). In the open system, the phase formation proceeded about 35 % faster at 37 °C and 100 % faster at 60 °C compared to 22 °C. In contrast, in the closed system even after 10 months at 60 °C struvite remained stable and the transformation barely started (< 2 wt.-%). The XRD data showed that after about 8 months at 37 °C and after 2 months at 60 °C in the open system amorphization of struvite occurs through the complete loss of ammonia and water.

Microscopic imaging revealed that both newberyite and dittmarite were characterized by pseudomorphic overgrowth after struvite, while showing similar optical properties. Yet, the kinetic data indicates different formation mechanisms for the two phases. The partial pressure of water and ammonia in the reacting atmosphere, which was documented by the differences in open and closed kinetic rates, as well as differences in the crystal structures were the main drivers for the breakdown of struvite to the two other magnesium phosphate phases.

As struvite is used as a slow-release fertilizer in agriculture, our results document that its transformation to newberyite leads to the loss of ammonia, which has important implications for fertilizer storage. Even at 22 °C, after 10 months 15 % of the ammonia is lost. Although at higher temperatures (≥ 37 °C) the transformation leads to the retaining of ammonia in the

dittmarite structure, such a temperature requires a higher energy demand for storage. Therefore, our study indicates that struvite fertilizer should not be stored at ambient conditions, but at temperatures below 22 °C and in closed containers.

Manning DAC (2008): Phosphate minerals, environmental pollution and sustainable agriculture. – Elements 4, 105-108

Le Corre KS, Valsami-Jones E, Hobbs P, Parsons SA (2009): Phosphorus recovery from wastewater by struvite crystallization: A review. - Crit Rev Environ Sci Technol 39, 433-477

Tansel B, Lunn G, Monje O (2018): Struvite formation and decomposition characteristics for ammonia and phosphorus recovery: A review of magnesium-ammonia-phosphate interactions. – Chemosphere 194, 504-514

Provenance studies on raw garnets from the Zillertal (Tyrol), Ahrntal (South Tyrol), and Radenthein (Carinthia)

S. Wagner¹, B. Zerobin², R. Köchl³, P. Tropper¹, G. Goldenberg²

¹*Institute of Mineralogy and Petrography, University of Innsbruck*

²*Department of Archaeologies, University of Innsbruck*

³*Department of History and European Ethnology, University of Innsbruck*
e-mail: simon.wagner@uibk.ac.at

There is evidence of the use of the mineral garnet as a gemstone in jewellery since the early Middle Ages. In the Alps, too, garnet is still used today in the form of traditional costume jewellery, especially the garnet variety almandine. From the middle of the 19th century, garnet mining began in the Zillertal, Ahrntal and Radenthein, of which all three remained important sites until the early 20th century. However, due to the export to the gemstone-cutting factories in the Czech Republic at the time, the raw garnets lost their actual origin and were henceforth traded as "Bohemian garnets". Nevertheless, a chemical differentiation and determination of origin is possible even in this state with suitable analytical methods (EPMA, micro-XRF, etc.). On a macroscopic level, it is not possible to distinguish visually between the different garnet deposits. The most significant features are the size and colour of cut garnets, since the true Bohemian garnets often only measure a few millimetres and show a more intense red colour than alpine garnets. A further criterion for distinguishing between the different alpine deposits can be achieved via the individual inclusion pattern, which can be attributed to the different conditions of garnet formation and differing host rock composition. Typical inclusions of Zillertal and Ahrntal garnet are, for example, chlorite, apatite, zircon, quartz, ilmenite, and epidote. In contrast, garnets from Radenthein show oriented growth, which is typically seen with the ilmenite and rutile inclusions. The clearest differences are due to chemical differences in the composition of the garnets, which can also be attributed to different formation conditions (P-T-X). Typically, these chemical differences can be clearly visualized by plotting certain oxides against each other. This method has proven to be very effective in distinguishing garnet deposits on a global scale and therefore forms the basic discrimination method in provenance studies (e.g. Then-Obłuska et al. 2021). On a local scale apparent chemical differences are only visible to a limited extent. However, the use of compositional data analysis allows a clearer distinction between the different alpine garnet deposits. In the case of chemical composition, certain conditions must be met to achieve a successful evaluation of discrimination features. With the help of software like *CoDaPack 2.0* (Comas-Cufi & Henestrosa 2011), these analyses can be carried easier and allow therefore a better differentiation between the different garnet deposits within Austria. Applying PCA on this big dataset, consisting of samples directly from the deposits and the former warehouse in Zell am Ziller, clearly shows that the biggest variance in the data set is produced by the three oxides MgO, MnO and CaO. By plotting these in a ternary diagram five different groups can be identified.

Petrological investigations on garnet-chlorite-mica shists of the Rosstrugg and Hornkees (Zemmgrund, Zillertal)

S. Wagner¹, B. Zerobin², R. Köchl³, P. Tropper¹, G. Goldenberg²

¹*Institute of Mineralogy and Petrography, University of Innsbruck*

²*Department of Archaeologies, University of Innsbruck*

³*Department of History and European Ethnology, University of Innsbruck*
e-mail: simon.wagner@uibk.ac.at

Geologically, the Zemmgrund (Zillertal) is part of the Tauern Window and belongs tectonostratigraphically to the Venediger Duplex (Subpenninic Nappes). The garnet deposits occur locally on the Rosstrugg and around the Hornkees glacier within ductile shear zones within the “Zentralgneisse”. Similar shear zones can be observed in other parts of the innermost Zillertal, for example, the Stilluptal. The garnet-bearing host-rocks can be described as chlorite-mica-shist, which formed during the alpine orogeny (Selverstone et al. 1991). Especially at the Rosstrugg and Hornkees these garnets can reach sizes of several millimetres and are usually of good quality (few inclusions, beautiful red colour, etc.), which is why they were also used to produce garnet jewellery and are also very popular among mineral collectors.

The samples of the garnet-bearing chlorite-mica-shist have been taken directly from the historic mining site at the Rosstrugg and the mineral site close to the Hornkees glacier. Both host rocks are mainly composed of Bt+Chl+Qz and show minor amounts of Fsp+Ms±Rt±Zrn±Ap±opaque phases. The garnets in this matrix show different sizes, often reaching several millimeters. Crack formation can also be observed depending on the thin section. The inclusion pattern of the garnets varies as well; typically, however, Chl+Ap+Zrn+Qz+Rt+Ilm can be found.

Regarding their geochemical composition, garnets have been analysed with the help of μ -XRF, EPMA and LA-ICP-MS. Continuous zoning can be observed in all garnet samples, with the almandine component showing the largest proportions from 60 mol% (core) to 73 mol% (rim). The trace element distribution of Co, Zn, or Zr, for example, correlates with the pattern of the almandine component, whereas e.g., Ti shows a decreasing concentration from the core to the rim. The same can be observed for Y, whose distribution is already clearly visible in the distribution images generated with μ -XRF. HREEs, such as Yb or Lu, follow the same trend.

The pressure and temperature of garnet formation have been calculated using *Thermocalc v.3.45* and the extension *TC_Comb* (Dolivo-Dobrovolsky 2023). The AveragePT calculations resulted in $T = 613 \pm 10$ °C and $P = 8.2 \pm 0.4$ kbar. Calculation of garnet isopleths using the program *Perplex* yielded garnet growth with decreasing pressures (approx. 8.9 kbar in the core and 7.7 kbar in the rim) and increasing temperatures (560 °C in the core and 590 °C in the rim). Additionally, pseudosection modelling [P-T, P-a(H₂O)] was done using *THERIAK-DOMINO* and the most current database *td-d62-mp50-05* (Tinkham 2022). The combination of geothermobarometry and thermodynamic modelling clearly shows that a (H₂O) greater than 0.6 must have been predominant. The obtained garnet ages (Lu-Hf-geochronology) of 32.5 Ma agree with the existing age data of the Alpine metamorphic event and correspond with the “Tauernkristallisation”.

Dolivo-Dobrovolsky D (2023): TC_Comb software

Silverstone J, Morteani G, Staude J-M (1991): Fluid channelling during ductile shearing: transformation of granodiorite into aluminous schist in the Tauern Window, Eastern Alps. - J Metamorph Geol 9, 419–431

Tinkham DK (2022): td-ds62-mp50-05 database

Anhydrite formation in planetary surface environments – The case of the Atacama Desert

N. Wehmann¹, C. Lenting¹, T.M. Stawski², L. Agudo Jácome², S. Jahn¹

¹*Institut für Geologie und Mineralogie, Universität zu Köln, Zùlpicher Straße 49b, 50674 Köln, Germany*

²*Bundesanstalt für Materialforschung und -prüfung (BAM), Department for Materials Engineering,
Unter den Eichen 87, 12205 Berlin, Germany
e-mail: n.wehmann@uni-koeln.de*

Gypsum ($\text{CaSO}_4 \cdot 2\text{H}_2\text{O}$), bassanite ($\text{CaSO}_4 \cdot 0.5\text{H}_2\text{O}$), and anhydrite (CaSO_4) are essential evaporite minerals for the evolution of hyper-arid surface environments on Earth and Mars (Voigt et al. 2019; Vaniman et al. 2018). The formation mechanism of especially anhydrite has been a matter of scientific debate for more than a century (van't Hoff et al. 1903). To date, there exists no model that can reliably predict anhydrite formation at earth's surface conditions. While thermodynamics favor its formation, it is hardly achieved on laboratory time scales at conditions fitting either the Atacama Desert on Earth, or the surface of Mars (Wehmann et al. 2023, *subm.*). In light of most recent developments (e.g. Stawski et al. 2016), that advocate for a complex, non-classical nucleation mechanism for all calcium sulphates, we present an analysis of natural samples from the Atacama Desert to identify key features that promote the nucleation and growth of anhydrite under planetary surface conditions. Our analyses reveal at least three distinct anhydrite facies, with differing mineralogy and micro- to nano-structures. The facies are (1) aeolian deposits with sub- μm grain sizes, (2) (sub-)surface nodules that formed from aeolian deposits and (3) selenites with secondary anhydrite rims. Possible mechanisms of their formation will be discussed.

Hoff JVT, Armstrong EF, Hinrichsen W, Weigert F Just G (1903). Gips und Anhydrit. - Z Phys Chem 45(1), 257-306

Stawski TM, Van Driessche AE, Ossorio M, Diego Rodriguez-Blanco J, Besselink R, Benning LG (2016): Formation of calcium sulfate through the aggregation of sub-3 nanometre primary species. - Nature Comm 7, 11177

Vaniman DT, Martínez GM, Rampe EB, Bristow TF, Blake DF, Yen AS, Sumner DY (2018): Gypsum, bassanite, and anhydrite at Gale crater, Mars. - Amer Miner 103, 1011-1020

Voigt C, Klipsch S, Herwartz D, Chong G, Staubwasser M (2020): The spatial distribution of soluble salts in the surface soil of the Atacama Desert and their relationship to hyperaridity. - Global and Planetary Change 184, 103077

Wehmann N, Lenting C, Jahn S (2023): Calcium sulfates in planetary surface environments. - Available at SSRN 4479259

Crystallography in energy applications

C. Weidenthaler

*¹Max-Planck-Institut für Kohlenforschung, Mülheim an der Ruhr, Germany
e-mail: weidenthaler@mpi-muelheim.mpg.de*

The energy transition requires the implementation of sustainable energy carriers. Hydrogen is one of these options, but the storage is still a challenge. Ammonia, NH₃, is intensively investigated as a suitable candidate as an H₂ storage medium and is already used for heavy-duty transportation systems. The efficient splitting of NH₃ into H₂ and N₂ for fuel cell applications requires the development of catalysts where supported transition metals are one amongst others.

To understand the function of a catalyst, it is inevitable to use in situ/operando techniques in addition to ex-situ analytics. This contribution presents a combination of different in situ techniques that were used to investigate structure-property relationships of several types of Co- and Ni-based catalysts supported on different oxides such as La₂O₃, Al₂O₃, and MgO. In addition to in situ X-ray diffraction experiments, X-ray total scattering and X-ray absorption methods reveal structure changes of the catalysts and the supports on different lengths scales from bulk to the atomic scale. In addition to the results obtained from structure studies, the reduction behaviour, surface chemistry, and catalytic activities will be included to the overall discussion.

For Co-based catalysts supported on Al₂O₃, it could be shown that a significant fraction of the Co catalysts reacts with Al₂O₃ and forms catalytically inactive CoAl₂O₄ (Weidenthaler et al. 2022). The Co content in the spinel cannot be compensated by higher metal loadings. Alumina is known to prevent sintering and a re-dispersion of metallic Co after the reaction was observed. However, the disadvantage of its tendency to form inactive cobalt aluminates predominates.

The second system, Co on basic La₂O₃ support, forms in situ during NH₃ cracking from a LaCoO₃ pre-catalyst. The structural transformation from LaCoO₃ to the catalysts via several intermediate phases was monitored by means of operando X-ray diffraction experiments. The catalytically active metallic Co neither reacts with La₂O₃ nor re-disperses after the reaction. The conversion for Co on La₂O₃ is comparable to the most active Co on Al₂O₃ catalyst, despite having multiple higher Co-loading.

The third system involves Ni on MgO, which shows a clear dependence of the catalytic conversion on the activation process and the associated structural changes.

Weidenthaler C, Schmidt W, Leiting S, Ternieden J, Kostis A, Ulucan TH, Budiyo E (2022): In-situ investigations of Co@Al₂O₃ ammonia decomposition catalysts: The interaction between support and catalyst. - Chem Cat Chem 14, e202200688

Confocal μ -XANES as a tool to analyse Fe oxidation state in heterogeneous samples: The case of melt inclusions in olivine from Hekla volcano

M. Wilke¹, R. Botcharnikov², J. Garrevoet³, M. Portnyagin⁴, K. Klimm⁵,
S. Krashenninikov^{1,6}, R. Almeev⁶, S. Moune⁷, G. Falkenberg³

¹*Institut für Geowissenschaften, Universität Potsdam, Germany*

²*Institut für Geowissenschaften, Johannes-Gutenberg Universität Mainz, Germany*

³*Deutsches Elektronen-Synchrotron, DESY, Hamburg, Germany*

⁴*GEOMAR Helmholtz-Zentrum für Ozeanforschung, Kiel, Germany*

⁵*Institut für Geowissenschaften, Goethe Universität Frankfurt, Germany*

⁶*Institut für Mineralogie, Leibniz Universität Hannover, Germany*

⁷*Observatoire de Physique du Globe de Clermont-Ferrand, Université Clermont Auvergne, France*

e-mail: wilkem@uni-potsdam.de

Here we present a confocal Fe K-edge μ -XANES method for the analysis of Fe oxidation state in melt inclusions of one-side polished samples, potentially applicable to any heterogeneous sample. The new technique allows for an analysis of small volumes with high spatial 3D resolution of $<100 \mu\text{m}^3$. Using a confocal setup, the probed volume is restricted to that just beneath the surface of the exposed object. This protocol avoids contamination of the signal by the host mineral and minimizes self-absorption effects. This technique has been calibrated and tested on a set of experimental glasses with a wide range of $\text{Fe}^{3+}/\sum\text{Fe}$ ratios. The method was applied to the analysis of natural melt inclusions trapped in forsteritic to fayalitic olivine crystals of the Hekla volcano, Iceland. Our measurements reveal changes in $\text{Fe}^{3+}/\sum\text{Fe}$ from 0.17 in basaltic up to 0.45 in dacitic melts, whereas magnetite-ilmenite equilibrium testifies redox conditions with $\text{Fe}^{3+}/\sum\text{Fe} \leq 0.20$ (close to FMQ, Fayalite-Magnetite-Quartz redox equilibrium) along the entire range of Hekla melt compositions. This discrepancy indicates that the oxidized nature of glasses in the melt inclusions could be related to post-entrapment process of diffusive hydrogen loss from inclusions and associated oxidation of Fe in the melt. The $\text{Fe}^{3+}/\sum\text{Fe}$ ratio in silicic melts is particularly susceptible to this process due to their low FeO content and it should be critically evaluated before petrological interpretation.

Investigating the metal sources of the Early Nordic Bronze Age through a multi-proxy approach

A. Wittke¹, B. Cornelis¹, D. Berger¹

¹*Curt-Engelhorn-Zentrum Archäometrie, Mannheim, Germany
e-mail: andreas.wittke@ceza.de*

The Early Nordic Bronze Age (NBA Period IB, 1600–1500 BC) is characterized by huge amounts of metal products reaching northern Germany and Scandinavia for the first time, demonstrated by the appearance of a refined repertoire of bronze products (Nørgaard et al, 2019). Examples for these products are the blades of swords and daggers of the Sögel and Wohlde district, which suddenly appear as highly sophisticated metal artefacts without local precursors. Both blade types have hilt-plates with four or five rivets, while Sögel blades have a rounded and Wohlde plates have a trapezoidal formed hilt-plate. One of the great desiderates of archaeologists is determining the origin of archaeological bronzes and their metal sources (copper and tin). To reconstruct the provenance of the source materials isotope and elemental compositions of metals have since become important tools. This work pursues a multi-isotope approach combining Pb, Cu and Sn isotopes with trace element composition (Berger et al. 2022) of about 300 blades of the Sögel and Wohlde type from the Early NBA to investigate the origin of the raw material sources and of the blades. Additionally, we search for evidence of source mixing and/or recycling to gain a better insight into the manufacturing practices and to validate the provenance analysis. For this, the blades are isotopically and chemically analysed and compared with ores and typologically related blades from other regions in Central and Southern Europe. This may help to reconstruct relationships between artefacts of different origins and to reveal cultural and trade networks. Moreover, a critical evaluation of the data will be undertaken against the background of potential metal/ore mixing and recycling.

First results of 49 blades from the Early NBA indicate the Alpine Mitterberg as a potential source region for the copper based on Pb and Cu isotope composition, and trace element patterns. The majority of the blades consists of low-impurity copper of chalcopyrite quality typical for the Mitterberg. However, some blades were likely produced from Slovakian copper ores and there could even be indications of mixing both copper sources. Regarding tin, the Erzgebirge would be a very likely supplier, but some regions of Cornwall are also possible because of matching Sn isotope values. Based on the isotopic data of a single blade (Pb, Cu, Sn), we are able to comprehend the manufacturing steps of the object and their meaning for the choice of source materials. In future research, more artefacts from the NBA and Central and Southern Europe, as well as copper ores of the Mitterberg and the Slovakian Ore Mountains will be studied to conduct statistical analysis and to check for mixing practices.

Berger D, Brüggemann G, Bunnefeld J-H, Pernicka E (2022): Identifying mixtures of metals by multi-isotope analysis: Disentangling the relationships of the Early Bronze Age swords of the Apa–Hajdúsámson type and associated objects. - *Archaeometry* 64, 44–74, <https://doi.org/10.1111/arc.12714>

Nørgaard HW, Pernicka E, Vandkilde H (2019): On the trail of Scandinavia's early metallurgy: Provenance, transfer and mixing. *PLoS ONE* 14, 1-32, <https://doi.org/10.1371/journal.pone.0219574>

Study of natural As_2S_3 glass

T. Witzke¹, G. Nénert¹, M. Gateshki¹

¹Malvern Panalytical B. V., Lelyweg 1, 7602 EA, Almelo, The Netherlands,
e-mail: thomas.witzke@malvernpanalytical.com

At the burning mine dump of the Lichtenberg open cast, Ronneburg, Thuringia, Germany (mined for uranium-bearing alum shale) and the burning mine dump of the Katerina coal mine, Radvanice, Czech Republic, orange-red to red glassy crusts and droplets with the composition As_2S_3 were found. The material was solidified from a melt, which was probably a sublimation product from a gas phase. X-ray diffraction showed that the material is amorphous. No peaks, but just a flat, very broad hump around $d = 5 \text{ \AA}$ were observed in the diffraction patterns.

To be able to characterize structurally this amorphous mineral, Pair Distribution Function (PDF) analysis has been carried out. Similarly, to previous studies on the synthetic materials (Georgiev et al., 2003), the PDF data show that this mineral is intrinsically phase separated into small As-rich (As_4S_4) and large S-rich clusters. We show in Fig. 1 the PDF fit of the as-collected data using the previously reported model. This result suggests that this new mineral is closely related to the synthetic As_2S_3 glass.

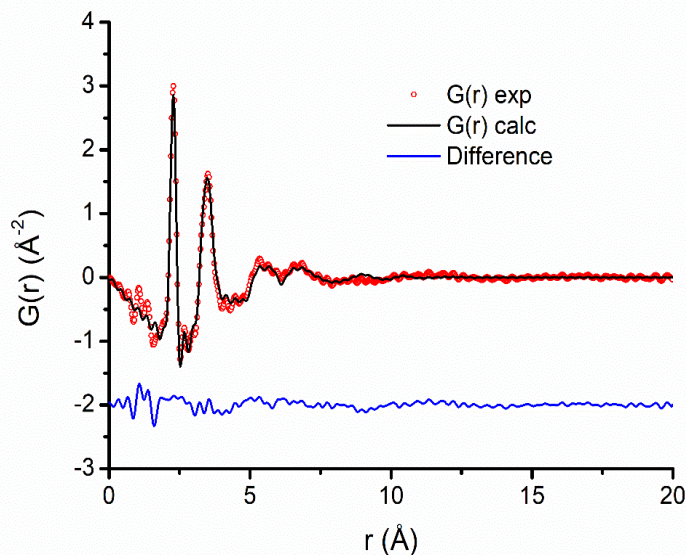


Figure 1: PDF fit of the experimental data using a phase separation model made of As_4S_4 and Sulfur cluster

Retrograde serpentinization and low-pressure metamorphic characteristics in the 3.8 Ga Isua Supracrustal belt, Greenland

J. Wolf¹, D. Sorger¹, S. Piazzolo², A.A.G. Webb³, T. Müller¹

¹*Geoscience Center Göttingen, Georg-August-University, Germany*

²*School of Earth and Environment, The University of Leeds, United Kingdom*

³*Division of Earth and Planetary Science and Laboratory for Space Research, University of Hong Kong, Hong Kong, China*

e-mail: j.wolf@stud.uni-goettingen.de

The Eoarchean Isua Supracrustal Belt (ISB) in West Greenland exposes one of the oldest rock records on Earth. Its tectonic setting is still subject of debate with interpretations ranging from plate tectonics to environments that are dominated by vertical tectonics. A first order question is the presence or absence of a metamorphic gradient within the belt. To that end, phase equilibria modeling combined with multiple geothermobarometric data convincingly suggested a homogeneous distribution of peak metamorphic conditions (550-600 °C; 0.8 - 1.0 GPa) (Ramírez-Salazar et al. 2021). However, recent studies of a dunite lens from the ISB suggested different metamorphic conditions varying from ultra-high pressure (Nutman et al. 2021) to low pressure deserpentinization (Guotana et al. 2022). In this study, we re-examine the petrography, mineral assemblages, reaction textures as well as the role of CO₂ in the metamorphism affecting ultramafic rocks from the specified lens B in the northwestern limb of the ISB. The texture of four different samples were analyzed using polarization microscopy, BSE imaging and EBSD measurements. Element x-ray maps and major element composition of major and accessory humite phases have been determined using EPMA. Phase equilibria modeling was done using the software package PerpleX to evaluate the role of CO₂.

Our petrographic observations show mineral assemblages of antigorite, olivine, magnesite, Ti-rich-humites and Fe-oxides. Antigorite (XMg = 0.99), magnesite, and Fe-oxide result from the breakdown reaction of olivine (XMg = 0.96). High forsterite content is interpreted to be the result of a hotter Archean mantle rather than deserpentinization. While the presence of accessory Ti-phases has been used as indicator for decompression through the breakdown reaction of Ti-chondrodite to form Ti-clinohumite, we present textural evidence of Ti-clinohumite being replaced by Ti-chondrodite pointing to a different reaction along a cooling path at lower pressures. The presence of carbonate instead of brucite highlights the role of CO₂ and its necessity to accurately describe phase relations for the metamorphic evolution of ultramafic rocks. Here, we present evidence from phase equilibria modeling, equally pointing to a simple cooling path at intermediate pressure conditions in agreement with metamorphic conditions obtained for the rest of the belt, rather than isothermal decompression from pressures higher than 2.0 GPa. The resulting lack of evidence for higher pressure conditions experienced by these mafic lenses thus removes a strong argument for the ISB to exhibit a metamorphic gradient, confirming the record of homogeneous metamorphic conditions within the belt.

- Guotana JM, Morishita T, Nishio I, Tamura A, Mizukami T, Tani K, Harigane Y, Szilas K, Pearson DG (2022): Deserpentinization and high-pressure (eclogite-facies) metamorphic features in the Eoarchean ultramafic body from Isua, Greenland. - *Geosci Front* 13, 101298, <https://doi.org/10.1016/j.gsf.2021.101298>
- Nutman AP, Scicchitano MR, Friend CRL, Bennett VC, Chivas AR (2021): Isua (Greenland) ~3700 Ma meta-serpentinite olivine Mg# and $\delta^{18}\text{O}$ signatures show connection between the early mantle and hydrosphere: Geodynamic implications. - *Precambrian Res.* 361, 106249, <https://doi.org/10.1016/j.precamres.2021.106249>
- Ramírez-Salazar A, Müller T, Piazzolo S, Webb AAG, Hauzenberger C, Zuo J, Haproff P, Harvey J, Wong TK, Charlton C (2021): Tectonics of the Isua Supracrustal Belt 1: P-T-X-d Constraints of a Poly-Metamorphic Terrane. - *Tectonics* 40, e2020TC006516. <https://doi.org/10.1029/2020TC006516>

Cement analysis by X-ray diffraction and X-ray fluorescence

S. Wollstadt¹, T. Füllmann¹, E. Hartmann¹

¹Rigaku Europe SE, Hugenottenallee 167, 63263 Neu-Isenburg, Germany
e-mail: elmar.hartmann@rigaku.com

Cement is one of the most important materials for construction and reacts with water to form hydrates, which gradually condense and harden. This hardening is caused when the formed hydrates coat cement particles and bind them together. A detailed understanding of the hydrate formation process is expected to lead to the elucidation of the mechanism of condensation and hardening. X-ray diffraction (XRD) techniques can identify crystalline hydrates such as ettringite and monocarbonate in cement. We report on the observation of changes in the crystalline phase or ordinary Portland cement over time with a water/cement ratio of 25% using a liquid sample holder which can prevent the sample from drying in an ambient environment by covering the sample surface with a film. Fig. 1 exemplifies changes in the XRD pattern of cement during a hydration reaction.

In addition, X-ray fluorescence (XRF) techniques are used to control the chemical composition of cement products and interim products. Since the fusion method can eliminate sample heterogeneity problems, such as grain size and mineralogical effects, it is possible to obtain high accuracy for cement samples and to establish calibrations using a variety of materials. ASTM C114-18 covers chemical analysis of hydraulic cements. In this standard, mainly procedures of wet chemical analysis are described and XRF spectrometry is mentioned as an example of “Rapid Test Methods”. In practice, XRF spectrometry has been used for chemical composition analysis of cement owing to its simple sample preparation and high precision. We will show quantitative analysis for Portland cements by the fusion method according to ASTM C114-18, as displayed in Table 1, using a multi-channel simultaneous wavelength dispersive XRF (WDXRF) spectrometer, which enables the simultaneous measurement of all the elements in the sample under investigation. The counting time of the measurement was 40 seconds for twelve elements in cement.

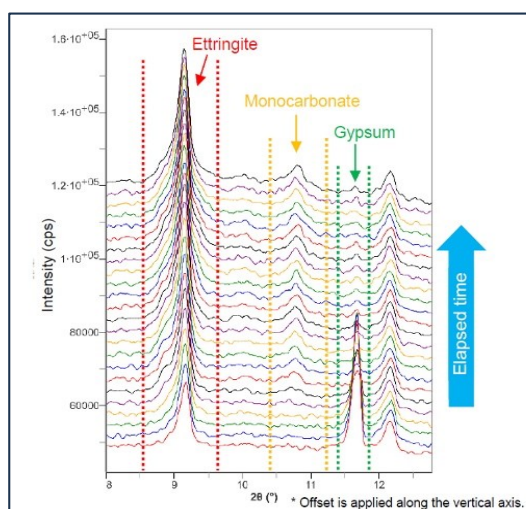


Figure 1. Overlaid X-ray diffraction patterns of hydrated cement.

Analysis component	Analysis range	Difference between duplicates		Qualified
		Limit (ASTM)	Maximum difference	
SiO ₂	18.637 – 22.38	0.16	0.05	✓
Al ₂ O ₃	3.875 – 7.06	0.20	0.01	✓
Fe ₂ O ₃	0.152 – 3.09	0.10	0.003	✓
CaO	57.58 – 67.87	0.20	0.14	✓
MgO	0.814 – 4.475	0.16	0.01	✓
SO ₃	2.086 – 4.622	0.10	0.01	✓
Na ₂ O	0.021 – 1.068	0.03	0.006	✓
K ₂ O	0.093 – 1.228	0.03	0.004	✓
TiO ₂	0.084 – 0.3663	0.02	0.003	✓
P ₂ O ₅	0.022 – 0.306	0.03	0.001	✓
ZnO	0.0048 – 0.107	0.03	0.0004	✓
Mn ₂ O ₃	0.0073 – 0.2588	0.03	0.001	✓

Table 1. Qualification test results (unit: mass%)

Stable tungsten (W) isotope behavior during the early diagenesis in the Gulf of California

R. Yang^{1,2}, M. Gutjahr², F. Scholz², F. Kurzweil¹, S. Eroglu³, C. Münker¹

¹*Institute of Geology und Mineralogy, University of Cologne, Zùlpicher StraÙe 49b, 50674 Cologne, Germany*

²*GEOMAR Helmholtz Centre for Ocean Research Kiel, WischhofstraÙe 1-3, 24148 Kiel, Germany*

³*Institute of Geology and Paleontology, Westfälische Wilhelms Universität,*

Correns StraÙe 24, 48149 Münster, Germany

e-mail: ryang2@uni-koeln.de

The stable W isotope system has recently emerged as a promising redox indicator, but its modern oceanic budget is not yet fully understood. Specifically, the mechanisms of W delivery to the sediments and its behavior during early diagenesis remain unknown.

In this study, three sediment cores in the gulf of California were thoroughly analyzed. Our findings indicate that W in marginal sediments is a combination of authigenic and detrital W components, with varying contributions at different depths. Authigenic W is likely bound to Mn oxides and released into the pore water in the Mn reduction zone. The delivery of W is primarily associated with Mn shuttling. Light W is adsorbed and released upon reductive dissolution of Mn oxides.

The sub-surface conditions in all the three cores are anoxic, leading to limited enrichment of W in sediments. Despite being geochemical twin elements, W and Mo display contrasting behaviors in sulfidic environments. Consequently, the distinctive behavior of W makes it a valuable indicator for identifying the cycling of Mn, an essential element for biological processes, and for tracing the oxidation history of the early Earth's oceans.

Unravelling the formation history of the Maronia Skarn, NE Greece: Insights from melilite group minerals

M. Zeug¹, A. Repstock², P. Voudouris³, H. Gevorgyan⁴, H. Schleicher⁵

¹ Landesamt für Geologie und Bergwesen Sachsen-Anhalt,
Fliederwegkaserne 13, 06130 Halle, Saale, Germany

² Geological Survey and Geophysics, Sächsisches Landesamt für Umwelt,
Landwirtschaft und Geologie, Pillnitzer Platz 3, 01326 Dresden, Germany

³ Department of Mineralogy and Petrology, National and Kapodistrian University of Athens,
University Campus-Zografou, 15784, Athens, Greece

⁴ Institute for Mineralogy, TU Bergakademie Freiberg, Brennhausgasse 4, 09599 Freiberg

⁵ Mineralogisch-Petrographisches Institut, Universität Hamburg, Grindelallee 48, 20146 Hamburg, Germany
e-mail: manuela.zeug@sachsen-anhalt.de / manuela.zeug@univie.ac.at

The Maronia skarn is situated in the northern region of the Aegean Sea, approximately 25 km west of Alexandroupolis in northeastern Greece. During the Oligocene (29.8 Ma) the Maronia pluton (monzonite, quartz monzonite, monzogabbro) intruded into Mesozoic metasediments of the Circum Rhodope Belt (Schaarschmidt et al. 2021). This intrusive event led to the development of a remarkable skarn mineralisation within the western metamorphic aureole caused by the contact between the pluton and the adjacent marbles. The western contact aureole extends 3km in length and up to 100m in width.

Skarn zones between the pluton and the marble were identified based on mineral assemblages and the chemical composition of granditic garnet, which is present in each skarn zone. Garnet crystals of the western contact aureole of the Maronia skarn correspond to the grossular-andradite solid solution series. The Maronia skarn contains a variety of unusual and remarkable mineralisation, including (i) Ti-Zr-Cr-rich garnet crystals, which occurrence is possibly unique worldwide (Voudouris & Katerinopoulos 2004, Katerinopoulou et al. 2009), (ii) predominantly Ti-rich dark brown andradite crystals (2–6 wt% TiO₂) that contain subhedral to euhedral titanite crystals [CaTi(SiO₄)O] in the core, and (iii) andradite-rich garnet (2–8 wt% TiO₂) within a melilitic skarn that contain perovskite (CaTiO₃) in the core. The skarn mineral assemblages (e.g. Ti-rich garnet, melilite, perovskite) in both the endoskarn and the exoskarn indicate a development in a silica-undersaturated magmatic environment (cf. Russel et al. 1999).

Melilite group minerals are restricted to the exoskarn and refer to gehlenite (Ca₂Al[AlSiO₇]-åkermanite (Ca₂Mg[Si₂O₇]) solid solution series. Various stages of skarn formation can be identified based on the appearance of the melilite solid solutions, which are reflected in four different zones in the Maronia exoskarn. The first zone is fine-grained consisting of clinopyroxene, interstitial melilite, and andradite-rich garnet, which may contain perovskite cores. This fine-grained zone is assumed to be closest to the pluton. The adjacent zone consists of almost tabular, slightly rounded cube-shaped crystals associated with interstitial andradite-rich garnet (2–8 wt% TiO₂) with or without perovskite-cores (Fig. 1). These melilite crystals are closer in composition to gehlenite suggesting a formation of a high-temperature skarn (Deer et al. 1992; Katona et al. 2003; Marinacea et al. 2011, and references therein) at a formation temperature exceeding 900°C in the prograde stage of skarn formation (cf. Mposkos & Doryphoros 1993). In the following zone melilite crystals show zoning with a gehlenitic core and an åkermanitic rim indicating the initial retrograde stage (cf. Reverdatto et al. 1979). Next to the latter zone, melilite solid solutions are completely replaced by vesuvianite representing a late retrograde stage during the cooling down at temperatures below melilite stability (~ 675 °C, Mposkos & Doryphoros 1993). Results of the

present study show that melilite crystals can be used to reveal the different stages of Maronia skarn evolution.

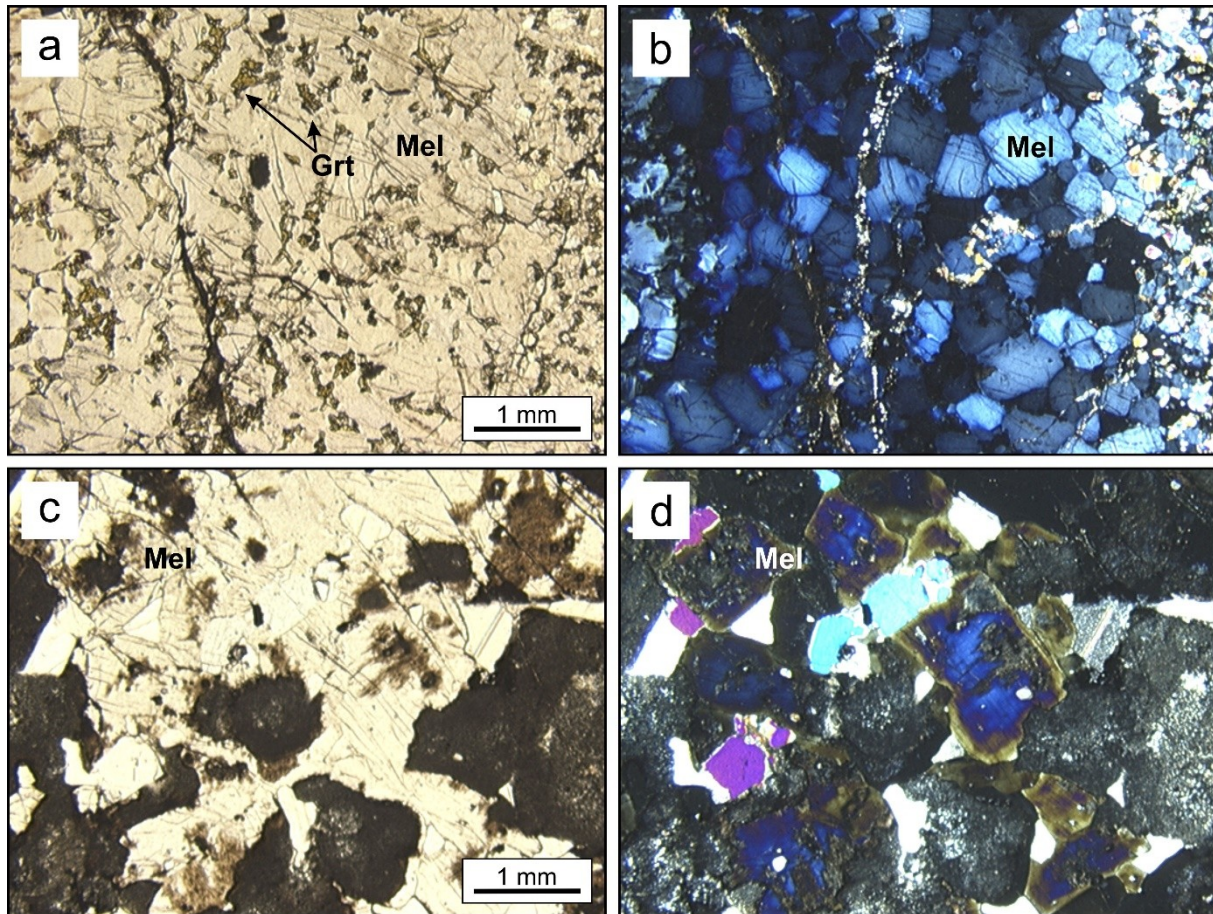


Figure 1. Plane-polarised (a and c) and cross-polarised (b and d) transmitted light photomicrographs of melilite zones in the Maronia skarn. The melilite in a and b is closer to the gehlenite endmember, suggesting a formation in the prograde stage. The melilite in c and d shows clear zonation of a gehlenite-rich core surrounded by an åkermanite-rich rim, which indicates an initial retrograde stage of skarn formation. Foto: M. Zeug

- Deer WA, Howie RA, Zussman J (1992): *An Introduction to the Rock-Forming Minerals* (second ed.). Longman, Hong Kong
- Katerinopoulou A, Katerinopoulos A, Voudouris P, Bieniok A, Musso M, Amthauer G (2009): A multi-analytical study of the crystal structure of unusual Ti–Zr–Cr-rich Andradite from the Maronia skarn, Rhodope massif, western Thrace, Greece. - *Miner Petrol* 95, 113–124
- Katona I, Pascal M-L, Fonteilles M, Verkaeren J (2003): The melilite (Gh50) skarns at Oravița, Banat, Romania: transition to gehlenite (Gh85) and to vesuvianite. *Can. Mineral.* 41, 1255–1270
- Marincea S, Dumitraș D-G, Ghineț C (2011) Gehlenite from three occurrences of high-temperature skarns, Romania: New mineralogical data
- Mposkos E, Doryphoros K (1993): High temperature skarns in the Maronia area (NE Greece). - *Bull Geol Soc Greece*, 23–35
- Reverdatto VV, Pertsev NN, Korolyuk VN (1979): P-T-Evolution and origin of zoning in melilite during the regressive stage of contact metamorphism in carbonate-bearing rocks. *Contrib Miner Petr* 70, 203–208
- Russell JK, Dipple GM, Lang JR, Lueck B (1999): Major-element discrimination of titanian andradite from magmatic and hydrothermal environments: an example from the Canadian Cordillera. *Europ J Miner* 11, 919–935
- Schaarschmidt A, Klemd R, Regelous M, Voudouris PC, Melfos V, Haase KM (2021) The formation of shoshonitic magma and its relationship to porphyry-type mineralisation: the Maronia pluton in NE Greece. *Lithos* 380–381, 105911
- Voudouris P, Katerinopoulos A (2004): New occurrences of mineral megacrysts in Tertiary magmatic-hydrothermal and epithermal environments in Greece. *Documenta Naturae* 151, 1–21

How to predict strength and optimum mix-designs of mineral-waste-based geopolymers

I. Zögl¹, O.Rudić², C. Grengg¹, F. Steindl¹, D. Etehad¹, M. Dietzel¹, S. Raič¹

¹*Institute of Applied Geoscience, Graz University of Technology*

²*Institute of Technology and Testing of Construction Material, Graz University of Technology*
e-mail: iris.zoegl@tugraz.at

Reducing the carbon footprint of building material production (*ca.* 9 % of anthropogenic CO₂) in the short term is essential to achieve global climate targets. In this regard, mineral wastes and industrial secondary raw materials show large potential as a low-CO₂ alternative to traditional carbonate-based binder systems. In order to promote and establish the use of mineral waste based binders as strong future competitors in the construction industry, optimal combinations of solid and liquid binder components have to be developed in so-called mix designs to meet material requirements. In this context, the desired material properties, such as adequate workability, high strength, improved chemical resistance and minimal shrinkage strongly depend on elemental ratios (*e.g.* Si/Al, Al/K) within the mix design. These are multi-variable challenges that are conventionally solved by changing one variable of the mix design at a time, until the desired results are achieved. In order to ensure a more time- and cost-efficient strategy, and to generate optimum experimental conditions, we are applying the Design of Experiment (DoE) and Response Surface Methodology (RSM) approaches to alkali-activated waste-based binder systems. DoE is a widely used procedure that seeks to predict a desired outcome (*e.g.* compressive strength, elemental ratios), which is then systematically optimized by a set of statistical techniques (RSM). In the current study, we evaluated the most desirable relative contents of the mix design components metakaolin, mineral wastes and aqueous potassium silicates (waterglass as alkaline activator) under the conditions of (i) maximizing the content of mineral wastes and (ii) achieving the desired material properties (*e.g.*, compressive strength). Preliminary results demonstrate how a minimum number of experimental runs and samples enables a refinement of possible mix-ratio-combinations. Re-iterations of these experimental procedures allow to accurately predict relevant material properties such as mechanical performance of the hardened mineral-waste-based binder material. Additionally, economic and ecological decisions could be already made during early stages of experimental approaches by including manufacturing costs and CO₂ emissions to the existing DoE models.